الجمهورية الجزائرية الديمقراطية الشعبية
People's Democratic Republic of Algeria
وزارة التعليم العالي والبحث العلمي
Ministry of Higher Education and Scientific Research

جامعة زيان عاشور بالجلفة
Université Ziane Achour de Djelfa

كلية العلوم و التكنولوجيا
Faculty of Science and Technology

Department: Civil Engineering

Order N°: . …. / 2024

Defense authorization N°……/2024

DOCTORAL THESIS

3rd Cycle Doctoral (D-LMD)

Presented by

YOUSFI MOHAMMED AMIN

With a view to obtaining the doctoral diploma in 3rd Cycle Doctoral (D-LMD)

Branch: Civil Engineering

Specialty: Geotechnical

Topic

Study of the Behavior of Soft Soils Treated by Granular Columns

Supported, on 15 /01/ 2024, before the jury composed of:

Last and first name	Grade	Institution of affiliation	Designation
Mr Nécira Brahim	MCA	University of Djelfa	President
Mr Guettala Salim	Professeur	University of Djelfa	Supervisor
Mr Labed Mohamed	MCB	University of Djelfa	Co-Supervisor
Mr Cheriet Fayssal	MCA	University of Djelfa	Examiner
Mr Djedid Tarek	MCA	University of El Oued	Examiner

Djelfa University, FST, 2024

الجمهورية الجزائرية الديمقراطية الشعبية
République Algérienne Démocratique et Populaire
وزارة التعليم العالي والبحث العلمي
Ministère de l'Enseignement Supérieur et de la Recherche Scientifique

جامعة زيان عاشور بالجلفة
Université Ziane Achour de Djelfa

كلية العلوم و التكنولوجيا
Faculté des Sciences et de la Technologie

Département : Génie Civil

N° d'Ordre : . …. / 2024

Autorisation de Soutenance N°……/2024

THESE DE DOCTORAT

Doctorat 3ème Cycle (D-LMD)

Présentée par

YOUSFI MOHAMMED AMIN

En vue de l'obtention du diplôme de Docteur en 3ème Cycle D-LMD

Filière : Génie Civil

Spécialité : Géotechnique

Thème

Étude du Comportement des Sols Compressibles Traites par des Colonnes Granulaires

Soutenue publiquement, le 15/01/2024, devant le jury composé de :

Nom et Prénom	Grade	Etablissement de rattachement	Désignation
Mr Nécira Brahim	MCA	Université de Djelfa	Président
Mr Guettala Salim	Professeur	Université de Djelfa	Directeur
Mr Labed Mohamed	MCB	Université de Djelfa	Co Directeur
Mr Cheriet Fayssal	MCA	Université de Djelfa	Examinateur
Mr Djedid Tarek	MCA	Université d'El Oued	Examinateur

Université de Djelfa, FST, 2024

Dedications

To my beloved late father, I am filled with both sorrow and gratitude as I embark on this milestone. Your constant support, encouragement, and belief in my abilities have been my driving force. Though you may not be here to witness this achievement, I dedicate this thesis to your loving memory.

To my dear mother, to all my family, and to my fiancée, your unwavering faith in me has been my guiding light. Your endless sacrifices, unwavering love, and constant prayers have been instrumental in my journey. I am eternally grateful for your presence and strength.

Thank you.

REMERCIEMENTS

I would like to begin by thanking Almighty God, the all-powerful and merciful, who has granted me the strength and patience to accomplish this work.

I want to start by expressing my deepest appreciation to Professor ***Salim Guettala****, my thesis advisor, for his unwavering support and guidance during the course of this research project. His commitment to excellence and vast expertise have played a crucial role in the successful culmination of this study.*

I would also like to extend my sincere thanks to the co-supervisor, Dr. ***Mohamed Labed****, for his significant contribution to this research. His presence, expertise, and attention to detail have played a crucial role in the successful outcome of this thesis.*

I would like to express my gratitude to Dr. ***Nécira Brahim****, a doctor at the University of Djelfa, for accepting the role of the chairperson for the defense of this thesis.*

My sincere thanks go to the members of the jury who accepted to be the examiners of this thesis and dedicated their time and thorough attention to assessing this work. I am immensely grateful for their interest in my research.

Dr. ***Cheriet Fayssal*** *from the University of Djelfa.*

Dr. ***Djedid Tarek*** *from the University of El-Oued.*

*A big thank you goes to Dr.****Imad Eddine Debbabi****, an esteemed scholar at the University of Biskra, and Dr.* ***Ali Farik****, a respected doctor from the University of El-Oued, for their valuable guidance, advice, and the provision of data and documents relevant to the scope of this research project.*

Finally, I would like to express my gratitude to all the individuals who have contributed directly or indirectly to the completion of this work.

YOUSFI Mohammed Amin

ABSTRACT

The granular column technique presents itself as a highly effective approach for reinforcing soft soils, offering substantial benefits such as improved bearing capacity and minimized settlement. However, when dealing with extremely soft soils, the bearing capacity diminishes to an extent where ordinary stone columns or sand columns no longer provide sufficient containment. To address this challenge, an apt solution is to integrate the columns with geosynthetics, imparting them with vital lateral confinement required for optimal performance. On the other hand, the use of recycled aggregate materials has become an effective modern technology for better soil reinforcement.

Recycled aggregates have been increasingly considered at the recent years, owing to the limited supply of natural aggregates coupled with the corresponding carbon footprint. The use of recycled aggregates aims to reduce energy consumption and thus contributes to reducing waste harmful to the environment. The objective of this thesis is to clarify the importance of using recycled aggregate materials in soil reinforcement and to demonstrate their effectiveness compared to natural aggregate. This study is based on a number of numerical tests using the finite element method of the PLAXIS 3D software with the elastic-perfectly plastic behavior model and the Mohr-Coulomb flow criterion for all materials.

In the present study, a unit cell model of soft soil treated by three types of granular columns: Ordinary Stone Columns (OSC), Sand-Fiber Mix (SFM) and Recycled Aggregate Porous concrete Pile (RAPP) was loaded to failure. Where an extensive study was conducted to investigate the effects of the column type; angle of friction, modulus of elasticity, column length and geosynthetic effective stiffness on the behavior of soft soils. Results of the numerical tests indicated that the bearing capacity of the columns of recycled aggregates is three times greater than that the columns of natural aggregates. The findings of this research are given in the form of load-settlement graphs, which made it possible to release constructive recommendations for the realization of the work on this technique.

Keywords: *Soft Soil, Granular column, Recycled aggregates, Numerical analysis, Unit cell, Bearing capacity, PLAXIS 3D.*

RÉSUMÉ

La technique des colonnes granulaires se présente comme une approche hautement efficace pour renforcer les sols compressibles, offrant des avantages substantiels tels qu'une capacité portante améliorée et une réduction de tassement. Cependant, lorsqu'il s'agit de sols extrêmement compressibles, la capacité portante diminue à un point où les colonnes ballastées ordinaires ou les colonnes de sable ne fournissent plus une confinement suffisante. Pour relever ce défi, une solution appropriée consiste à intégrer les colonnes avec des géosynthétiques, leur conférant une confinement latérale primordiale nécessaire pour une performance optimale. D'autre part, l'utilisation des matériaux d'agrégats recyclés est devenue une technologie moderne efficace pour un meilleur renforcement des sols.

Au cours des dernières années, les agrégats recyclés ont été de plus en plus pris en considération en raison de la rareté des agrégats naturels et de leur empreinte carbone correspondante. L'utilisation d'agrégats recyclés vise à réduire la consommation d'énergie et contribue ainsi à la réduction des déchets nocifs pour l'environnement. L'objectif de cette thèse est de clarifier l'importance de l'utilisation des matériaux d'agrégats recyclés dans le renforcement des sols et de démontrer leur efficacité par rapport aux agrégats naturels. Cette étude repose sur un certain nombre de tests numériques utilisant la méthode des éléments finis du logiciel PLAXIS 3D avec un modèle de comportement élastique-parfaitement plastique avec le critère d'écoulement de Mohr-Coulomb pour tous les matériaux utilisés.

Dans la présente étude, un modèle de cellule unitaire de sol compressible traité par trois types de colonnes granulaires a été chargé jusqu'à la rupture : des colonnes ballastées ordinaires (OSC), un mélange de sable et de fibres (SFM) et des pieux en béton poreux d'agrégats recyclés (RAPP). Une étude approfondie a été menée pour examiner les effets du type de colonne, de l'angle de frottement, du module d'élasticité, de la longueur de la colonne et de la rigidité effective du géosynthétique sur le comportement des sols mous. Les résultats des tests numériques ont indiqué que la capacité portante des colonnes d'agrégats recyclés est trois fois supérieure à celle des colonnes d'agrégats naturels. Les résultats de cette recherche sont présentés sous forme de graphiques de chargement et de tassement, ce qui a permis de formuler des recommandations constructives pour la mise en œuvre de cette technique.

Mots-clés : *Sol compressible, Colonne granulaire, Agrégats recyclés, Analyse numérique, Cellule unitaire, Capacité portante, PLAXIS 3D.*

الملخص

تعتبر تقنية الأعمدة الحجرية منهجًا فعالًا لتعزيز التربة الضعيفة، حيث توفر فوائد كبيرة مثل تحسين قدرة التحمل وتقليل نسبة الهبوط. ومع ذلك، عند التعامل مع تربة ضعيفة للغاية، تقل قدرة التحمل إلى حد يجعل الأعمدة العادية من الحجر أو الرمل لا توفر الاحتواء الكافي. لحل هذه التحديات، الحل المناسب هو دمج الأعمدة مع الجيوسنتيتيك، لمنحها الحصر الجانبي الضروري للأداء الأمثل. من ناحية أخرى، أصبح استخدام مواد الركام المعاد تدويرها تكنولوجيا حديثة فعالة لتعزيز التربة بشكل أفضل.

إن المواد الركامية المعاد تدويرها أصبحت محل اهتمام متزايد في السنوات الأخيرة، نظرًا للإمداد المحدود للمواد الركامية الطبيعية والتأثير الكربوني المرتبط بها. يهدف استخدام المواد الركامية المعاد تدويرها إلى تقليل استهلاك الطاقات الحيوية وبالتالي المساهمة في الحد من النفايات الضارة للبيئة. يهدف هذا البحث إلى توضيح أهمية استخدام مواد الركام المعاد تدويرها في تعزيز التربة وإظهار فعاليتها مقارنةً بالمواد الركامية الطبيعية. تعتمد هذه الدراسة على عدد من الاختبارات العددية باستخدام طريقة العناصر المحدودة في برنامج PLAXIS 3D، وذلك باستخدام نموذج السلوك المرن-البلاستيكي المثالي ومعيار تدفق مور-كولومب لجميع المواد المستخدمة.

تم في هاته الدراسة إنشاء نموذج خلية وحدة للتربة الناعمة المعالجة بواسطة ثلاثة أنواع من الأعمدة الحبيبية: أعمدة الحجر العادية (OSC)، ومزيج الرمل مع الألياف (SFM)، والخوازيق من الخرسانة المسامية المعاد تدويرها (RAPP) حتى الانهيار. تم إجراء دراسة شاملة لاستكشاف تأثير نوع العمود، وزاوية الاحتكاك، ومعامل المرونة، وطول العمود، وصلادة الجيوصطناعي الفعالة على سلوك التربة الناعمة. أظهرت نتائج الاختبارات العددية أن قدرة تحمل أعمدة الركام المعاد تدويرها أكبر بثلاث مرات من قدرة تحمل أعمدة الركام الطبيعي. تم تقديم نتائج هذا البحث في شكل مخططات تحميل-تسوية، مما سمح بإصدار توصيات بناءة لتنفيذ العمل بهذه التقنية.

الكلمات المفتاحية:

التربة الضعيفة، العمود الحبيبي، الركام المعاد تدويره، التحليل العددي، خلية الوحدة، قدرة التحمل، PLAXIS 3D.

SUMMARY

Chapter 01: Bibliographical Study on Compressible Soils

Chapter 02: Ground Improvement Technique for Soft Soils Using stone Columns

Chapter 03: Numerical Modelling and Behavioural Laws

Chapter 04: Numerical Analysis of a 3D Unit Cell Model for Soft Soil Reinforced with Different Granular Columns

LIST OF FIGURES

Chapter 01: Bibliographical Study on Compressible Soils

Chapter 02: Ground Improvement Technique for Soft Soils Using stone Columns

Chapter 03: Numerical Modelling and Behavioural Laws

Chapter 04: Numerical Analysis of a 3D Unit Cell Model for Soft Soil Reinforced with Different Granular Columns

LIST OF TABLES

LIST OF ABBREVIATIONS

B	*Foundation width*
c	*Soil cohesion*
D_f	*Foundation embedment*
q	*Load*
q_u	*Ultimate bearing capacity*
q_{adm}	*Allowable bearing capacity*
D_r	*Relative density*
Q_u	*Ultimate load*
$\mathcal{S}_c$, $\mathcal{S}_q$, $\mathcal{S}_\gamma$	*Shape coefficients*
d_q, d_γ	*Depth coefficients*
I_D	*Density index*
i_β	*Bearing capacity reduction factor*
K_s	*Punching shear resistance coefficient*
i_e	*Safety factor of bearing capacity*
EA	*Normal stiffness*
EI	*Flexural stiffness*
E	*Young's modulus*
d/B	*Aspect ratio*
G_u	*Ultimate shear modulus*
G	*Shear modulus*
D_r	*Relative density*
K_0	*Coefficient of earth pressure at rest*
γ	*Soil unit weight*
δ_u	*Unit displacement*
ε	*Deformation*
τ	*Shear stress*
ν	*Poisson's ratio*
σ	*Stress*
σ_n	*Normal stresses*
φ	*Internal friction angle of the soil*
φ_u	*Ultimate friction angle*
ψ	*Dilation angle of the soil*
S	*Settlement*
TxDOT	*Texas Department of Transportation cited by (Vipulanandan)*
NTCP	*Number of the Texas Cone Penetration*
σ_z	*Principal stress*
P	*The applied load*
P_p	*The passive force*
ε_x, ε_y	*Radial deformations*
σ'_z	*Effective stress*
ΔH_i	*Final settlement*
σ'_p	*The preconsolidation pressure*

Cc	*The compression index*
Cg	*The swelling index*
OCR	*The over consolidation ratio*
Eoed	*Oedometer modulus*
Δσ'	*The range of stress*
t_s	*Settlement at time*
U	*The degree of consolidation*
τ	*The shear strength*
(UU)	*Unconsolidated Undrained test*
(CU)	*Consolidated Undrained test*
(CD)	*Consolidated Drained test*
Nγ	*Area Factor*
Nc	*Cohesion Factor*
Nq	*Depth Factor*
i_γ, i_q, i_c	*Reduction factors*
S_γ, S_q, S_c	*Shape coefficients*
UC	*Unit Cell Model*
GFRP	*Glass Fiber Reinforced Polymer*
PVD	*Prefabricated vertical drains*
(S)	*Spacing of Stone Columns*
(D)	*Diameter of Stone Columns*
(de)	*Arrangement of stone columns*
(Ac)	*The area of the stone column*
$\Delta\sigma v_{,c}$	*Vertical stress on the columns*
n.	*The stress concentration ratio*
β	*Settlement reduction factor*
S_0	*Settlement before treatment*
Hc	*Column length*
EA	*The axial stiffness*
J	*Geotextile encasement*

(LEM)	
(M-C)	*Linear Elastic Model*
(HSM)	*Criterion of Mohr-Coulomb*
(SSM)	*Hardening Soil Model*
(SSCM)	*Soft Soil Model*
(JRM)	*Soft Soil Creep Model*
(MCC)	*The Jointed Rock Model*
(HBM)	*Modified Cam-Clay Model*
(UDSM)	*Hoek-Brown Model*
(GP)	*User-defined Soil Models*
(US)	*Granular Pile*
(OSC)	*Unreinforced soil*
(SFM)	*Ordinary Stone Columns*
(RAPP)	*Sand-Fiber Mix*
	Recycled Aggregate Porous Concrete Pile

General Introduction

Granular columns are commonly used in civil engineering to mitigate settlement and enhance the bearing capacity of soft soil. This technique involves replacing a portion of weak soil (typically 10-40%) with a compacted granular material contained within cylindrical columns (Boumekik et al., 2021). Noteworthy applications of this technique encompass the stabilization of isolated and strip foundation soils, support for embankments, reconstruction of weakly cohesive soils, reduction of liquefaction potential, and acceleration of soil consolidation (Adalier & Elgamal, 2004; Castro, 2014). Settlement caused by structures and buildings poses a significant stability issue within the realm of soil mechanics, primarily due to the low stresses and high compressibility exhibited by soft soils. Ordinary Stone Columns (OSC) are specifically installed within soft soil to mitigate settlement while simultaneously enhancing both the structural and load-bearing capabilities (GREENWOOD DA, 1970; Han & Ye, 2001).

Numerous researchers have endeavored to examine the behavior of Sand-Fiber Mix (SFM) or geogrids using both numerical and experimental methods. For instance (Ambily & Gandhi, 2007; Hasanzadeh & Shooshpasha, 2017; Malarvizhi & Ilamparuthi, 2008; Murugesan & Rajagopal, 2010) conducted comprehensive parametric studies utilizing random fibers. These studies aimed to investigate the behavior of SFM and analyze the influence of fiber length, fiber depth, and fiber quantity within the sand pile on its bearing capacity. In a different study,(Kim et al., 2012) conducted both experimental and numerical analyses to explore the behavior of Recycled Aggregate Porous Concrete Pile (RAPP) as a substitute for traditional granular columns, such as compression columns, in weak soil. This innovative system entails incorporating porous concrete and recycled aggregates within the soil. Hasan and Samadhiya, (2016) and You et al (2016) provided the mechanical properties of the utilized recycled aggregates that form the basis of their study on RAPP.

Numerous theoretical and experimental studies have been conducted and published, primarily focusing on the case where the foundation is subjected to vertical loads at the center. These studies, conducted by (Gupta et al., 2022; Hanna et al., 2013; Kang et al., 2023; W. E. T, 1995), have elucidated that the ultimate bearing capacity of reinforced soils and the failure behavior of vertically loaded stone columns are contingent upon the geometric and physical properties of both the surrounding soils and stone columns. Furthermore, other investigations have

classified potential failure modes of single columns, identifying three distinct patterns: shearing failure, bulging failure, and general punching failure. Notable contributions in this regard have been made by (Debbabi et al., 2020; Mohamed, 2022; Ng, 2018).

The unit cell model has been endorsed by several authors (e.g., Indraratna et al., 2013; Miranda et al., 2015; Pulko & Majes, 2005)Its model consists of a single granular column with an infinitely equivalent circular area and it's used according to measures that simulate the presence of a column within an infinitely large group of granular columns.

Comparing the results with previous works is an essential step in validating findings and understanding their significance in the research. In the case of the present study, there are several previous works that can be used as a basis for comparison. Eg, (Kim et al., 2012) investigated the bearing capacity of recycled aggregate porous concrete piles (RAPP) compared to traditional compression columns. They found that RAPP had a higher bearing capacity than the traditional columns, which is consistent with the findings of the present study. Similarly, (Miranda & Da Costa, 2016)conducted a study on the behavior of stone columns reinforced with geotextiles. They found that the vertical bearing capacity of the columns increased with increasing geotextile stiffness, which is consistent with the findings of the present study regarding the impact of geotextiles on column stiffness. In terms of the impact of Young's modulus on the bearing capacity of granular columns, previous works have mixed results. Eg, (Ambily & Gandhi, 2007) found that the stiffness of geogrids used in stone columns had a significant impact on their bearing capacity, while (Malarvizhi & Ilamparuthi, 2008) found that the stiffness of geogrids had a more significant impact on the bearing capacity of soft clay columns. These results are consistent with the current study, which found that the effect of Young's modulus on the bearing capacity of granular columns varies with the column material. Moreover, previous studies have also investigated the impact of geotextiles on the bearing capacity of granular columns. Eg, (DİLBAS, 2021)conducted a study on the behavior of recycled aggregate concrete-filled steel tube columns reinforced with geotextiles. They found that the use of geotextiles significantly improved the bearing capacity and stiffness of the columns.

Several studies have emphasized the widespread use of natural aggregates in strengthening soft soils by granular columns (Malarvizhi & Ilamparuthi, 2008; Sexton et al., 2014), while recycled aggregates have been studied less sharply because this recyclable material is still being

researched and developed(Alabi & Mahachi, 2020; Kim et al., 2012; Petkovic et al., 2004; Zaharieva et al., 2003). For this purpose, we made this research contribution.

The study is organized as follows: firstly, the Finite Element Method (FEM) model used in this study is introduced. The validity of the proposed model is established by comparing it with experimental and numerical data from previous studies (Basu, 2009; Hasan & Samadhiya, 2016), demonstrating good agreement. The geometry and geotechnical characteristics used in the comparison studies are identical to those employed in this research. Subsequently, a comprehensive parametric study is conducted to assess the sensitivity of the desired outcomes (i.e., load-settlement results) to variations in key parameters. The study investigates the effectiveness of three different column types (OSC, SFM, and RAPP) in enhancing the response, as well as the influence of reinforcement material, friction angle, encasement stiffness, and column length. Notably, this research contribution focuses on the behavior of recycled aggregate (RAPP) as an alternative to natural aggregates and stones (OSC, SFM) in reinforced particle columns. It is worth mentioning that RAPP is a relatively new and emerging material in this field.

Chapter 01:
Bibliographical Study on Compressible Soils

Chapter 01: Bibliographical Study on Compressible Soils

1.1.Introduction

Civil engineering encounters a prevalent and considerable challenge in dealing with soft soil deposits, mainly due to their tendency to settle excessively and their low bearing capacity. These problematic soils are found across the globe with great frequency, particularly in major urban centers where land is at a premium. Building on weak soil deposits presents considerable challenges that include excess settlement and low shear strength. Being aware of the geological and geotechnical characteristics of compressible soils is an essential step towards finding effective solutions to these issues. This chapter aims to provide an insightful overview of the unique properties and challenges associated with these soils, which includes discussing the physical properties of weak soils, the factors that contribute to their formation, and the engineering techniques used to overcome their adverse effects.

Compressible soils are soils that undergo significant deformation under the influence of a load. Within this category of compressible soils are included silts, peat, and soft clays (Mahfoud, 1990). This class of soils generally exhibits the following properties:

- A predominantly clayey or organic nature,
- A high water content and low bulk density,
- Very low permeability,
- Low shear strength and high compressibility.

In these soils, the liquid phase plays a crucial role and is largely responsible for the delayed nature of the deformations they undergo under the weight of typical structures. This non-instantaneous response to external loads varies according to:

- The soil type,
- The degree of saturation,
- The rate at which the imposed load is applied.

According to the definition provided by (Ahmad et al., 2010), a soft soil is characterized as a mineral mixture consisting of hydrous aluminum, silicates, quartz, feldspars, carbonates, oxides, hydroxides, and organic materials. Additionally, soft soil is distinguished by having a shear strength below 25 kPa.

Terzaghi et al., (1996) proposed that the consistency of clay can be characterized by its shear strength Cu. They classified clay as very soft if its undrained shear strength is below 25 kPa, and as soft when the strength falls between 25 kPa and 50 kPa.

According to the Texas Department of Transportation (TxDOT) (cited by Vipulanandan, 2009), clay is considered soft when the number of blows from the Texas Cone Penetration Test is less than or equal to 20 blows for 300 mm of penetration (NTCP ≤ 20) (Table 1.1).

Table 1.1: Soil classification according to TxDOT(Vipulanandan et al., 2009)

Density(Granular)	**Consistency (Cohesive)**	**Number of Blows/300mm**	**Field Identification**
Very Loose	Very Soft	0 to 8	Core (height twice diameter) sags under own weight
Loose	Soft	8 to 20	Core can be pinched or imprinted easily with finger
Slightly Compact	Stiff	20 to 40	Core can be imprinted with considerable pressure
Compact	Very Stiff	40 to 80	Core can only be imprinted slightly with fingers
Dense	Hard	80 to 5/100 (125mm/100)	Core cannot be imprinted with fingers but can be penetrated with pencil
Very Dense	Very Hard	5/100 to 0/100 (125mm/100 to 0 mm/100)	Core cannot be penetrated with pencil

1.2. Definition of compressible soils

Compressible soils exhibit several distinct characteristics, including a composition that is primarily clayey with varying amounts of organic matter that may or may not be significant. Typically, these soils exhibit high water content and low apparent specific weight, often approaching saturation. They also have very low shear strength, and their high compressibility

leads to significant settlement even under minimal loads. Although the rate of settlement decreases over time, it may take several years for it to fully subside.

Compressible soils are typically of recent formation, dating back only a few thousand years. These soils almost always contain organic matter, which may be present in varying amounts Compressible soils are classified into several categories including: Soft clays, Silts, Peat, Vases, Loons and Marls.

1.3. Type of compressible soils

1.3.1. CLAYS

Clays are fine-grained sedimentary rocks with a particle size smaller than 5 μm, composed largely of specific minerals, usually silicates of aluminium that are more or less hydrated. They have a layered structure that explains their plasticity or a fibrous structure that accounts for their absorption qualities. Clays absorb water and form an impermeable paste (permeability less than 0.2 mm/h), commonly called clay soil, coloured by iron oxides in ochre, red, or green. Some clays, such as those in the Montmorillonite family, can swell when they absorb water and, conversely, decrease in volume due to dryness, resulting in surface cracking and even deep fissures up to 2 to 4 metres deep. In addition, under a load, such as that of a building, some of the absorbed water trapped between the clay particles is displaced, leading to significant settlement of the soil (Magnan et al., n.d.).

1.3.2. SILTS

Silts, composed of silt, loess, and limestone, have a siliceous skeleton with fine-grained siliceous limestone. Their particle size is between that of sand and clay, and their clay content varies. They are poorly permeable and constitute fertile agricultural land. However, their bearing capacity is mediocre and should therefore be avoided for foundations (Schlosser et al., 1984).

1.3.3. PEATS

Peats are natural organic deposits with high levels of organic matter, water, and saturation. They are characterized by a content of decomposed plant fibres that form an anisotropic structure, which has a significant influence on their mechanical strength. Unlike clay consolidation, peat settlement does not typically follow the conventional laws.

Assessing the preconsolidation pressure in peat soils presents a challenge, as they are commonly assumed to be normally consolidated. The consolidation phase in peats is typically short and challenging to define precisely. Moreover, secondary compression tends to be the prevailing mechanism. Oedometer tests reveal extremely high compression indices for peats, often greater than 1.

Permeability in peats generally displays a considerably higher horizontal component compared to the vertical direction. During settlement, the permeability in peats experiences a significant decrease (DEBBABI, 2021).

1.3.4. MARLS

Marls are both clayey and calcareous. Depending on their composition, there are three main categories:

- clayey marls containing 5 to 35% of calcium carbonate;
- true marls and marlylime stones, with rates ranging respectively from 35 to 65% and 65 to 95%.

Like clays, clayey marls have the disadvantage of cracking at a certain depth in cases of drought. Marls have often been exploited in open pit or underground quarries to produce lime with clayey marls, hydraulic lime with true marls, and cement with limestone or marlylime stones. They have also been used to amend agricultural land. In general, marls are a good-to-moderate foundation soil in the absence of gypsum. However, they are mediocre or even dangerous when very clayey at outcrop or when located above a mass of gypsum, with the risk of sinkhole formation. Marls are relatively soft rocks that undergo very active surface geodynamics, and their fragility makes them very vulnerable to natural and human hazards. A combination of natural and anthropogenic factors has caused intense water erosion, resulting in soil degradation and a significant decrease in productivity.

It can be concluded that the evolution of fine soils is due to the presence of clay minerals such as marls, clays, etc., which exhibit great sensitivity to air (shrinkage, cracking, progressive disintegration of soil layers) and a strong affinity for water (with the classic consequences of humidification: swelling, deconsolidation, loss of mechanical characteristics) (Schlosser et al., 1984).

1.4. Study the one-dimensional compressibility of soils through consolidation testing

In 1910, Frontar, a French researcher, pioneered the development of the first equipment specifically designed for conducting one-dimensional compression testing. In 1919, the Swedish Geotechnical Commission performed the unidimensional consolidation test using a clayey soil sample placed between two layers of sand (refer to Figure 1.1). This testing method was later adapted by (Terzaghi et al., 1996) to design the consolidometer, which is now commonly referred to as the oedometer.

1.4.1. Study hypothesis

The study of one-dimensional compressibility of soils is based on a fundamental hypothesis, which assumes that there is no horizontal deformation, as the soil is effectively confined by the surrounding soil mass. Since water and grains are considered incompressible, deformations can only occur due to the movement of grains among themselves.

The principle of the oedometer test involves applying a constant vertical total stress on a soil sample:

- $\sigma_z = P/S$ (principal stress, where P is the applied load)
- Radial deformations are zero ($\varepsilon_x = \varepsilon_y = 0$, as the walls are considered rigid)
- A drainage system allows water to evacuate from the sample in symmetrical upward and downward paths, while keeping the soil saturated.

The dissipation of pore water pressure resulting from drainage allows the soil to be subjected, after a sufficient waiting period, to an effective stress σ'_z that is equal to the applied stress σ_z. Comparators are used to measure the corresponding settlement ΔH, and thus calculate the axial deformation:

$$\varepsilon_z = \Delta H/H. \quad (1.1)$$

In practical terms, the applied load P is typically doubled every 24 hours. Due to the small thickness of the samples (to minimize lateral friction), the pore water pressures are generally dissipated, resulting in $\sigma'_z = \sigma_z$.

The study of soil compressibility through oedometer testing provides two types of curves that can determine numerous parameters related to this phenomenon:

- A compressibility curve: e - log (σ'_z) (see Figure 1.1).

- Consolidation curves: e - log (t). A curve of this type can be plotted for each value of the applied stress σ'_z, corresponding to each loading stage(Terzaghi et al., 1996) (see Figure 1.2).

1.4.2. Compressibility of compressible soils

The final settlement (typically measured 24 hours after applying the load) ΔH_i is measured for each value of σ'_z, starting from a known initial state e_0 and H_0.

Using the relationship $\Delta H_i / H_0 = \Delta e_i / (1 + e_0)$, the value of Δe_i can be calculated for all values of ΔH_i (i.e., all values of σ'_z).

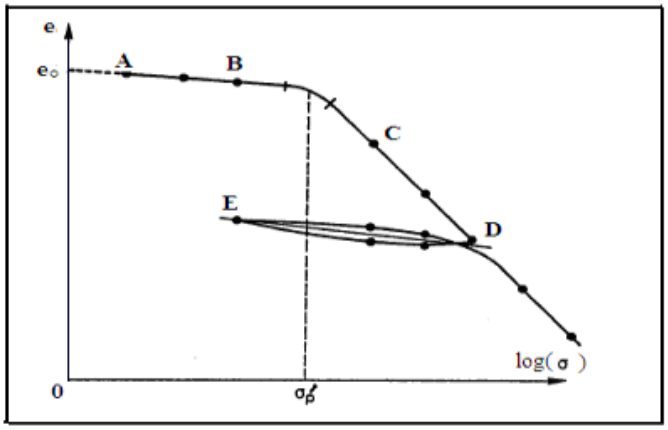

Figure 1.1: Compressibility curve

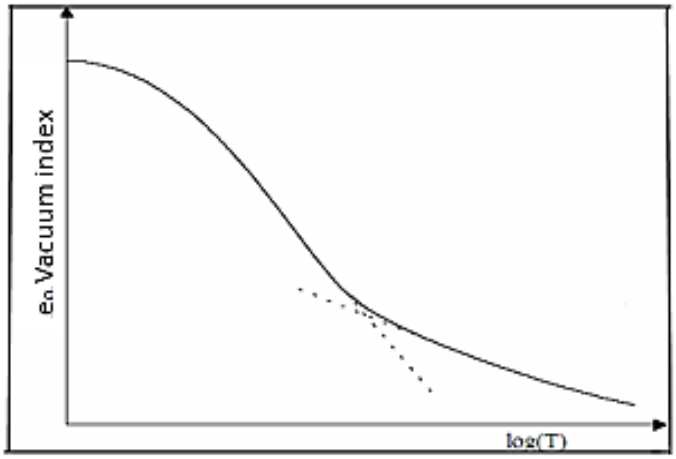

Figure 1.2: Typical consolidation curve

The compressibility curve (e - log σ'_z) is then plotted (see Figure 1.1). It consists of two straight-line segments connected by an arc. After reaching the desired maximum load (point D), a unloading-reloading cycle can be performed. The following observations can be made:

- Segments AB and ED are approximately parallel. In the AB zone (known as the recompression zone), settlements are minimal due to water presence in the sample.

- Zone BC: This is the transition zone. The stress at which transition occurs is known as the preconsolidation stress and is denoted as σ'_p. Beyond this stress, the soil exhibits high compressibility even for small variations in stress.
- Zone CD, known as the virgin compression zone, where the change in void ratio is proportional to the change in logarithm of applied effective pressure.

This curve allows us to determine three characteristics of the compressible soil being studied: the preconsolidation pressure σ'p, the compression index Cc, and the swelling index Cg (Das, 2021).

1.4.2.1. Preconsolidation pressure

The preconsolidation pressure σ'_p is an important property of a compressible soil. It represents the threshold beyond which irreversible displacements occur, indicating a transition from an elastic behavior to a plastic behavior.

The compressibility curve allows for the graphical determination of the preconsolidation pressure σ'_p:

✓ Determination of the preconsolidation stress:

The preconsolidation stress σ'_p is determined through a compressibility test using the Casagrande graphical construction on the (e-log(σ')) curve(Figure 1.3).

- Let A be the point where the curvature radius is minimal.
- Draw the horizontal line AH from point A.
- From point A, draw the tangent AT at the beginning of the virgin compression curve.
- Draw the bisector AB' of the angle HAT.
- Extend the linear portion of the virgin compression zone until it intersects the bisector AB' at point B.
- Point B corresponds to the preconsolidation stress σ'_p.

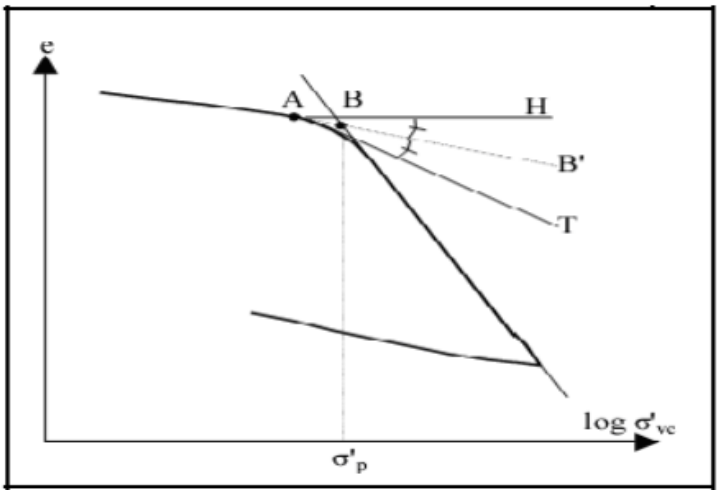

Figure 1.3: Determination of the preconsolidation stress based on the Casagrande construction.

There can be several cases depending on the relative values of σ'_p and the current effective stress due to the weight of the soil, σ'_z.

- When $\sigma'_z<\sigma'_p$, the soil undergoes very little deformation because it has already been consolidated, during its history, under a pressure that, at its maximum value, was equal to σ'_p. In this case, the soil is considered to be overconsolidated. Normally consolidated soft soils are known for their high compressibility.
- When $\sigma'_z = \sigma'_p$, the preconsolidation stress is equal to the stress due to the weight of the soil, indicating that the soil is normally consolidated.
- When $\sigma'_z>\sigma'_p$, the soil is much more deformable as it is subjected to stresses higher than any it has experienced before. This case is generally rare and not permanent. It can typically be found in soils recently deposited through geological processes or human intervention. The soil in question has not yet reached equilibrium with the weight of the soil, and the pore water pressure is higher than the hydrostatic pressure. The corresponding portion of the curve is called the virgin compression curve.

The over consolidation ratio (OCR), denoted as $OCR = \sigma'_p / \sigma'_z$, characterizes the initial over consolidated state of the soil. Its value for different soft clays (compressible soils) ranges from 1.2 to 3.0 (Das, 2021).

a - The compression index (Cc)

It's the main parameter for characterizing compressible soils. It is defined as $Cc = -\Delta e/\Delta\log(\sigma)$ (During the compression phase, the slope of the curve is greater for σ'_z than for σ'_p), and is a dimensionless number.

The values of Cc for different types of compressible soils (clays) are as follows (Table 1.2).

Table 1.2: Magnitude of compression index for different types of compressible soils (Costet et al., 1969)

Types of compressible soils (clays)	**The values of C_c**
- Kaolinites (stiff)	$0,1 < C_c < 0,25$
- Illites	$0,25 < C_c < 0,8$
-Montmorillonites (soft)	$0,8 < C_c < 2,5$

Alternatively, for sands, we can consider the following:

- Incompressible: **Cc**< 0.02
- Weakly compressible: 0.02 <**Cc**< 0.05
- Slightly compressible: 0.05 <**Cc**< 0.10
- Moderately compressible (Kaolinites): 0.10 <**Cc**< 0.20
- Fairly compressible (Montmorillonites): 0.20 <**Cc**< 0.30
- Highly compressible (Illites): 0.30 <**Cc**< 0.50
- Extremely compressible (Montmorillonites): **Cc**> 0.50

b - The swelling index (Cg):

It's defined as the average slope (with the sign) of a loading-unloading cycle. It is denoted as Cg.

It can be calculated using the equation; $Cs = \Delta e/\Delta log(\sigma)$, with Cg < Cc.

c - Oedometer Modulus (E_{oed}):

The oedometer modulus is the parameter that relates deformations to stresses in a constitutive law. In the case of oedometer loading (uniaxial deformation), it can be written as:

$\sigma' = -E_{oed}(\Delta H/H)$ where *Eoed* has the dimensions of stress. (1.2)

$E_{oed} = -\sigma'_z/(\Delta H/H) = -\Delta\sigma'(1+e)/\Delta\varepsilon = ((1+\varepsilon)/Cc)(\Delta\sigma'/\log(1+\Delta\sigma'/\sigma')) = 1/m_v$. (1.3)

For unidimensional compression, the oedometer modulus is related to the elastic modulus E by the following equation:

$E = E_{oed}(1+v)(1-2v)/(1+v)$ (1.4)

where v is usually between 0.12 and 0.35. Therefore:

E / E_{oed}=0,623 à 0,967 (1.5)

$1/m_v = -\Delta e/\Delta\sigma'(1+e)$ This is called the coefficient of volumetric compressibility. (1.6)

It is important to note that the oedometer modulus is not constant (unlike the Young's modulus of a material with linear elastic behavior). It depends on both the initial stress state considered σ' and the range of stress Δσ'.

It is evident that the oedometer modulus is not constant (unlike the Young's modulus of a material with linear elastic behavior). It depends on both the initial stress state considered σ' and the stress range Δσ' (BETEHI, 2010).

1.4.3. Consolidation of compressible soils

Consolidation is a fundamental process in civil engineering that involves the gradual compression and settlement of soils over time. This process is not instantaneous but can span several years, especially when dealing with thick compressible layers and low permeability. The study of consolidation aims to understand the variations in the height of soil samples as a function of time. Consolidation can be divided into two distinct phases: primary and secondary consolidation (Figure 1.4).

1.4.3. Primary and secondary consolidation.

In all that has been said, the variable of time has not been considered. However, the settlement phenomenon is far from being instantaneous; it can sometimes last for years if the compressible layer is thick and has low permeability. The study of settlement rate therefore presents considerable practical importance. It has already been observed, in relation to the oedometer experiment, that the permeability of the material plays a major role in this matter, as settlement is only possible in a saturated material if water can be expelled.

The evolution of settlement under constant load over time can be studied using the oedometer. Two roughly linear branches can be discerned on the representative curve of this test (settlement, logarithm of time), with their extensions intersecting at point A (Figure 1.4). The left branch BC represents what is called primary consolidation; the resistance offered to the

drainage of excess water is the sole cause of this phenomenon. This phenomenon is entirely comparable to the creep of a solid with delayed elasticity, which is interpreted in rheology using generalized Kelvin-Voigt models.

On the other hand, the right branch CD represents secondary consolidation, which is slower and seems to be the result of a progressive arrangement of the soil structure, linked to the deformations of the absorbed layers. It is a viscous flow, and settlement increases as long as the overload is applied.

Therefore, clays behave as viscoelastic materials. The study of secondary consolidation is quite challenging. In the absence of secondary consolidation, the left branch of Figure 1.4 would have had a horizontal asymptote passing approximately through point A. By definition, point A determines the primary settlement, which can be identified with the settlement calculated earlier.

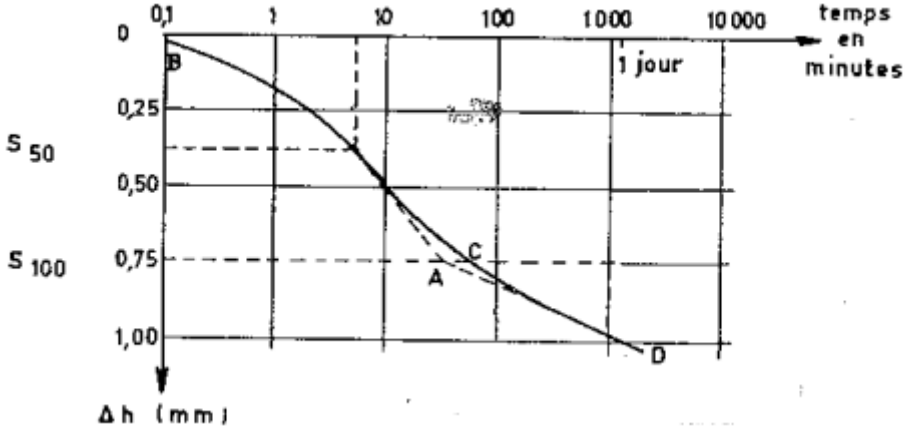

Figure 1.4: Primary and Secondary Consolidation (Costet et al., 1969).

In the following paragraphs, the particular case of one-dimensional vertical consolidation will be considered. The mechanism of primary consolidation is as follows. The application of the load system creates an additional pressure σ_c. At the moment of loading, this pressure is fully taken up by the interstitial water, which is thus subjected to an excess pressure $u = \sigma_c$. Under the action of this excess pressure, a portion of the water escapes from the compressible layer, allowing settlement. The excess pressure decreases in the water, and the difference $\sigma_c - u$ is then supported by the additional effective pressure σ in the grains, which corresponds to the observed settlement. The phenomenon continues until the interstitial water comes to rest, that is, until $u = 0$; the total pressure σ' is then fully supported by the granular skeleton, $\sigma' = \sigma_c$, and the

settlement becomes the final settlement. It should be noted that throughout this article, σ_c, σ', and u represent increases in stresses and not the actual stresses in the soil during consolidation.

Figure 1.5 shows a mechanical device with analogous behavior: the displacement of the spring under the loads is limited by the water contained in the cylinder; however, this water can only be evacuated through narrow holes drilled in the piston. The figure illustrates the evolution of the phenomenon.

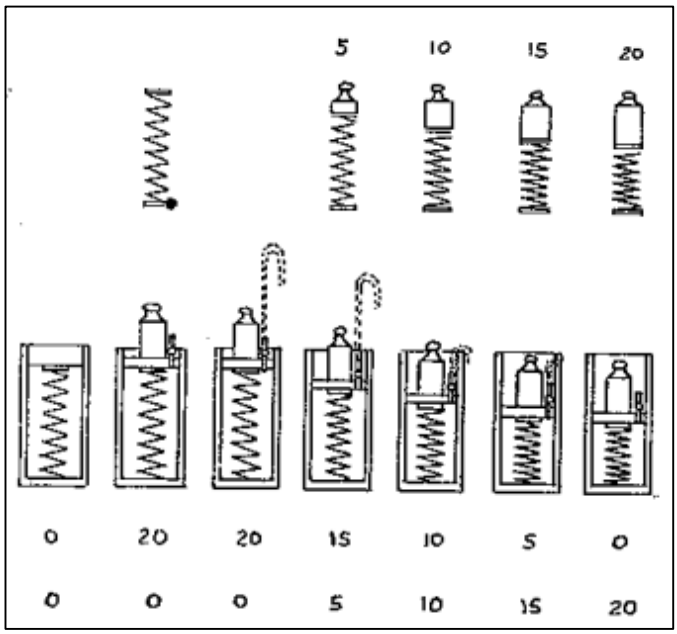

Figure 1.5: Consolidations -Mechanical analogy- (Costet et al., 1969).

Hence, settlement gradually increases as time progresses until it reaches the final settlement, which may take a prolonged duration (theoretically infinite). The degree of consolidation U is the ratio of settlement at a specific time *ts* to the final settlement *s*, and it varies as a function of time. The problem of consolidation involves determining this function.

1.4.4. Shear strength

The shear behavior of fine soils can vary depending on whether sufficient time is allowed for the dissipation of interstitial overpressures during shearing. Therefore, a distinction is made between short-term (undrained) shear strength and long-term (drained) shear strength. Additionally, the characteristics of shear strength to be considered differ depending on whether it involves new shear movements (peak strength) or reactivations of old shear movements (residual strength) (DURVILLE & SEVE, 1996). Typical values of cohesion and friction angle are presented in Table 1.3.

Table 1.3: Typical values of mechanical characteristics for selected soils (DURVILLE & SEVE, 1996).

Soil Type	r (kN/m3)	c'pic (kPa)	φ' pic (degrees)	C'r (kPa)	φ' r (degrees)	Cu (kPa)
Organic Silt	13 to 15	0 to 10	25 to 32	0	25 to 30	14 to 18
Soft Clay	15 to 19	0 to 10	28 to 34	0 to 5	10 to 15	< 25
Stiff, Non-Fissured Clay	18 to 20	10 to 40	15 to 25	0 to 5	6 to 15	80 to 200
Silt	17 to 19	0 to 40	25 to 35	0	20 to 30	40 to 50
Sand	16 to 21	0	30 to 45	0	25 to 35	
Sand and Gravel	16122	0	35 to 48	0	30 to 35	

The shear strength behavior of soils can exhibit two basic typesdepending on various factors such as soil type, stress levels, water content, and particle characteristics. The common types of shear strength behavior in soils are:

- Short-term behavior: This occurs at the beginning of loading when water supports any increase in total stresses. Deformation occurs at constant volume, and the behavior, involving both grains and water, is described by total stresses. The limit equilibrium state is reached when $\tau = cu + \sigma \tan \varphi u$.
- Long-term behavior: This occurs after primary consolidation. Water is in a hydrostatic regime, and the grains support the additional load. Deformation occurs with volume variation, and the behavioris described by effective stresses. The limit equilibrium state is reached when $\tau = c' + \sigma - u \tan \varphi'$.

Figure 1.6 provides a schematic representation of the different types of shear strength analysis for soils.

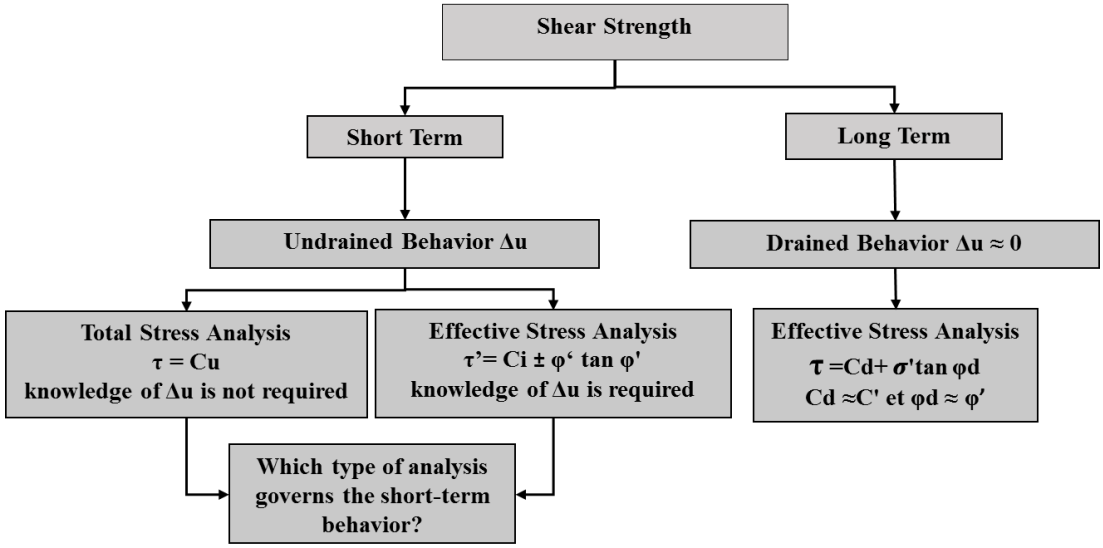

Figure 1.6: Types of geotechnical analysis (Kempfert & Gebreselassie, 2006).

According to(Schlosser et al., 1984), three types of shear tests can be conducted to determine different mechanical parameters of a soil:

1.4.4.1. Unconsolidated Undrained (UU) test:

The UU test represents the short-term behavior of the soil. It involves applying hydrostatic pressure ($\boldsymbol{\sigma 3}$) and performing shearing under closed drainage conditions. The shear strength of the soil is generally constant (φ = 0) and referred to as "Undrained cohesion" (Cu). Cu reflects the current strength of the soil and allows for the determination of immediate bearing capacity of a foundation, stability analysis of a slope, retaining wall, etc.

1.4.4.2. Consolidated Undrained (CU) test:

In the CU test, each specimen is consolidated under open drainage conditions to a specified hydrostatic pressure ($\boldsymbol{\sigma_3}$), and then sheared at constant volume under closed drainage. This test enables the study of the variation of undrained shear strength (Cc_u and φc_u) with consolidation pressure. By measuring the pore pressure during shearing, the effective characteristics (C' and φ') of saturated soils can be determined, without the need for the time-consuming consolidated-drained (CD) test, especially for less permeable soils.

1.4.4.3. Consolidated Drained (CD) test:

In the CD test, the soil specimen is first consolidated under open drainage conditions to a prescribed hydrostatic pressure ($\boldsymbol{\sigma_3}$), and subsequently sheared under the same pressure while maintaining open drainage. It is important to apply the deviator stress gradually to ensure the pore pressure remains zero throughout the test.

The CD test provides valuable insights into the effective behavior of the soil. The parameters Cd and φd obtained from this test are crucial for conducting long-term stability analyses.

1.5. An overview of the bearing capacity of a shallow foundation

The study of the bearing capacity of shallow foundations, especially when subjected to specific loading cases, is not only a topic of proven interest but also one of the most important subjects in geotechnical engineering.

Determining the bearing capacity of foundations is one of the most significant problems in soil mechanics. The allowable pressure, also known as the maximum pressure or stress that can

be applied by a structure on soil without excessive settlements and risk of soil failure, needs to be determined. Two types of elements need to be analyzed for a shallow foundation:

- The bearing capacity of the foundation, i.e., verifying that the soils (and possibly the foundation material) can effectively support the transmitted load.
- Settlement under operational loads. The determination of bearing capacity typically relies on evaluating the mechanical properties of soils, which can be measured either in a laboratory setting or in situ. Sometimes, the determination of the bearing capacity is done through loading tests, although this is very rare for shallow foundations.

The foundation does not rest on the surface of the soil; typically, it is placed at a depth D after excavation. The base of the footing is then chosen as the reference plane where compression stresses equal to Q_u/B act at the location of the footing, and $q_s = \gamma D$ outside.

This new diagram summarizes the equivalent problem that replaces the actual case in order to solve foundation problems (Figure 1.7).

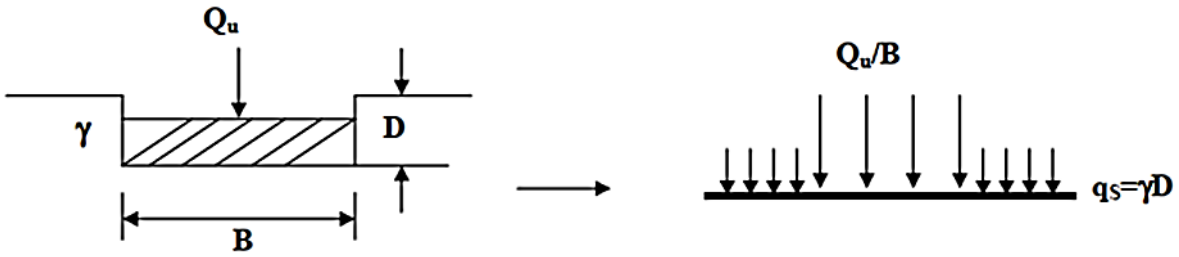

Figure 1.7: Equivalent Problem (Benmoussa, 2006).

1.5.1. Definition of bearing capacity

In the field of civil engineering, the bearing capacity of a foundation refers to its ability to support an increasing load without experiencing excessive deformations or structural failures. Initially, when the applied load is small, the soil behavior is essentially linear, meaning that vertical displacements increase proportionally with the load.

However, as the load increases and reaches a critical value known as the limit load (Q_d), the soil deformations become non-proportional to the load. Finally, when the load reaches a maximum value called the ultimate load (Q_L), the displacements become uncontrollable, indicating that the soil is no longer capable of supporting any additional load (Figure 1.8).

It should be noted that the bearing capacity of a shallow foundation varies with the increase in the applied load, as indicated by R. Frank in his research (Frank et al., 1999).

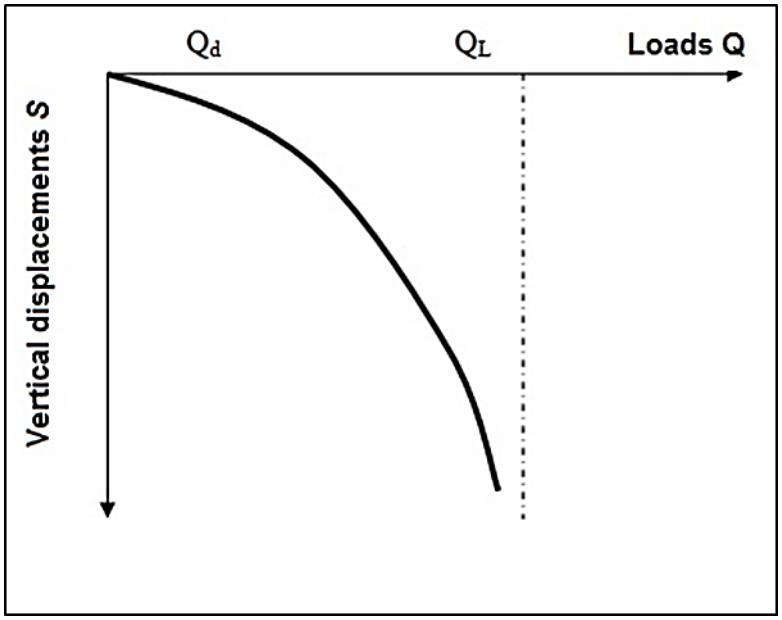

Figure 1.8: Load-Displacement Curve

1.5.2. Methods for calculating bearing capacity for vertical loading

To date, there is no rigorous mathematical solution that allows for the analysis of the soil failure phenomenon. Numerous methods have been proposed, but all involve certain simplifying approximations regarding soil properties and the displacements that occur, approximations that do not fully correspond to observed phenomena.

Despite these limitations, comparisons between the ultimate bearing capacities of small-scale models and large-scale foundations show that the margin of error is slightly larger than for stability problems in other materials (Rima, 2012).

Stability studies at failure, often referred to as total shear, are based on the assumption that the soil behaves as an ideal plastic material. This assumption was first put forward by Prandtl regarding the deformation of metals and was later applied to the study of soils by Terzaghi, Meyerhof, Buisman, Caquot & Kérisel, and De Beer &Vesic...

Their general approach to the problem is as follows: an infinitely long and B-width foundation exerts an average pressure q_u on a homogeneous soil with a specific weight of γ. The load acting on the foundation is vertical, constant, and exerted in the axis of the footing. Thus, we are confronted with a two-dimensional problem.

1.5.2.1. Rankine's Theory (Rankine's Wedge) :

The principle of Rankine's method in 1856 is to calculate the thrust and bearing forces based on an approximation of the stress state in the soil at the contact with a retaining wall. If F is the stress exerted by the soil on the retaining wall, the thrust or bearing force per unit length of the retaining wall can be expressed as:

$$\vec{F} = \int \vec{f}.dz \tag{1.7}$$

Figure (1.9) depicts a footing with a high length-to-width ratio (L/B) and an embedment depth D, resting on a soil with cohesion C and an angle of friction φ.

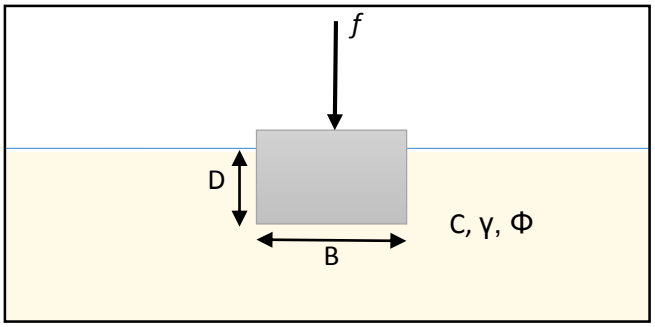

Figure 1.9: Footing Resting on a Soil (c.φ).

For Rankine, the problem is reduced to studying the equilibrium beneath the end of the foundation, between an active wedge under the half sole and a passive wedge on the outside (*a* and *b* in Figure 1.10) (BENMOUSSA., 2013).

Figure (1.10.b) represents the Rankine wedges used in this analysis.

- Wedge I is an active wedge.
- Wedge II is a passive wedge.

The horizontal or lateral resistances acting on the interface of the two wedges are denoted by "P" and are characterized by equal magnitudes but opposite directions.

However, the force P associated with wedge *a* represents the active pressure, while the force P of wedge *b* represents the passive pressure.

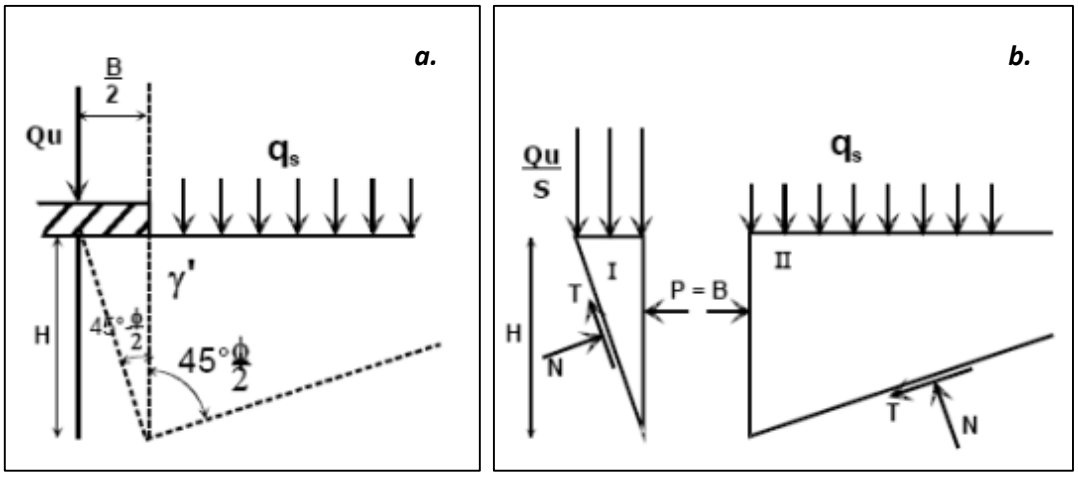

Figure 1.10: Rankine Equilibrium (Rankine, 1857).

- For the passive case (wedge *a*), we have:

$$P = \frac{1}{2}\gamma.K_P.H^2 + 2.C.H\sqrt{K_P} + q.K_P.H \tag{1.8}$$

Therefore,

$$K_P = \tan^2\left(45 + \frac{\varphi}{2}\right) \tag{1.9}$$

- For the active case(wedge *b*), we have:

$$P = \frac{1}{2}\gamma.K_a.H^2 + 2.C.H\sqrt{K_a} + q_u.K_a.H \tag{1.10}$$

Therefore,

$$K_a = \tan^2\left(45 - \frac{\varphi}{2}\right) \tag{1.11}$$

Assuming that both resultant forces have the same magnitude, we can write:

$$P = \frac{1}{2}\gamma.K_P.H^2 + 2.C.H\sqrt{K_P} + q.K_P.H = P = \frac{1}{2}\gamma.K_a.H^2 + 2.C.H\sqrt{K_a} + q_u.K_a.H \tag{1.12}$$

The expression that gives the maximum load that the footing can support is:

$$q_u = \frac{1}{2}\gamma.H.\left(\frac{1}{K_a}\right).\left(K_a - k_P\right) + \frac{2.C}{K_a}.\left(\sqrt{K_P} + \sqrt{K_a}\right) + q.K_P^2 \tag{1.13}$$

However,

$$K_P = \frac{1}{K_a} \tag{1.14}$$

then according to Figure (1.10):

$$H = \frac{B}{2\tan\left(45 - \frac{\varphi}{2}\right)} = \frac{B}{2\sqrt{K_a}} \tag{1.15}$$

So, the expression for q_u becomes:

$$q_u = \frac{1}{4}\gamma.B.K_P^{3/2}.\left(K_P - K_P^{-1}\right) + 2.C.K_P.\left(K_P^{1/2} + K_P^{-1/2}\right) + q.K_P^2 \tag{1.16}$$

Or alternatively:

$$q_u = \frac{1}{4}\gamma.B.\left(K_P^{5/2} - K_P^{1/2}\right) + 2.C.\left(K_P^{3/2} + K_P^{1/2}\right) + q.K_P^2 \tag{1.17}$$

Which can be written in a condensed form as:

The bearing capacity:

$$q_U = C.N_C + q.N_q + \frac{1}{2}\gamma.B.N_\gamma \tag{1.18}$$

With;

$$N_\gamma = \frac{1}{2}\left(K_P^{5/2} - K_P^{1/2}\right), \quad N_C = 2\left(K_P^{3/2} + K_P^{1/2}\right), \quad N_q = K_P^2 \tag{1.19}$$

Where:

The Rankine theory is just a very rough approximation of the actual behavior of soil. In reality, experiments on scaled models show that beneath the foundation, a wedge is formed, limited by inclined planar forces that penetrate with the footing and behave as a solid body. It exerts a thrust on the adjacent soil, which reacts with friction between soil-to-soil contacts.

1.5.2.2. Prandtl Theory

According to Prandtl, the failure mechanism beneath the foundation assumes that the foundation base is smooth, thus an active state of Rankineis developed in the AA'O corner (Figure 1.11).

The system is formed by three successive zones.

- Zone I in Rankine active earth pressure equilibrium.
- Zone II in Prandtl equilibrium.
- Zone III in Rankine passive earth pressure equilibrium.

In Zones I and III, the sliding line family consists of straight lines.

In Zone II, one sliding line family is formed by curves. These are sliding lines belonging to the same family that are homothetic to each other and form logarithmic spirals. The other sliding line family consists of straight lines, making an angle of φ with the normal at the intersection points with the spirals, and all having a change of direction point at the intersection of the two surcharges.

It should be noted that the logarithmic spirals can be expressed in polar coordinates as:

$$\left(r = r\ .e^{\theta tan\varphi}\right)$$

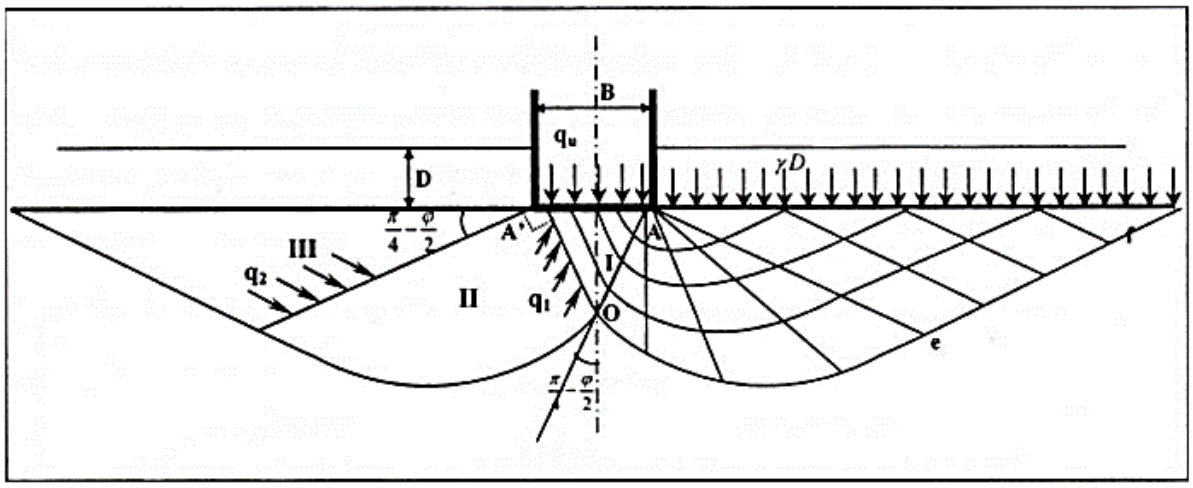

Figure 1.11: Failure mechanism of a foundation with a smooth base (Prandtl, 1921).

The problem is reduced to studying the equilibrium of the block (AO_e) by stating that the moment at A of the sum of forces is zero. The two-dimensional problem of a weightless granular soil with internal friction angle φ and loaded normally on its surface by two uniform distributions, was first solved by (Prandtl, 1921).

Let q_1 and q_2 be the intensities of the critical stresses acting respectively on the polar radii AO and A_e. The equilibrium of Rankine active and passive earth pressure in a weightless medium is given by:

$$q_1 = q_u.\tan\left(\frac{\pi}{4}-\frac{\varphi}{2}\right) \text{ and } q_2 = \gamma.D.\tan\left(\frac{\pi}{4}+\frac{\varphi}{2}\right) \quad (1.20)$$

We can translate the equilibrium of the block AO_e by stating that the moment at A of the sum of applied forces is zero.

$$\frac{AO}{2}.AO.q_1.\tan\varphi - \frac{Ae}{2}.Ae.q_2.\tan\varphi = 0 \text{ and } \frac{AO}{Ae} = e^{-\varepsilon\tan\varphi} \quad (1.21)$$

Therefore, q_1 and $q_2$are related by the following equation in Prandtl's equilibrium:

$$\frac{q1}{q2} = \left(\frac{AO}{Ae}\right)^2 = e^{-2\varepsilon.\tan\varphi} = e^{-\pi.\tan\varphi} \quad (1.22)$$

Since the angle ε formed by AO and Ae is equal to π/2.

We ultimately obtain the following equation:

$$q_u = \gamma.D.\tan^2\left(\frac{\pi}{4}+\frac{\varphi}{2}\right).e^{\pi.\tan\varphi} \quad (1.23)$$

That is to say,

$$N_q = \tan^2\left(\frac{\pi}{4}+\frac{\varphi}{2}\right).e^{\pi.\tan\varphi} \quad (1.24)$$

This formula is sometimes referred to as the Prandtl-Caquot formula, as both authors independently published it around 1920.

1.5.2.3. Terzaghi's Theory

a. Terzaghi's Assumption

Based on the theory of ultimate bearing capacity for a shallow foundation (rigid, continuous, and with a rough base) supported by a homogeneous soil of sufficient depth, (Terzaghi, 1943b)defines the geometric parameters of the shallow foundation as follows:

$B \le D_f$(B: Width of the footing, D_f: Depth of embedment).

The failure surface in the soil caused by the ultimate load (q_u); the failure surface of the soil beneath the foundation can be divided into three main zones (Figure 1.12). These are:

Zone 1 'abc': A rigid punch is formed under the base of the footing, which sinks into the soil by displacing it on either side up to the surface. The inclination of faces ac and bc with the horizontal is the angle $\alpha = \varphi$ (soil friction angle);

Zone 2 'bcf': The soil in these parts is completely plasticized and is displaced towards the surface. Significant displacements and shear: generalized failure (referred to as Prandtl's radial shear zone);

Zone 3 'bfg': The external zone is only subjected to much lower stresses that do not cause failure (this is the passive Zone 3 of Rankine). The inclined lines in this zone make an angle of $\pm (45-\varphi/2)$ with the horizontal. It should be noted that the radial shear zone '2' and the passive Rankine zone '3' also exist to the left of the elastic triangle zone abc, but they are not shown. The line cf is a logarithmic spiral arc defined by the equation $\left(r = r_0 .e^{\theta \tan\varphi}\right)$.

The lines bf and fg are straight lines. In principle, the line *fg* continues to the surface of the soil, but Terzaghi assumed that the soil above the level of the footing base is replaced by a surcharge equal to γD_f.

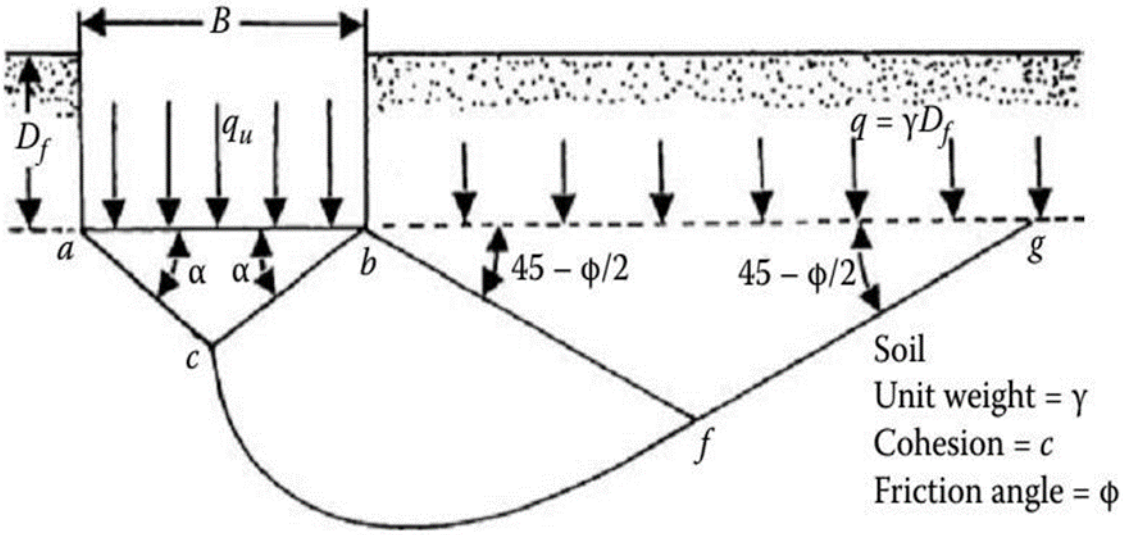

Figure 1.12: Soil failure surface under ultimate load of a rigid strip footing according to Terzaghi, (Das, 2021).

The shear stress that can be mobilized by the soil is given by:

$$\tau = \sigma' \tan\varphi + c \tag{1.25}$$

Where σ' represents the effective normal stress and *c* denotes the cohesion. The ultimate bearing capacity of the foundation, q_u, can be assessed by analyzing the faces ac and *bc* of the triangle *abc* and evaluating the passive forces acting on each face, leading to failure.

It is important to highlight that the passive force P_p is influenced by various factors, including the surcharge $q = \gamma.D_f$, cohesion *c*, unit weight γ, and internal friction angle *φ* of the soil.

In accordance with Figure 1.13, the passive force P_p acting on the face *bc* per unit length of the foundation can be expressed as:

$$P_p = P_{pq} + P_{pc} + P_{p\gamma} \tag{1.26}$$

Where P_{pq}, P_{pc}, and $P_{p\gamma}$ are the components of the passive force due to q, c, and γ respectively.

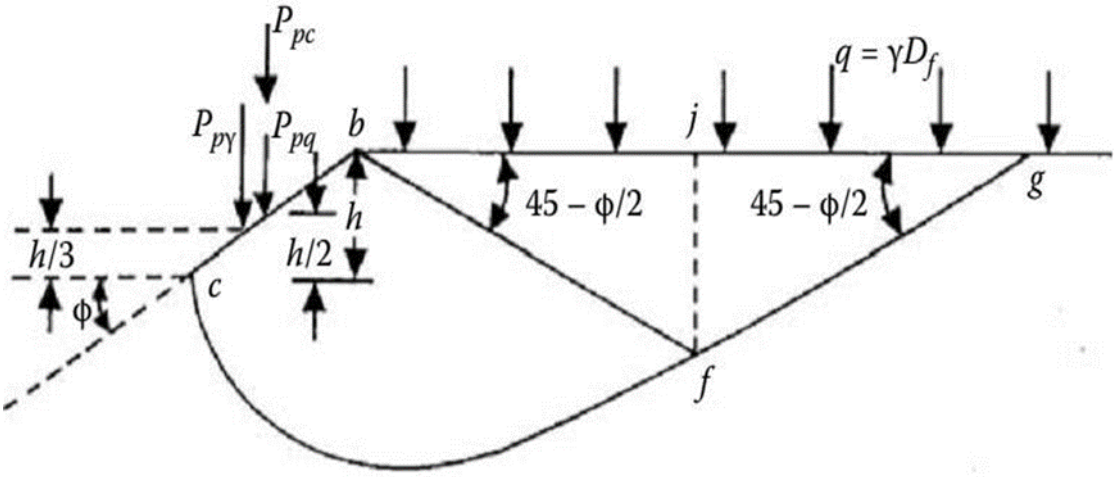

Figure 1.13: Passive forces acting on the face *bc* of the triangle *abc* (Das, 2017).

It is crucial to acknowledge that P_{pq}, P_{pc}, and $P_{p\gamma}$act in the vertical direction, and as the face *bc* is inclined at an angle φ to the horizontal, P_{pq}, P_{pc}, and $P_{p\gamma}$ will also have an angle *φ* with the normal to *bc*. To determine the values of P_{pq}, P_{pc}, and $P_{p\gamma}$, the method of superposition can be employed; however, it should be noted that this method is not an exact solution.

Thus, it has been demonstrated that:

$$q_q(B \times 1) = 2Ppq \tag{1.27}$$

$$q_q = \frac{2P_{pq}}{B} = q\left[\frac{e^{2\left(\frac{2\pi}{4}-\frac{\varphi}{2}\right)tan\varphi}}{2cos^2\left(45+\frac{\varphi}{2}\right)}\right] = qN_q \tag{1.28}$$

Similarly, the expressions for q_c and q_γ terms have been demonstrated:

$$q_c = c.\cot\varphi\left[\frac{e^{2\left(\frac{2\pi}{4}-\frac{\varphi}{2}\right)tan\varphi}}{2cos^2\left(45+\frac{\varphi}{2}\right)}-1\right] = cN_c = c.\cot\varphi(N_q-1) \quad (1.29)$$

$$q_\gamma = \frac{1}{B}\left[\frac{1}{4}\gamma B^2 K_{P\gamma}\tan^2\varphi - \frac{B^2}{4}\gamma\tan\varphi\right] = \frac{1}{2}\gamma B\left(\frac{1}{2}K_{P\gamma}\tan^2\varphi - \frac{\tan\varphi}{4}\right) = \frac{1}{2}\gamma B N_\gamma \quad (1.30)$$

Where $K_{p\gamma}$ is the coefficient of passive earth pressure.

The ultimate bearing capacity per unit area of the foundation (i.e., the ultimate bearing capacity q_u) can be expressed as follows for a soil with cohesion c and unit weight γ:

$$q_u = q_c + q_q + q_\gamma \quad (1.31)$$

Through the substitution of the previously derived equations for q_q, qc, and q_γ, the expression for the bearing capacity can be obtained. The equation consists of three terms, each associated with distinct factors. The first term corresponds to the soil cohesion, while the second term is influenced by the footing depth and surcharge pressure. The third term is influenced by the footing width and the length of the shear stress zone. The bearing capacity factors, N_c, N_q, and N_γ, are solely influenced by the internal friction angle, φ. This solution was derived by Terzaghi utilizing the method of limit equilibrium.

The general expression for bearing capacity was written by (Terzaghi, 1943a)in the following form:

• Strip footing:

$$q_u = c\,N_c + q\,N_q + 0.5\gamma B\,N_\gamma \quad (1.32)$$

• Square footing:

$$q_u = 1.3\,c\,N_c + \gamma\,D\,N_q + 0.4\,\gamma\,B\,N_\gamma \quad (1.33)$$

• Circular footing:

$$q_u = 1.3\,c\,N_c + \gamma\,D\,N_q + 0.3\,\gamma\,B\,N_\gamma \quad (1.34)$$

The following expressions are for the three bearing capacity factors:

$$N_c = cot\varphi(N_q - 1) \tag{1.35}$$

$$N_q = \frac{(e^{2\left(\frac{3\pi}{4}-\frac{\varphi}{2}\right)tan\ \varphi})}{2cos^2(45 + \frac{\varphi}{2})} \tag{1.36}$$

$$N_\gamma = \frac{1}{2}K_{p\gamma}tan^2\varphi - \frac{tan\varphi}{2} \tag{1.37}$$

The values of the factors are presented in Table 2.1, with the values of N_γ obtained from (Das, 2021).

Table 1.4: Bearing capacity factors according to Terzaghi (Das, 2021).

φ	N_c	N_q	N_γ	φ	N_c	N_q	N_γ
0	5.70	1.00	0.00	26	27.09	14.21	11.35
2	6.30	1.22	0.18	28	31.61	17.81	15.15
4	6.97	1.49	0.38	30	37.16	22.46	19.73
6	7.73	1.81	0.62	32	44.04	28.52	27.49
8	8.60	2.21	0.91	34	52.64	36.51	36.96
10	9.61	2.69	1.25	36	63.53	47.16	51.70
12	10.76	3.29	1.70	38	77.50	61.55	73.47
14	12.11	4.02	2.23	40	95.67	81.27	100.3 9
16	13.68	4.92	2.94	42	119.67	108.75	165.69
18	15.52	6.04	3.87	44	151.95	147.74	248.29
20	11.69	7.44	4.97	46	196.22	204.20	426.96
22	20.27	9.19	6.91	48	258.29	287.86	742.61
24	23.36	11.40	8.85	50	347.52	415.16	1153.15

b. General formula for the ultimate load:

Terzaghi hypothesized that the maximum load that could be applied to a foundation on the surface of a soil could be approximately considered as the resultant of the maximum loads (the

principle of superposition of an ultimate load of the foundation) (Guetari, 2019). See Figure 1.14 which consists of superimposing the following three states:

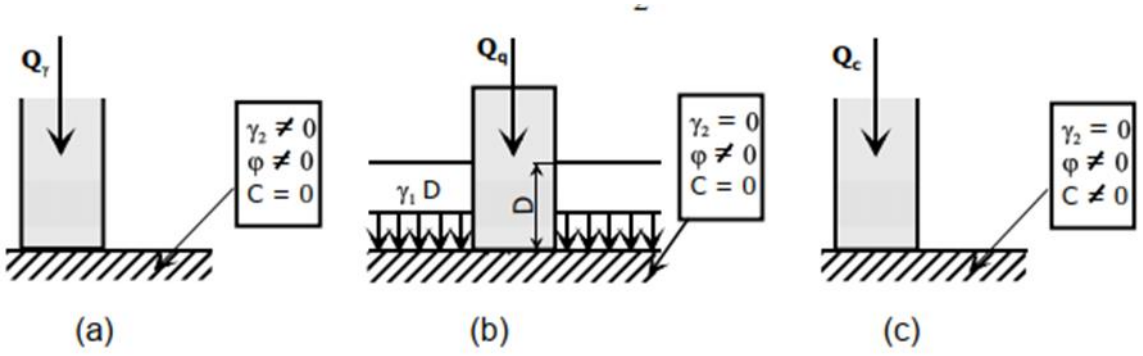

Figure 1.14: Superposition principle.

c: cohesion of the soil.

γ: unit weight.

D and B are respectively the depth and width of the foundation.

N_c, N_q, and N_γ: bearing capacity factors depend on the friction angle (φ).

- The first term is called the cohesion term (proportional to c).
- The second term is called the depth term (proportional to D).
- The third term is called the surface term (proportional to B).

Many authors have solved the problem by making different assumptions on the roughness of the footing and the shape of the zone at the ultimate limit state. Although the numerical values may sometimes differ significantly, all these studies lead to Terzaghi's general formula.

Thus, the bearing capacity problem reduces to determine the factors affecting the bearing capacity N_c, N_q, and N_γ. After proposing this approach, various studies have been conducted to evaluate these factors.

1.5.2.4. Meyerhof's Theory

In 1951, Meyerhof proposed a supplementary theory for determining the bearing capacity of rough, shallow, and deep foundations. Figure 1.15 illustrates the assumed rupture surface at the ultimate load for a continuous shallow foundation, as described by (G. Meyerhof, 1963). The figure depicts an elastic triangular zone labeled as *abc*, a zone of radial shear labeled as *bcd*, with cd forming an arc of a logarithmic spiral, and a mixed shear zone labeled as *bde*, where

the shear varies between radial and planar shear, depending on the depth and roughness of the footing. The plane be is referred to as the equivalent free surface, with normal and shear stresses denoted as P_o and S_o, respectively. In addition, (G. G. Meyerhof, 1951) utilized the general formula prescribed by (Terzaghi, 1943a) to calculate the bearing capacity. The expressions established by Prandtl Reissner were employed to determine the N_c and N_q factors. However, an approximate formula proposed by Meyerhof himself was employed for calculating the N_γ factor.

The superposition method was utilized to determine the ultimate bearing capacity *q* of a continuous footing, which considered the contribution of cohesion *c*, P_o, *γ*, and *φ*, and can be expressed as follows:

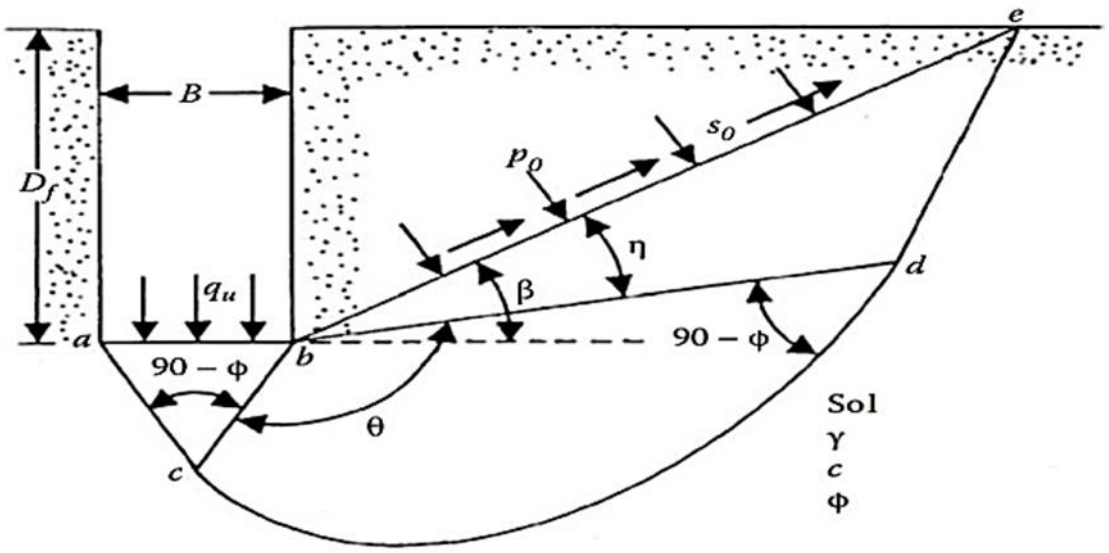

Figure 1.15 : The slip lines for a rough shallow foundation, according to (G. G. Meyerhof, 1951).

$$q_u = c\left[(N_q - 1)\cot\varphi\right] + q\left[e^{\pi\tan\varphi}.tan^2\left(\frac{\pi}{4} - \frac{\varphi}{2}\right)\right] + \gamma B\left[\left(N_q - 1\right)\tan\varphi(1.4\varphi)\right] \tag{1.38}$$

$$\begin{aligned} N_c &= (N_q - 1)\cot\varphi \\ N_q &= tan^2(\frac{\pi}{4} - \frac{\varphi}{2}) \\ N_\gamma &= \left(N_q - 1\right)\tan(1.4\varphi) \end{aligned} \tag{1.39}$$

For circular and rectangular footings with sides *B* and *L*, partial factors have been proposed, initiated by (Skempton, 1951) for clay soils, by interpolation between the case of strip footings and circular footings:

$$S_c = 1 + 0.2\frac{B}{L}\tan^2\left(\frac{\pi}{4} + \frac{\varphi}{2}\right)$$

(1.40)

$$S_\gamma = S_q = 1 \text{ si } \varphi = 0 \tag{1.41}$$

$$S_\gamma = S_q = 1 + 0.1\frac{B}{L}\tan^2\left(\frac{\pi}{4} + \frac{\varphi}{2}\right) \text{ si } \varphi \succ 10^\circ \tag{1.42}$$

For rectangular foundations, an interpolation is also proposed to correct the value of the internal friction angle, which is 10% higher in plane strain failures (φ_p) than in triaxial tests (φ_t):

$$\varphi = \varphi_p = \left(1.1 - 0.1\frac{B}{L}\right).\varphi_t \tag{1.43}$$

If there is water in the soil or if the soil is not homogeneous, it is recommended to use average values of the buoyant unit weight (underwater) and non-buoyant unit weight (in the absence of water), cohesion c, and internal friction angle φ_t:

- Up to two times B below the base of strip footings,
- Up to one times B below the base of circular and square footings.

To take into account the soil resistance above the foundation base, other partial factors are used.

$$d_c = 1 + 0.2\frac{D}{B}\tan^2\left(\frac{\pi}{4} + \frac{\varphi}{2}\right) \tag{1.44}$$

$$\boldsymbol{d_\gamma = d_q = 1} \quad \text{si} \quad \varphi = 0 \tag{1.45}$$

$$d_\gamma = d_q \text{ si } \varphi \succ 10^\circ \tag{1.46}$$

Meyerhof also indicates that, for eccentric loads, the practice is to calculate the bearing capacity on a reduced width B' strip footing:

$$B' = B - 2e \tag{1.47}$$

For inclined loads, the works of (Gg. Meyerhof, 1953; Schultze & Schwick, 1952)have defined reduction factors equal to:

$$i_\gamma = \left(1 - \frac{\delta}{\varphi}\right)^2$$
$$i_q = \left(1 - \frac{\delta}{90}\right)^2 \quad (1.48)$$
$$i_c = \left(1 - \frac{\delta}{90}\right)^2$$

In the general case, the formula for calculating the soil bearing capacity takes the form:

$$q_{\max} = c.S_c.d_c.i_c.N_c + q.S_q.d_q.i_q.N_q + \frac{1}{2}\gamma B.S_\gamma.d_\gamma.i_\gamma.N_\gamma \quad (1.49)$$

Meyerhof draws the reader's attention to the link between resistance and displacement: under inclined and eccentric loads, a shallow foundation can horizontally move from 5 to 20% of the foundation width and rotate from 1 to 5 degrees, depending on the soil density or stiffness and the foundation embedment depth.

These displacements are necessary to mobilize the soil resistance and can have a significant influence on the structures it supports. To limit foundation displacements, they need to be widened or embedded more deeply.

On the other hand, if the foundation's stiffness is low compared to that of the soil, a different approach needs to be used, for example, with reaction coefficients.

1.5.2.5. Hansen's Method

(Hansen, 1970)summarizes his recommendations for calculating the bearing capacity of shallow foundations following the general framework introduced by Terzaghi, except that the width of the foundation is taken as B instead of 2B. The three factors adopted by (Hansen, 1970)are as follows:

$$N_c = (N_q - 1)\cot\varphi$$
$$N_q = e^{\pi\tan\varphi}.\tan^2\left(\frac{\pi}{4} + \frac{\varphi}{2}\right) \quad (1.50)$$
$$N_\gamma = 1.5(N_q - 1)\tan\varphi$$

The results of the empirical formula for N_γ (equations 1.50, 1.51) are in good agreement with the values calculated by (Lundgrenand Mortensen, 1953)using the failure mechanism presented in Figure 1.16. The superposition of the three terms N_γ, N_q, and N_c leads to an underestimation

of the foundation bearing capacity, which generally remains below 20% of Lundgren and Mortensen's values. Furthermore, in 1961, Hansen proposed a different expression for N_γ:

$$N_\gamma = 1.8(N_q - 1)tan\varphi \quad (1.51)$$

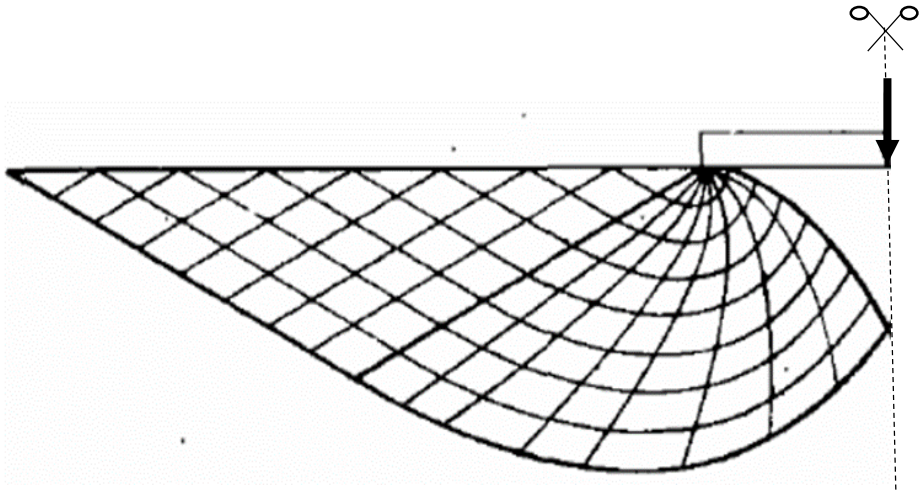

Figure 1.16: Rupture mechanism for the calculation of N_γ according to (Lundgrenand Mortensen, 1953).

1.5.2.6. Vesić's Method:

(Vesic, 1974) presents the development of the analysis of bearing capacity of shallow foundations. He recalls that the history of early works on the subject began with Rankine in 1857 and was described in Terzaghi's first treatise on soil mechanics (1925).

Vesić describes the calculation method by superposition of bearing capacity with the Prandtl and Reissner factors N_c and N_q. For N_γ, he indicates that the tabulated solution of (Caquot & Kérisel, 1948) can be represented with less than 10% error over the range $15 < \varphi < 45$ degrees (less than 5% error between 20 and 40 degrees) by the expression:

$$N_\gamma = 2(N_q - 1)tan\varphi \quad (1.52)$$

The superposition of the three bearing capacity terms gives a approximate estimation by default (from 17 to 10% at most for $\varphi = 30$ to 40 degrees), but it is exact for $\varphi = 0$ degrees. The author indicates that choosing a friction angle in plane strain is not necessarily the best solution to improve the accuracy of the calculated bearing capacity. Considering the progressive failure of

the soil under various stress levels seems to be a more promising approach. For the corrective coefficients applied to each term of equation (2.8), Vesić provides the following expressions:

- **Shape coefficients:**

$$S_c = 1 + \frac{B}{L}.\frac{N_q}{N_c} = 1 + \frac{B}{L}.\frac{N_q}{N_c - 1}.\tan\varphi$$
$$S_q = 1 + \frac{B}{L}\tan\varphi \qquad (1.53)$$
$$S_\gamma = 1 + 0.4\frac{B}{L}$$

- **Depth coefficients (for D/B ≤ 1, according to(Hansen, 1970):**

$$d_q = 1 + \frac{2D}{B}.\tan\varphi(1 - \sin\varphi)^2 \qquad (1.54)$$
$$d_\gamma = 1$$

The effect of soil compressibility and foundation size is then extensively discussed. The decrease in soil strength as the size of the foundation increases appears to be caused by three factors:

- the Mohr circles envelope is not a straight line;
- failure develops progressively along the failure surface;
- there are zones of lower strength in all natural soils.

This decrease is primarily due to the term. Equations are proposed to account for this.

1.6. Conclusion

In this chapter, we delve into a comprehensive bibliographical study on compressible soils, a crucial topic in the field of civil engineering. Compressible soils refer to those that undergo significant changes in volume and density under applied loads or changes in moisture content. Understanding the behavior and characteristics of compressible soils is essential for designing and constructing stable foundations and structures.

This study aims to provide a thorough analysis of the various aspects related to compressible soils, such as their definition, types, one-dimensional compressibility, consolidation, shear strength, and bearing capacity of shallow foundations. By examining the existing literature and

research findings, we aim to enhance our understanding of the behavior and properties of compressible soils, This enables us to make important decisions in determining how to reinforce them. The main focus of the discussion was the significance of the bearing capacity of shallow foundations as a critical criterion in geotechnical engineering. The study conducted in this thesis is based on analyzing the variations in output obtained from bearing capacity curves.

Chapter 02:

Ground Improvement Technique for Soft Soils Using stone Columns

Chapter 02: Ground Improvement Technique for Soft Soils Using stone Columns

2.1. Introduction

Soil reinforcement through stone columns is a common technique used for its simplicity in construction and its effectiveness in improving the load-bearing capacity of soft soils while reducing settlements. Additionally, this technique has drainage capabilities and can reduce the risk of soil liquefaction. In cases where the soil is extremely soft, it may be necessary to confine the columns within geogrids to ensure the required performance of the columns.

The stone column technique involves creating a cylindrical opening in soft soil and filling it with granular material. The technique replaces a certain percentage of soft soil with granular material that has better resistance and rigidity properties than natural soil.

The following is a literature review on the main technical and mechanical characteristics of soil reinforcement through a group of stone columns supporting a surface foundation. The review primarily covers common techniques for installing columns and the behavior of stone columns (isolated or grouped) under vertical loading, including the different properties of column granular material, soft soil, and confinement geosynthetics.

2.2. Application areas of soil improvement techniques:

Soil improvement techniques are an essential aspect of geotechnical engineering. These techniques aim to modify the properties of soil to make it more suitable for different projects and to enhance the performance of structures built on it. This section specifically focuses on the application areas of soil improvement techniques, including methods for improving soft soil and reinforcing compressible soil using geosynthetic materials and stone columns. Soft soil is characterised by its low bearing capacity, which makes it a significant challenge for geotechnical engineers. Therefore, different techniques have been developed to improve the properties of soft soil, including soil nailing, prefabricated vertical drains, compaction grouting, columns of lime-cement-treated soils, and dynamic compaction. Similarly, compressible soil reinforcement is an essential technique for stabilising soil and enhancing the stability of built structures. In this part, we discuss the practical applications of these techniques and their benefits in terms of effectiveness, cost, and environmental impact. The following section will discuss various Techniques for improving soft soil:

2.2.1. Soil nailing:

Soil nailing is a soil reinforcement technique that involves the installation of steel reinforcement bars or fibers, known as soil nails, into the soil at a specific spacing and depth. The soil nails are usually installed at an angle between 10 and 30 degrees to the horizontal and are grouted into the surrounding soil to create a solid shear-resistant bond between the soil and the nail.

Soil nailing is typically used in sloped excavations, retaining walls, and tunnels to stabilize and reinforce the soil. The technique can also be used to improve the load-bearing capacity of the soil and reduce lateral movement. Soil nailing is often used in areas where space is limited or where conventional stabilization techniques are not feasible.

The installation of soil nails involves several steps. First, a drilling machine is used to create a hole in the soil at a specific angle and depth. Then, a steel bar or fiber is inserted into the hole and grouted with a cementitious grout. Multiple soil nails are installed in a grid pattern to create a reinforced soil mass that can withstand the applied loads (Figure 2.1).

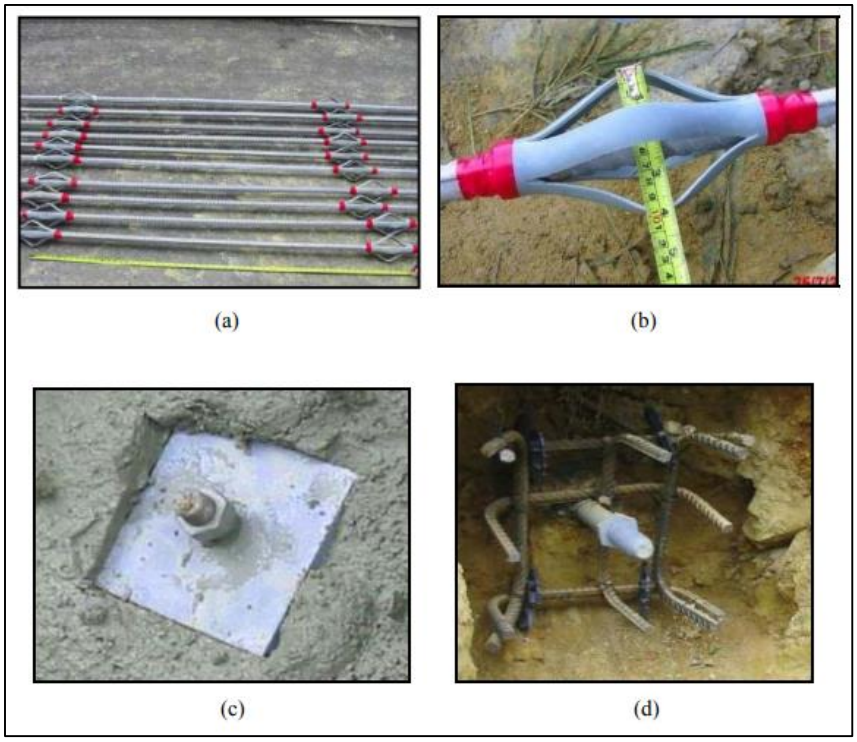

Figure 2.1: Various elements of soil nailing (Yeung, 2008), **a.** Soil nail reinforcement Bars, **b.** Typical Centralizers, **c.** Steel plate and Steel nuts head, **d.** Steel plate and Steel nuts head.

Soil nailing provides several advantages over other soil stabilization techniques. The technique is flexible and can be tailored to the specific soil conditions and project requirements.

Soil nailing is also quick and relatively simple to install, requiring minimal excavation and disturbance to the surrounding soil. The technique can also be used in combination with other stabilization techniques to enhance its effectiveness. The effectiveness of soil nailing as a soil reinforcement technique has been established through various studies. (Zhu et al., 2011) conducted a field pullout testing and performance evaluation of Glass Fiber Reinforced Polymer (GFRP) soil nails. The study examined the load transfer mechanism and the performance of GFRP soil nails in reinforcing soil slopes. The study concluded that GFRP soil nails are a promising alternative to traditional steel soil nails, offering advantages such as high tensile strength, corrosion resistance, and ease of installation. The results of the study can inform the design and implementation of GFRP soil nail systems in geotechnical engineering projects. On the other hand, (Prashant & Mukherjee, 2010)investigated the use of soil nailing for the stabilization of steep slopes near railway tracks. The study concluded that soil nailing was an effective technique for slope stabilization, reducing the risk of slope failure and improving safety near railway tracks. The study also highlighted the importance of proper design and installation of soil nailing systems to ensure their effectiveness.

Soil nailing is not without limitations, however. The technique may not be suitable for some soil types, such as loose or cohesive soils, which may not provide sufficient shear resistance to the soil nail. In addition, the technique can be expensive, particularly if specialized equipment is required for drilling and grouting. Overall, soil nailing is a proven and effective soil reinforcement technique that can improve the stability, bearing capacity, and overall performance of the soil. Proper design and installation, taking into account soil conditions and project requirements, are important for the successful implementation of the technique.

2.2.2. Prefabricated vertical drains:

Prefabricated vertical drains, also known as wick drains, are a soil improvement technique used to accelerate the consolidation process of soft soils. This technique involves the insertion of plastic or composite drains, which have a cylindrical core wrapped in a geotextile filter fabric, into the soil at a specific spacing. The prefabricated vertical drains act as a drainage path for the soil water, which facilitates the transfer of water from the soil to the surface, reducing the time required for consolidation. The installation process of prefabricated vertical drains typically involves drilling a hole into the soil to the required depth and inserting the wick drain into the soil. The wick drain is then surrounded by either a sand blanket or a secondary layer of filter material to prevent the clogging of the drain. Multiple wick drains are installed in a predetermined pattern and are connected to a drainage system that allows the soil water to be

removed from the soil. (Indraratna et al., 2010)studied the performance and prediction of prefabricated vertical drains (PVDs) in improving soft soils. The research evaluated the effectiveness of PVDs in accelerating consolidation and reducing time-dependent settlement in soft soils, as well as providing a method for predicting the long-term performance of PVD installations. The study concluded that PVDs are a cost-effective and efficient technique for improving soft soil properties, especially in combination with appropriate surcharge loading regimes. The findings of the study can help inform the use of PVDs in similar geotechnical engineering projects (Figure 2.2).

The use of prefabricated vertical drains offers several advantages over other soil improvement techniques. The technique is relatively simple and requires minimal excavation, disturbance, or settlement to the site. The wick drains can also be installed quickly, accelerating the consolidation process of the soil and reducing the total project duration. However, the effectiveness of prefabricated vertical drains depends on several factors, such as the soil type, moisture content, and depth of the soil layer to be improved. The drains must be installed at the correct spacing to ensure that the soil is adequately drained. The effectiveness of the technique can also be affected by other factors, such as clogging of the filter fabric, inappropriate installation, or insufficient drainage capacity, which can lead to prolonged consolidation times or reduced effectiveness of the consolidation process.

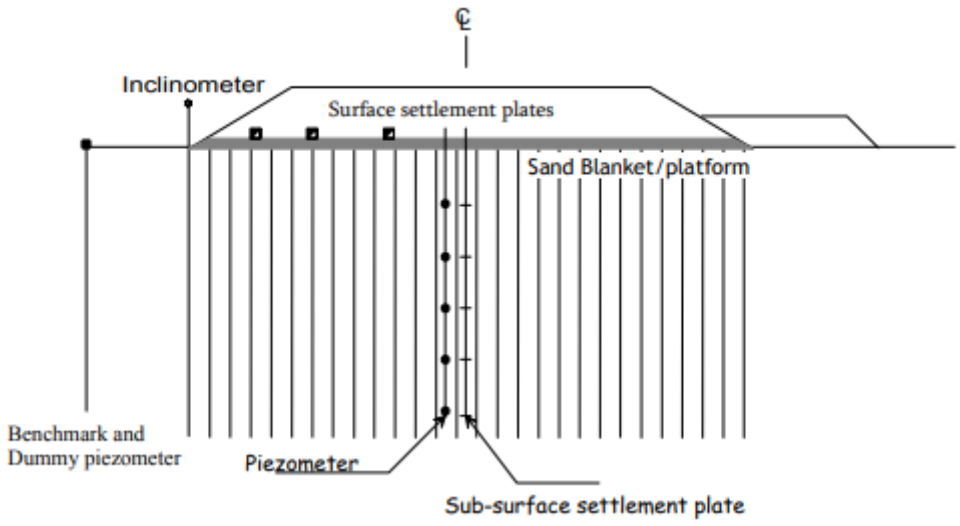

Figure 2.2: Vertical drain system with preloading (Indraratna et al., 2010).

2.2.3. Compaction Grouting

The process of compaction grouting involves injecting low workability cement paste into the soil without entering the soil pores, resulting in a homogeneous cement mass that extends and moves the soil before finally compacting it. This method is effective for improving liquefaction and can be used in various circumstances, including treatment under existing structures, urban areas with low levels of vibration and noise, and narrow spaces.

The compaction procedure utilizing the bottom-up injection technology comprises multiple sequential stages. Initially, the foundation soil of existing or future foundations is drilled to install injection pipes. Subsequently, the injection process is initiated, and a mixture is introduced through the pipes, exerting pressure on the surrounding soil. The injection pipes are then incrementally raised by a specific distance, typically ranging from 0.3-1.5 m, and the process is repeated. This stepwise injection procedure is continued until the entire soil layer is treated, with each injection incrementally increasing the density and pressure to stabilize the soil layer. Ultimately, this technique aims to achieve controlled elevation of the soil surface or mitigate the settlement of existing structures induced by local factors. This method has been discussed in the works of(Morales & Morales, 2003; Sayehvand & Kalantari, 2012), as well as (Welsh & Burke, 2000).

According to a report by (R. P. Orense et al., 2000),Compaction grouting encompasses the injection of an inflexible grout, consisting of a blend of soil-cement-water mixture, incorporating silt sizes to confer plasticity, as well as sand and gravel to induce internal friction. The grout formulation is specifically engineered to prevent permeation into the native soil, instead facilitating the controlled expansion of the grout bulb mass, displacing the surrounding soil. The fundamental objective of employing compaction grouting is to improve the compactness of soft, loose, or disturbed soil for various purposes including settlement management, structural realignment, augmentation of soil bearing capacity, and mitigation of liquefaction susceptibility.

A comprehensive analysis of the application of compaction grouting for remediation of liquefaction was presented by (R. Orense, 2008). The study included two case histories, one involving the implementation in an open unrestricted space, such as an airport runway, and another conducted beneath an existing manufacturing plant. The findings from these cases provided valuable insights into the effectiveness of the compaction grouting technique. Post-treatment data indicated that compaction grouting successfully enhanced the SPT resistance,

thereby mitigating the risk of liquefaction. The method of construction, whether "bottom-up," "top-down," or a combination of both, influenced the level of effectiveness and resulted in ground heave. Significantly, the technique demonstrated the highest efficacy in sandy soils with lower fines content. Moreover, compaction grouting also led to increased strength and lateral earth pressure within the ground. Figure 2.3 illustrates the application of this method.

In the study conducted by (R. Orense, 2008), two case studies were examined to illustrate the application of compaction grouting for liquefaction remediation. One case focused on the implementation of compaction grouting in an open unrestricted space, such as airport runways, while the second case involved its usage beneath an existing manufacturing plant. A thorough evaluation of the technique's effectiveness yielded several key observations. Analysis of the post-treatment data demonstrated that compaction grouting successfully improved the SPT resistance, effectively mitigating the risk of liquefaction. The method of construction employed, whether it followed a "bottom-up," "top-down," or a combination approach, influenced the efficacy of the technique and the resulting ground heave. Moreover, the compaction grouting method exhibited its highest effectiveness in sandy soils with a lower fines content. Additionally, compaction grouting contributed to increased ground strength and lateral earth pressure. Figure 2.3 presents an illustration of the compaction grouting technique.

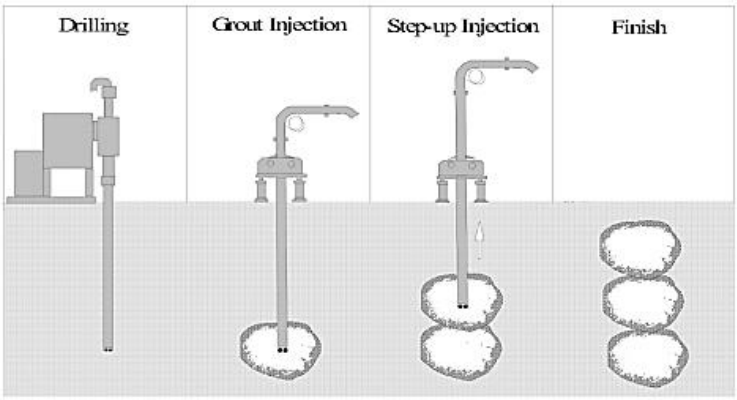

Figure 2.3: Compaction-grouting implementation (R. Orense, 2008).

(Wakeman et al., 2010) conducted a study that showcased the successful application of compaction grouting in densifying a thick, loose sand layer reaching depths of up to 40 feet at a large development site in an urban environment. The densification process resulted in a significant increase in the factor of safety against liquefaction and effectively reduced potential settlement induced by liquefaction to less than 0.5 inches. To ensure quality control and assurance, automated data acquisition and processing techniques were employed, along with three-dimensional visualization components. The ground improvement program was rigorously

validated by comparing cone penetration test (CPT) results obtained before and after the treatment. The densification of the loose sand layer led to a remarkable increase of over 100% in cone tip resistance, elevating the factor of safety against liquefaction from approximately 1 to over 1.5. Additionally, the initially anticipated liquefaction-induced settlement, projected to range from 2 to 5 inches, was effectively diminished to negligible amounts.

2.2.4. Columns of lime-cement treated soils

This is a technique for improving the geomechanical characteristics of poor fine-grained soils, which has been widely used in France where full-scale experimental tests have been carried out by specialized companies for the benefit of the SNCF. Initially, this technique was used to treat stability issues affecting embankment slopes made of clay and impacting railway networks, resulting in significant maintenance costs. The technique involves the use of a double hollow auger with a diameter of 150 mm to create real in situ treated soil columns by injecting a cement, lime, or lime-cement grout. The execution steps are summarized as follows (CARTIER et al., 1986):

- Disaggregation of the soil without extraction by the auger to a pre-set depth;
- Injection and mixing of binders to homogenize the treatment;
- Compaction of the soil column through successive passes so that the short-term compactness is only slightly different from that of the embankment prior to treatment.

Laboratory tests were carried out on samples using a highly plastic silt (WL = 59, Ip = 18) treated with varying percentages of lime and cement (from 6% to 12%). These tests revealed that treatments with 8% lime and 10% cement offer better resistance after 28 days of age (CARTIER et al., 1986). Different tests have confirmed that the improvement provided by lime-cement grouts is entirely satisfactory. In fact, it is the long-term action of lime that promotes the formation of compounds resulting from pozzolanic reactions, which link the attacked particles and create an overall texture. This technique falls under the category of reinforcement processes primarily intended for compressible fine soil deposits. The diagram of the execution operations is represented in Figure 2.4.

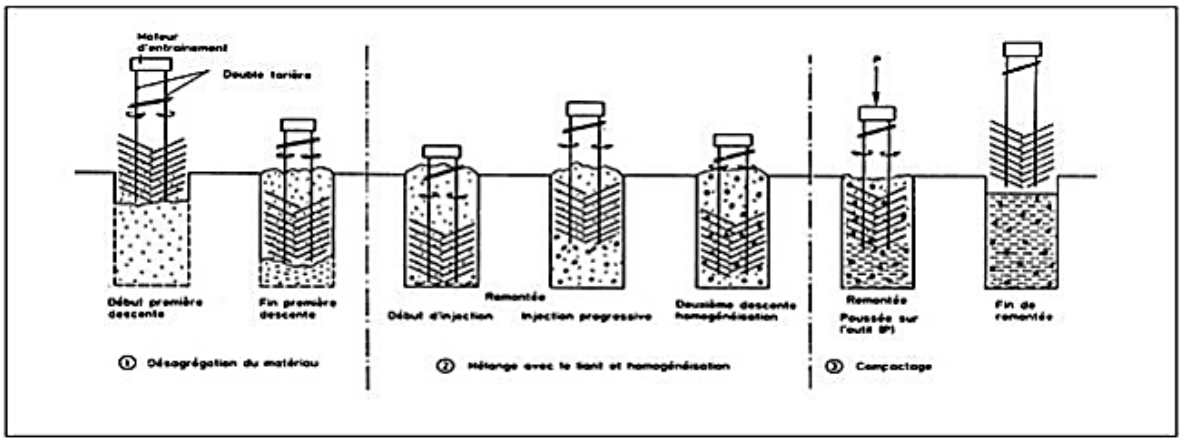

Figure 2.4: Procedure for creating treated soil columns (CARTIER et al., 1986)**.**

2.2.5. Dynamic compaction:

Dynamic compaction is a ground improvement technique that involves the use of heavy equipment, such as a crane-mounted drop weight or a high-energy hydraulic hammer, to impact the soil surface repeatedly over a large area. The repeated impact of the equipment causes the soil particles to rearrange, creating a denser and stiffer soil layer. The technique is commonly used on soft or loose soils that have poor bearing capacity, high compressibility, or that are prone to liquefaction.

The heavy equipment used in dynamic compaction can deliver impacts with a high energy density, resulting in a significant increase in soil density and stiffness. The depth of compaction depends on several factors, including the energy of the impact, the number of impacts, the soil type, and the water content. Typically, the technique is applied to fill soils or low-density natural soils. In some cases, the technique can also be used on more cohesive soils to enhance their stiffness and strength (Figure 2.5).

The technique is typically used to enhance the bearing capacity of the soil, reduce the potential for settlement, and to increase the resistance of the soil to liquefaction during seismic events. The depth of treatment depends on the thickness of the soft soil layer to be improved and the required bearing capacity of the improved layer. Dynamic compaction is often used in conjunction with other ground improvement techniques, such as stone columns or soil mixing, to improve the overall performance of the soil.

The effectiveness of dynamic compaction as a soil reinforcement technique has been established through various studies. (Feng et al., 2010)found that high energy dynamic

compaction (HEDC) is effective in improving the geotechnical properties of soil in coastal reclamation areas. In addition,(Liang et al., 2015) developed a new method using vacuum preloading and preloading with surcharge to improve the mechanical properties of soft soil.

One of the advantages of dynamic compaction is that it is a cost-effective and efficient technique for reinforcing large areas of soil quickly. The technique is relatively simple to implement, requires minimal excavation, and produces minimal waste materials. However, the technique has some limitations. For example, the technique may not be suitable for soils that are too soft, too wet, or have a high organic content. Further, the technique can result in some ground vibrations and noise, which could be a concern in urban areas.

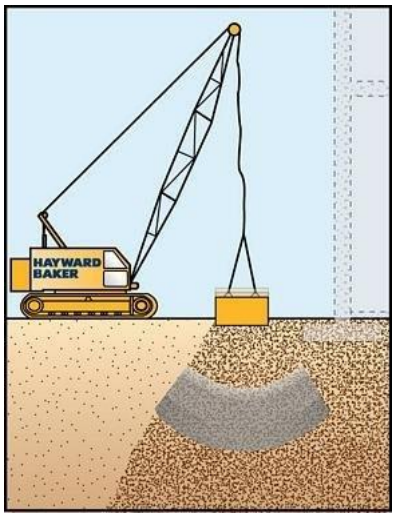

Figure 2.5: Dynamic compaction technique (Singh et al., 2016).

2.2.6. Reinforcement of compressible soil by geosynthetics materials

2.2.6.1. Definitions and Types of Geosynthetics

Geosynthetics are synthetic sheets that come into contact with soil and have been used in civil engineering for approximately two decades. Typically implemented as sheets, the primary functions of geosynthetics include drainage, filtration, separation, and reinforcement. Integrating geosynthetics into the structure enables several benefits, including reduction in the quantity of required materials, utilization of low-quality materials, prevention of interpenetration between layers, and reinforcement of a soft soil embankment to mitigate significant deformation (Holtz, 2001).

Geotextiles are products made of polymers and are commonly utilised in geotechnical and civil engineering due to their permeable nature. They can either be woven, nonwoven, or knitted and serve multiple functions in soil, such as filtration, separation, and reinforcement.

Geogrids are specifically engineered to provide soil reinforcement by offering an open and regular network of elements that can withstand traction forces. Typically composed of planar polymer structures, geogrids are manufactured through techniques such as extrusion, bonding, or interlacing. Essentially, a geogrid's dimension dictates the size of the mesh and allows for the penetration of large soil elements to create an interlocking effect for soil confinement.

Geomembranes are low-permeability geosynthetics that are commonly manufactured as sheets composed of either synthetic, bituminous, or bentonite materials. They have various uses in geotechnical, environmental, hydraulic, or transportation applications.

Geocomposites refer to the combination of two or more materials during the manufacturing process of geosynthetics. They can consist of various combinations such as geotextile-geonets, geotextile-geogrids, geotextile-geomembranes, geomembrane-geonets, geotextile-polymer cores, and three-dimensional cell structures made from the same polymer. The possibilities for geocomposites are nearly endless and can be highly useful in geotechnical engineering for functions like separation and reinforcement, as well as for pavement layers and reinforcement during reprocessing.

The primary components of geosynthetics consist of synthetic fibres, selected for their economic viability and ability to withstand the harmful effects of both chemical and biological factors present in soil. These fibres are produced through the process of spinning and stretching macromolecules, which are also referred to as polymers (Berrabah, 2015).

The geosynthetic sheets frequently comprise the following polymers:

- **Vinyls**, including polyvinyl chloride (PVC), are commonly utilised as drainage systems due to their exceptional resilience against water, chemical, and microbial damage.

- **Acrylics**, whether in resin or emulsion form, can be utilized for consolidating geosynthetics in the field of geotechnical engineering.

- **Polyamides,** including Nylon (PA); are typically avoided due to their heightened sensitivity to water, making them an uncommon choice.

- **Polyesters** (PET) are an appealing choice due to their impressive mechanical properties as well as their ability to resist the harmful impact of acids and microorganisms. However, they are prone to surface damage from bases.

- **Polyolefins,** including polyethylene (PE) and polypropylene (PP), are extensively utilised because of their cost-effectiveness, excellent mechanical properties, and high resistance to chemical damage.

2.2.6.2. Functions of Geosynthetics

The mechanical and hydraulic characteristics of soil can be enhanced through the implementation of geosynthetics. This can provide the following benefits, as illustrated in Figure 2.6:

a-Separation: A geotextile can be used to prevent the blending of two materials that possess distinct characteristics, serving as a means of preventing their intermingling.

b-Reinforcement: this involves leveraging the strength and resistance capabilities of geotextiles or comparable materials to enhance the mechanical properties of soil.

c-Protection: through the use of a geotextile, which is commonly found in the form of a geomembrane, it is possible to prevent localised harm or damage to a specific material.

d-Waterproofing: involves managing or controlling the movement of liquid or gas through a particular material.

e-Filtration: involves the use of a geotextile to retain soil or other particles when subjected to hydraulic forces, while still allowing fluids to flow through or into the geotextile.

f-Drainage: encompasses activities such as collecting and transporting rainwater, groundwater, or other liquids within the plane of a geotextile or similar materials.

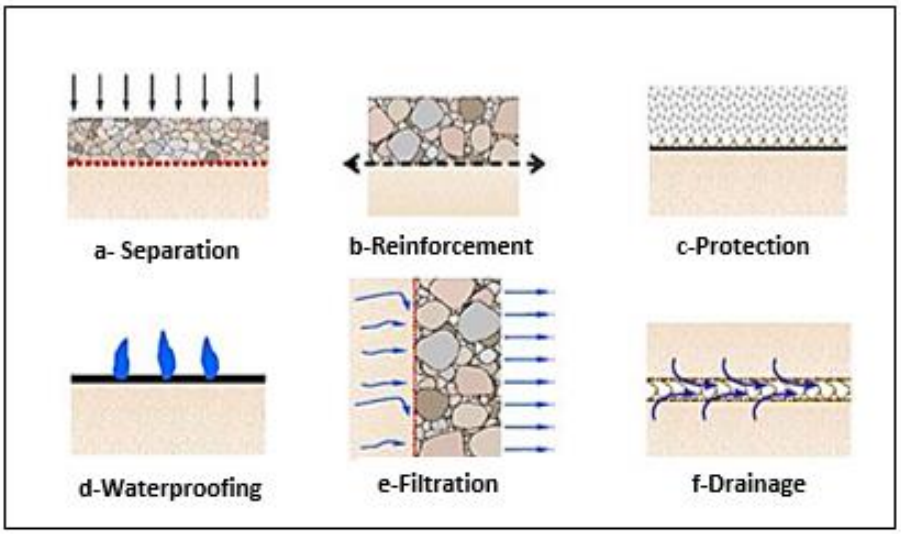

Figure 2.6: Main roles of geosynthetic materials.

Geosyntheticsare typically categorized based on their primary function, but they may also be capable of fulfilling one or more secondary functions in certain applications. Therefore, when calculating and determining the design characteristics of geosynthetics, it is crucial to factor in both their primary and secondary functions.

Geomembranes are a versatile construction material with a wide range of applications. In hydraulic systems, they are commonly used to create canals or basins for purposes such as irrigation, drinking water supply, or wastewater lagooning. They are also used in water-related applications such as water-resistant barriers for dikes, dams, and navigable canals. Additionally, geomembranesare frequently employed for sealing municipal or industrial waste storage facilities that contain waste from animal, plant, or chemical sources. With natural waterproof sites being scarce and regulations becoming increasingly strict, the utilization of geomembranes has become a popular solution for waterproofing needs.

The selection of geotextiles and related products is based on the specific requirements of the structure in which they are used. Geotextiles possess a wide range of tensile strength and rigidity, making them well-suited for soil reinforcement in structures like reinforced walls.

Geotextiles were initially adopted for road construction, where they continue to be utilized as reinforcements, separators, drains, filters, and for slope erosion control. In the construction of coastal structures, such as groynes and sea defences, geotextiles provide an advantageous alternative to traditional techniques like filter mats or pile curtains.

Geotextiles are particularly useful in hydraulic works, as they allow the creation of continuous, permeable, and filtering interfaces. They are therefore used either in addition to a traditional structure to reinforce the safety of the structure, or more often, as a replacement for expensive and calibrated natural materials. In this case, they allow for savings because they replace materials that are generally expensive, and their implementation is much easier for the realization of inclined or vertical interfaces.

2.2.7. Reinforcement by Granular Columns:

The initial soil, or unimproved state, is essentially identified by its particle size distribution curve, which remains an essential factor in determining the appropriate soil improvement technique. Given the two major classes of well-known soils, namely powdery or fine soils, it is natural to understand that there is a difference between the appropriate improvement techniques for each of these classes. Additionally, knowing that there is a good majority of soils belonging

to the category of intermediate soils, other derivative techniques can be considered. Figure 2.7 illustrates the clear difference between the techniques executable in fine soils on the one hand, and granular soils on the other hand. While for intermediate soils, the possibilities for improvement have not diversified. The experience gained in the field of soil treatment has allowed us to draw the following conclusions (Dhouib & Blondeau, 2005): It is possible to carry out dynamic, static compaction (also known as horizontal static compaction: CHS), or radial vibration compaction (vibroflotation or vibrocompaction), or to perform soil-cement mortar columns (Jet-Grouting) in more or less fine sandy-gravelly materials. When dealing with soils that primarily consist of fine to very fine particles and are at the limits of compaction processes (as shown in Figure 2.7), the application of ballasted columns, rigid inclusions, and lime-cement soil columns becomes necessary. The implementation of ballasted columns relies on the presence of sufficient and permanent lateral restraint provided by the treated medium to prevent lateral expansion of the cohesionless ballast material. However, when the soils to be treated are soft, compressible, and contain organic materials, the ground may not offer permanent resistance to the lateral expansion of the ballasted column. In such cases, soil improvement through ballasted columns may be unfeasible due to the evolving behavior of organic materials and their tendency to exhibit creep deformations. Consequently, the incorporation of rigid inclusions becomes necessary. On the other hand, in situations where the soil consists of organic materials with high natural water content, the dry incorporation of lime-cement columns proves to be a viable solution. In contrast, for soils with low natural water content, the wet method (Deep soil mixing) can be employed for the same technique.

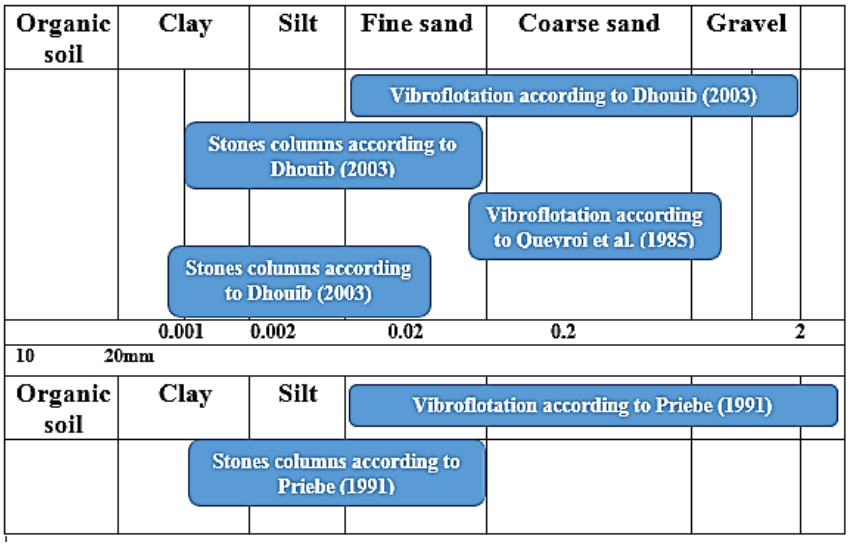

Figure 2.7: General diagram of the application of soil improvement techniques (Dhouib & Blondeau, 2005)

2.2.7.1. Definition of stone columns

Stone columns are a soil reinforcement method that involves incorporating compacted stone columns into the soil. This technique is suitable for clayey or silty soils containing more than 10% to 15% silt and clay. Stone columns are not foundation elements; their purpose is to confer new global and/or local characteristics to the soil under the structure to be built. This is to ensure that the different infrastructure elements of the structure (isolated or continuous footings, slabs, earthworks, etc.) have predictable and justifiable behaviour in accordance with the regulations and tolerances applicable to the structure's construction and operation. Stone columns allow for the control of the behaviour of the future structure's shallow foundations. The material used for the stone column is a high-bearing powder material, and the column acts as a drain. This not only increases the existing soil's load-bearing capacity but also increases the soil's consolidation speed (Auvray, 2010).

2.2.7.2. Column types

When the firm soil layer is located at a depth far below the soft soil layer, the column is then installed in the soft layer (Figure 2.8-a). The load carried by the column is supported by the lateral friction developed along the column. In this case, the column is called "floating"(Barksdale & Bachus, 1983).

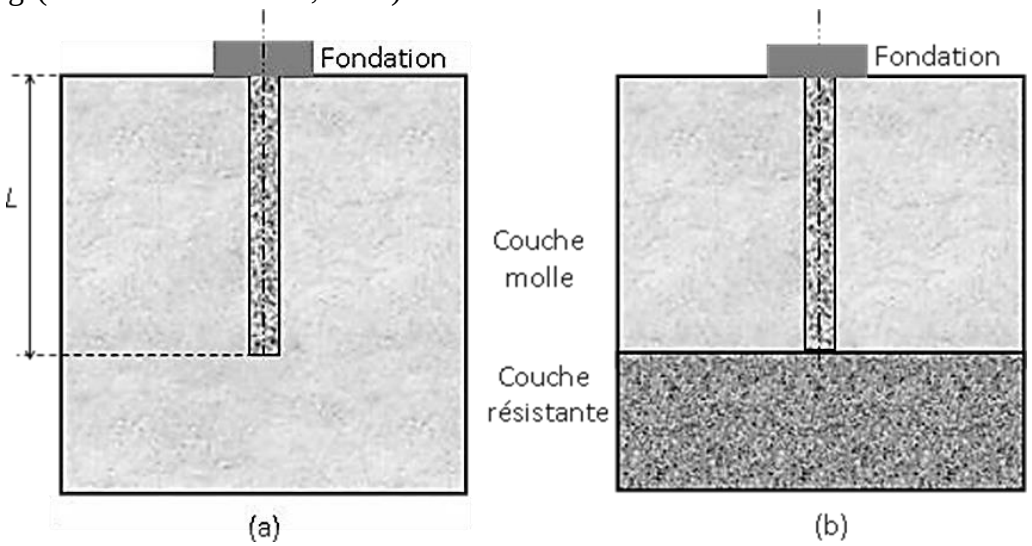

Figure 2.8: Types of stone columns, (a): floating, (b): bearing (Nour El Islam, 2021.)**.**

However, if the firm layer is located at a depth close to the surface of the soil, the column can be installed on the firm layer. In this case, the column is called "bearing columns at the tip". The loads are then supported by the resistance at the tip of the column (Figure 2.8-b). Generally, the choice between floating and bearing columns is made based on cost considerations and technical limitations of the drilling machines used.

2.2.7.3. Fundamental Design Parameters

Improving bearing capacity and minimizing settlement are influenced by crucial design parameters such as column spacing, diameter, and arrangement (triangular, square, or hexagonal pattern).

a) Spacing of Stone Columns (*S*)

The design of stone columns should be customised to the site, and it is not possible to provide definitive guidelines for maximum and minimum column spacing.

b) Diameter of Stone Columns (*D*)

The diameter D of the column plays an important role in increasing the bearing capacity and reducing the resulting settlement (Greenwood, 1991). The dimensions of ballasted columns typically depend on the type of soil to be reinforced, the densification of materials, and the construction technique used(Bell, 2004). The diameter D of the column generally varies between 0.7 m and 1.1 m. The length L of the column depends on the soil encountered at the site and usually ranges between 6 and 20 m (Raju & Sondermann, 2005). Additionally,(Balaam & Booker, 1985; Hughes & Withers, 1974) have reported that the diameter D affects the transfer of applied loads on the columns and have indicated that the effect of these loads is limited to a zone not exceeding a distance of 2.5D in the surrounding soil of the column (Boumekik et al., 2021).

In soft soils, the installation of stone columns is a self-compensating process, meaning that the diameter of the column formed is larger as the soil becomes softer. The final diameter of a hole is typically larger than the initial diameter of the probe or casing due to the lateral displacement of stones caused by vibrations or ramming. The vibroflot installation method (with a diameter of 300–500 mm) can produce column diameters ranging from 0.6 m in stiff clays to 1.1 m in very soft cohesive soils (Ranjan, 1989).

c) Arrangement of stone columns (d_e)

The ideal layout for installing stone columns is in an equilateral triangular pattern due to its high density packing. However, square and hexagonal patterns are also feasible options. (Figure 2.9) depicts a standard layout for equilateral triangular, square, and hexagonal patterns.

Each column has an influence domain that is characterised by the equivalent diameter (d_e). According to (Balaam & Booker, 1981), the value of the diameter de can be determined based on s and the type of pattern:

• Triangular pattern (Figure 1.5-a):

$$de = \sqrt[4]{\frac{12}{\pi^2}} S = 1.05S \tag{2.1}$$

• Square pattern (Figure 1.5-b):

$$de = \sqrt[4]{\frac{16}{\pi^2}} S = 1.13S \tag{2.2}$$

• Hexagonal pattern (Figure 1.5-c):

$$de = \sqrt[4]{\frac{27}{\pi^2}} S = 1.29S \tag{2.3}$$

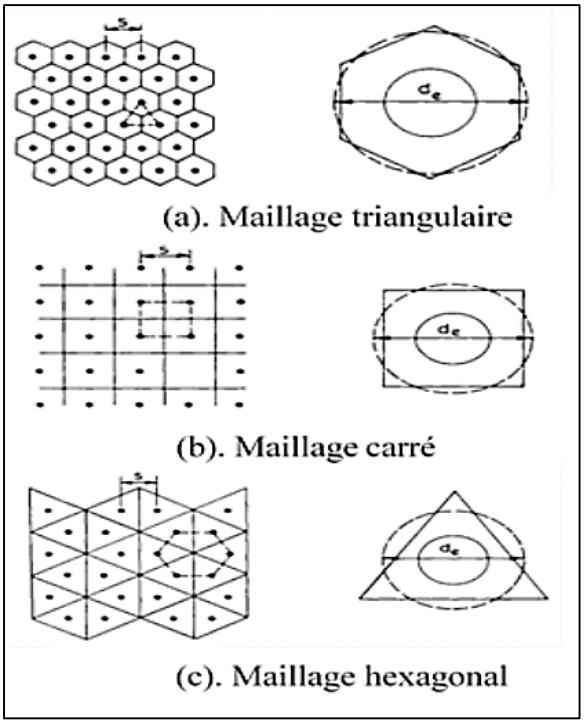

Figure 2.9: Arrangement and influence domain of ballasted columns (Balaam & Booker, 1981).

d) Coefficient of Substitution

The coefficient of substitution (α) or rate of incorporation is the ratio of the area of the stone column (Ac) to the area of its influence domain (A):

$$\alpha = Ac/A \tag{2.4}$$

e) Stress concentration ratio

In the presence of a uniform load ($\Delta\sigma v_0$) applied to a soil mass, the enhanced strength and stiffness of stone columns compared to the surrounding soil lead to stress concentration on the

columns ($\Delta\sigma v,_c$) and a reduction in stress on the soil ($\Delta\sigma v,_s$), as depicted in Figure 2.10. The stress concentration ratio (n) is defined as the ratio of the vertical stress applied to the column to the stress exerted on the surrounding soil:

$$n = \Delta\sigma v,c/\Delta\sigma v,s \tag{2.5}$$

The value of (n) is influenced by the relative stiffness of the stone column compared to the surrounding soil and typically falls within the range of 2 to 6 (Aboshi, 1979).

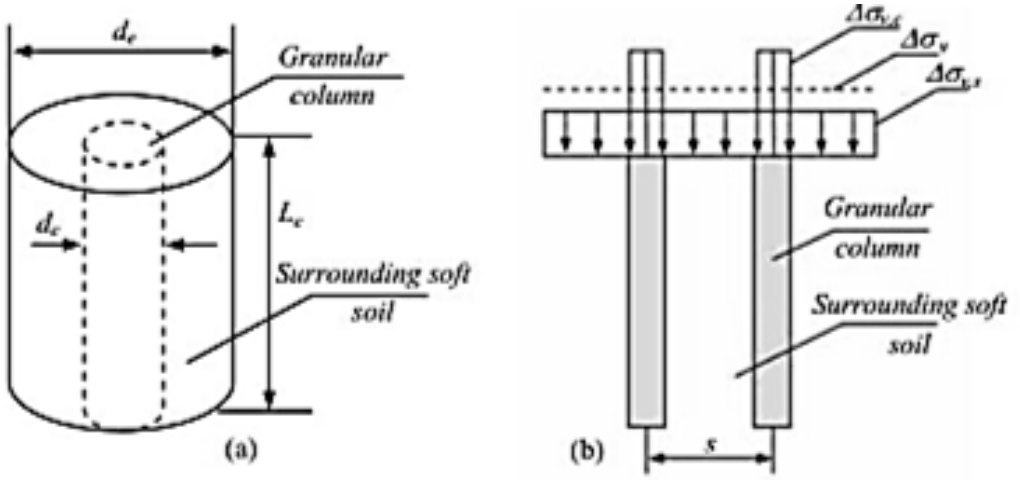

Figure 2.10: a. Unit cell scheme;**b.** Stress distribution.

f) Settlement reduction factor

The estimation of settlement reduction is generally the dominant design criterion in soils treated by ballasted columns (Figure 2.11). Most analytical design methods provide a direct prediction of the settlement reduction factor (β), which is defined as the ratio of soil settlement before treatment (S_0) divided by the settlement of the composite medium obtained after treatment (S_f), i.e.:

$$\beta = S_0 / S_f \tag{2.6}$$

Depending on the mesh density and the encountered geotechnical conditions, this factor is generally between 1.5 and 4 under distributed loads (CFMS, 2011).

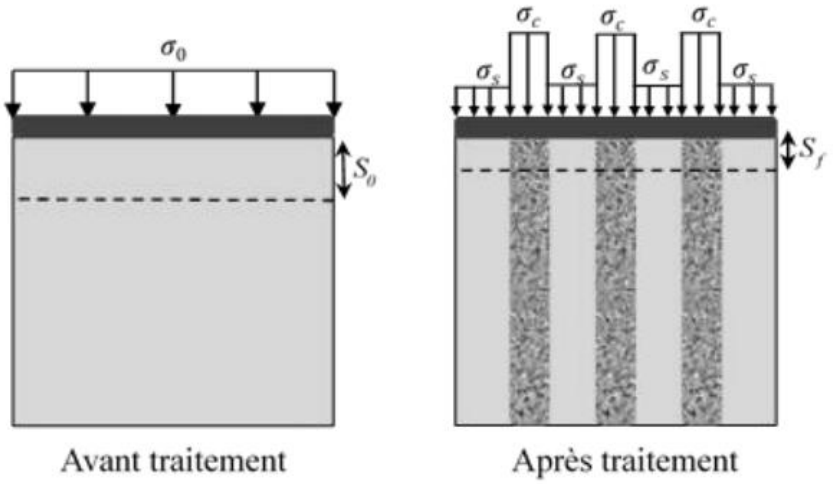

Figure 2.11: Principle of stress concentration and settlement reduction (Basu, 2009).

2.2.7.4. Failure Mechanism

Various publications (Ambily & Gandhi, 2007b; Brauns, 1978; Hughes et al., 1975; Hughes & Withers, 1974; Mohanty & Samanta, 2015; Shivashankar et al., 2011) relating to the ultimate bearing capacity of an isolated column revolve around three failure modes (Figure 2.12), which correspond to geometric configurations, according to (Datye, 1982):

- Lateral expansion failure (often the controlling failure mode) (Figure 2.12-a);
- General shear failure (rare failure mode, for short columns) (Figure 2.12-b);
- Punching shear failure (floating columns) (Figure 2.12-c).

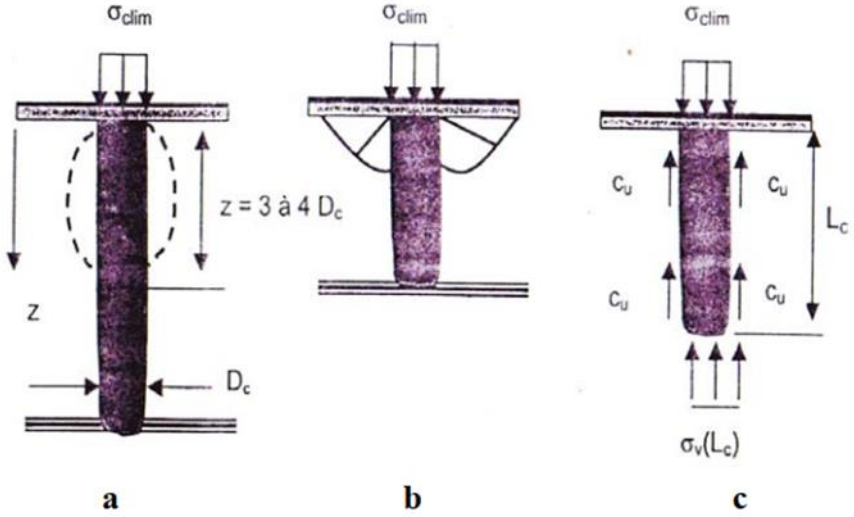

Figure 2.12: Types of failure in a head-loaded isolated column executed in a homogeneous compressible layer according to (Datye, 1982).

2.2.7.4.1. Lateral expansion failure

In 1974, Hughes and Withers conducted the first investigation with reduced models on the failure mode of a sand column installed in a homogeneous clay layer, specifically the "Kaolin clay".

The authors observed that vertical and lateral deformations are produced in the upper part of the column (Figure 2.13). Additionally, only the clay at a radial distance of 2.5d is laterally stretched, while the vertical displacement of the columns was not extended below 4d. To confirm these results, (Hughes et al., 1975) conducted full-scale loading tests on an isolated ballasted column. The loading was performed by a circular plate of 0.66 m diameter, slightly smaller than the column's diameter. After loading, the soil surrounding the column was excavated to determine its shape. The authors found that the column's shape was similar to that observed by (Hughes & Withers, 1974). Furthermore, the predicted expansion was limited to the upper zone. Based on reduced model tests, (Ambily & Gandhi, 2007a) found that the maximum expansion is concentrated at a depth of 0.5d from the top.

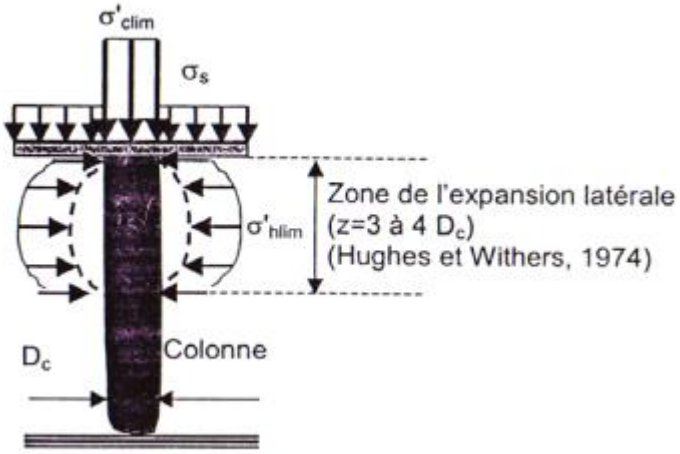

Figure 2.13: Deformation of an isolated sand column (reduced model) under axial head load (Hughes & Withers, 1974).

When the column is installed in a layered soil, (Shivashankar et al., 2011) observed that expansion occurs only in the weakest soil layer, and the expansion increases with the thickness of the layer due to less lateral confinement offered by this soil layer. Through laboratory testing and numerical studies, (Mohanty & Samanta, 2015) found that lateral expansion of the column is greater in layered soils than in homogeneous soils. According to the authors, the length of lateral expansion increases with the thickness of the upper layer but is limited to a length of 2d.

Additionally, the maximum depth of expansion is found at a depth of 0.5d to 0.8d and is independent of the thickness of the upper layer when it exceeds 2d.

2.2.7.4.2. Generalized Shear Failure

Generalized shear failure typically occurs in columns beneath rigid foundations. Figure 2.14 illustrates the most well-known contribution on this subject (Brauns, 1978), which considered the case of axisymmetric failure of a composite material volume, "Ballast-Soil," limited by a truncated conical surface centered on the axis of the column and developed to a depth denoted by *h* (Soyez, 1985), expressed as follows:

$$h = d \tan\left(\frac{\pi}{4} + \frac{\varphi_c}{2}\right) \tag{2.7}$$

With φc being the internal friction angle of the ballast material.

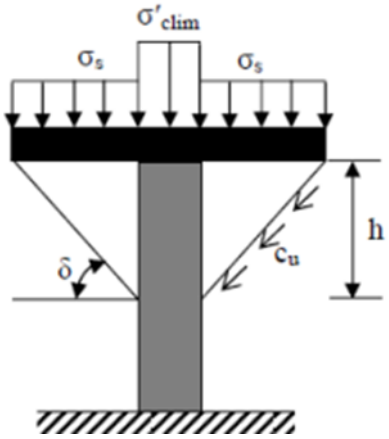

Figure 2.14: Generalized Shear Failure of an Isolated Ballasted Column under Axial Head Load, based on (Brauns, 1978).

The angle δ can be quickly determined using the chart in Figure 2.15. In the special case where σ_s is equal to zero, the curve in Figure I.26 directly provides δ as a function of φ_c.

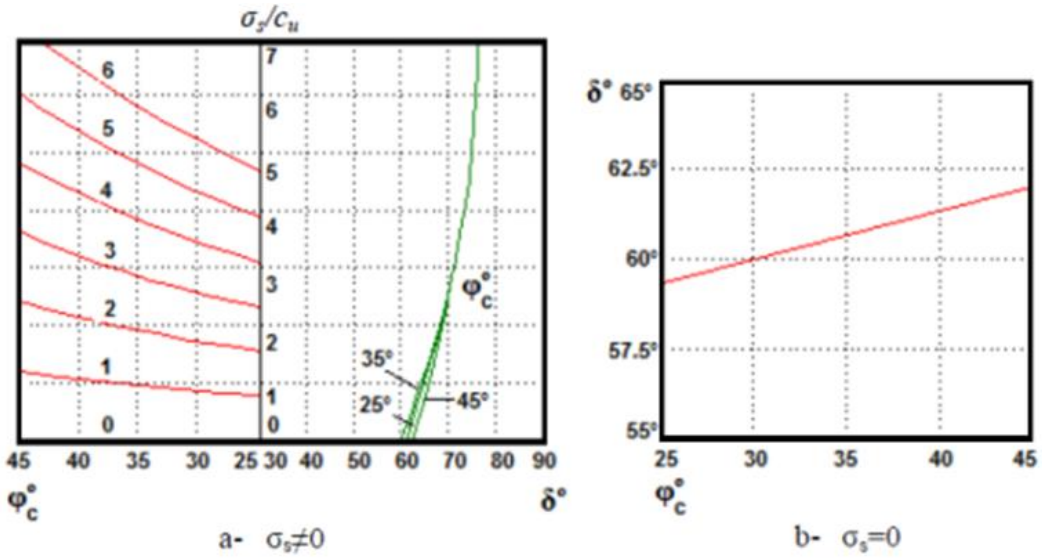

Figure 2.15: Practical Determination of δ (Brauns, 1978).

2.2.7.4.3. Punching Failure

For floating columns, punching failure occurs when the soil resistance under the column tip is unable to balance the vertical stress (z) transmitted through the column (Figure 2.16). The vertical stress within the column at depth z can be expressed, according to(Brauns, 1980), by the following equation:

$$(z) = \sigma_{v,0} + z(\gamma - 2r_c/c_u) \quad (2.8)$$

(2.8)

Where:

- $\sigma v_{,0}$: the vertical stress applied at the top of the column;
- γ_c: unit weight of the column;
- r_c: initial radius of the column.

To avoid punching failure, the vertical stress σv (L_{min}) must not exceed the limit vertical stress $\sigma v*$ at the base of the column, which is typically taken as $9cu$ for piles. The treatment depth should satisfy the following condition:

$$L_{min} < L < L_{max}$$

$$L_{\min} = \frac{1}{2} r_c \left(\frac{\sigma_{v.0}}{c_u} - 9 \right) \quad (2.9)$$

$$L_{max} = \frac{1}{2} r_c \left(\frac{\sigma_{v.0}}{c_u} \right)$$

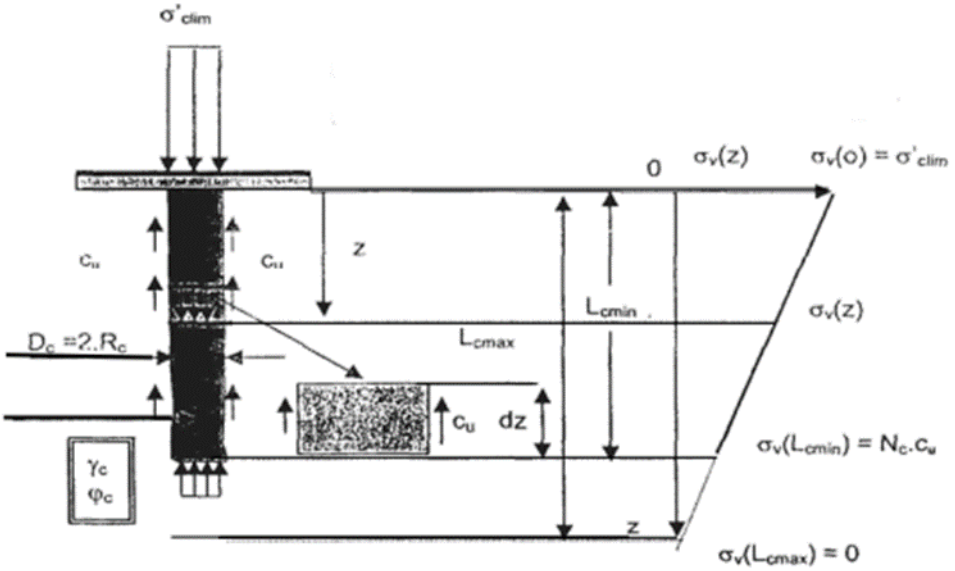

Figure 2.16: Punching Failure of an Isolated Floating Ballasted Column under Axial Head Load (Brauns, 1980).

2.2.7.5. Treatment Objective

The objective of improving soil through stone columns is to implement a "mesh" of columns made up of gravelly materials, which densifies the compressible layers and makes them capable of bearing loads from foundations. The treatment of soil through stone columns involves the following actions:

- Increasing the load-bearing capacity of the soil;
- Reducing total and differential settlements;
- Reducing consolidation time by creating draining elements;
- Reducing the risks induced by liquefaction phenomena during earthquakes;
- Increasing the equivalent characteristics of the treated soil mass (horizontal shear resistance, internal friction angle, and deformation parameters).

By achieving these objectives, the technique of improving soil through stone columns can significantly enhance the performance and safety of a structure.

2.2.7.6. Application areas of stone columns

Stone columns have various application areas that have evolved over the years based on technological advancements and desired improvements. The following list, although not exhaustive, highlights the variability of applications (HOUDA, 2010):

- Road and railway embankments;
- Buildings such as single or multi-story residential units, industrial buildings like offices, warehouses, production areas, silos, wastewater treatment plants (settling tanks, ancillary facilities);
- Airport runways;
- Slope stabilisation.

2.2.7.7. Installation technique of stone columns

The aggregates constituting the columns are installed using two installation techniques: the displacement method or the replacement method (Mokhtari & Kalantari, 2012).

2.2.7.7.1. Case of ordinary stone columns

The input materials must be of quality and controlled granulometry, as homogeneous as possible (natural aggregates, rolled or crushed). The crossing of compact layers or obstacles can be facilitated by prior drilling, with or without terrain extraction. Any excavated volume is filled and compacted by input material.

Figures 1, 2, and 3 show the installation methods used for the installation of stone columns, taken from (Taube & Herridge, 2002). The columns are constructed either by piling or by vibro-flotation(Priebe, 1991). The latter method includes vibro-displacement (dry bottom feeding method) and vibro-replacement (wet or dry top feeding method) (Nour El Islam, 2021).

a) Columns executed by wet method

In this wet method, pressurized water is used to facilitate penetration and the creation of a cylindrical opening. The aggregates (such as ballast or gravel) are placed in the cavity that has already been drilled in several layers, and then they are compacted by air or water pressure (Figure 2.17).

The execution of stone columns using the wet method, also referred to as vibro replacement, involves the following steps:

- **Drilling:** The process begins by utilizing self-drilling techniques and water launching to reach the desired depth.
- **Vibrator removal:** Once the drilling is completed, the vibrator is removed from the hole. In some cases, additional ramming may be conducted to ensure proper compaction.
- **Ballast placement:** The ballast material is then introduced into the pre-drilled hole, either by free fall or gravitational dropping.
- **Compaction:** The ballast is compacted by making successive passes, ensuring proper compaction until the column is fully formed.

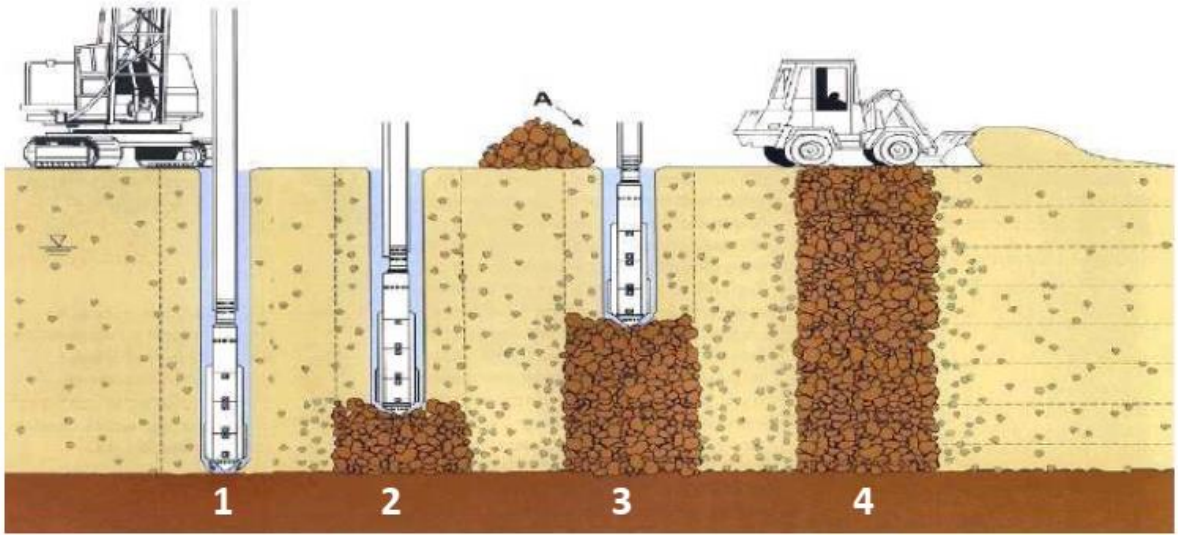

Figure 2.17: Procedure for installing a wet method column (Raju & Sondermann, 2005)

b) Columns executed by the dry method:

The implementation of ballasted columns by the dry method (Figure 2.18), also known as vibro-displacement, consists of:

- Self-driving the vibrator directly into the ground by displacement using air to the designated depth;
- Gradually lifting the vibrator while allowing the ballast supplied by a loader in a bucket sliding along the mast to descend by gravity and air pressure;
- Compacting the ballast by successive passes of about 0.5 inches until the column is finished.

There are several references that provide detailed presentations of these installation techniques, including(Barksdale & Bachus, 1983; Mitchell & Huber, 1985; Raju & Sondermann, 2005), and (Egan et al., 2008).

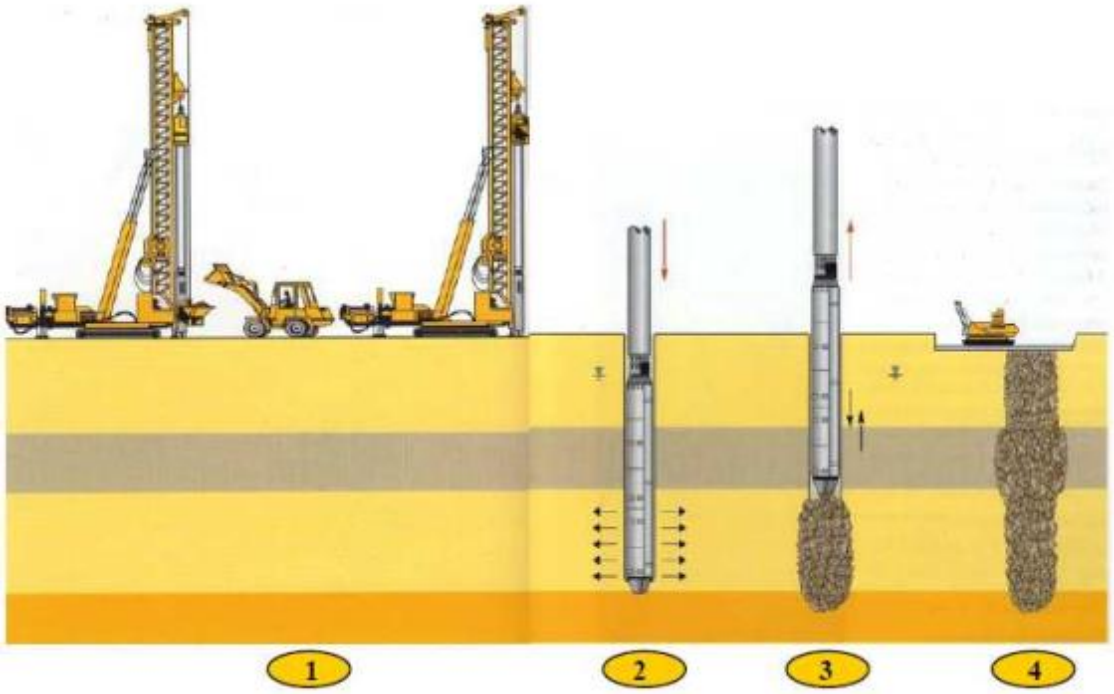

Figure 2.18: Procedure for installing a dry method column (Raju et al., 2004).

c) Piled stone columns ("Franki Gravel Piles"):

The implementation of piled ballasted columns (also known as "gravel piles") using the "Franki" method requires the following steps:

- preparation of the "Franki" driving plug using gravel;
- driving the tube to the desired depth with an internal tamper;
- removal of the gravel plug;
- formation of the column by driving loads of gravel and extracting the tube;
- finishing of the column.

The technique of piled stone columns using the "Franki" method ensures the creation of a densely compacted column with a diameter varying according to the quality of the gravel used (Figure 2.19) (Zighmi, 2011).

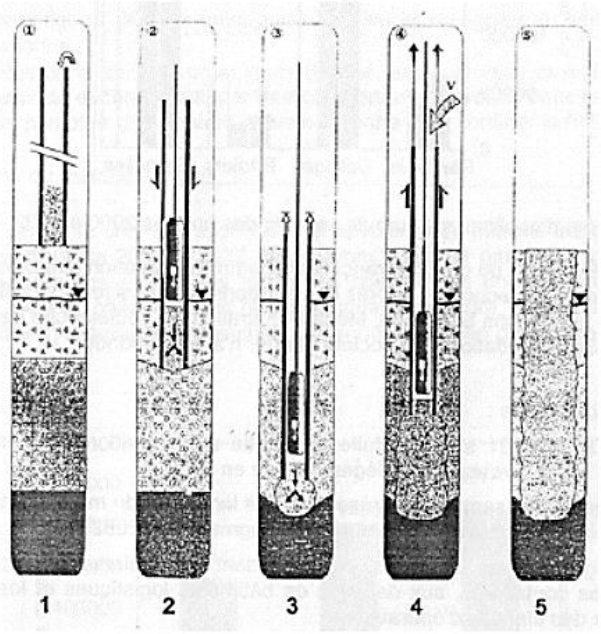

Figure 2.19: Wet top feeding method presented (Raju & Sondermann, 2005).

2.2.7.7.2. Case of stone columns confined to geosynthetics

There are two methods for installing ballasted columns confined by geosynthetics, which are described by (Tandel et al., 2012): (a) the displacement method and (b) the replacement method.

a) Displacement method

This method is generally used in soft soils (Cu <15 kPa). The technique involves driving a closed-ended steel tube into the loose soil, then placing the geosynthetic and filling it with granular material. Due to the vibration of the granular material, the tube's end opens, and it moves upward. Figure 2.20 shows the principle of the displacement method (Alexiew et al., 2005).

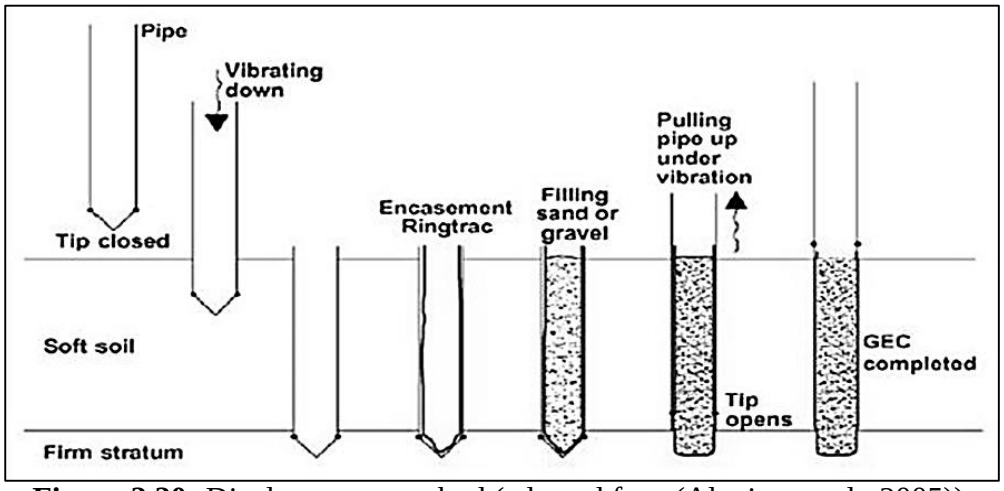

Figure 2.20: Displacement method (adapted from(Alexiew et al., 2005))

b) Replacement method

This installation method is employed when the soil exhibits a favorable penetration resistance. The procedure begins by installing a steel tube into the soil until it reaches a resistant layer. Subsequently, the soil within the tube is excavated using an auger. Once the excavation is complete, a geosynthetic material is positioned and then filled with granular material. Finally, the steel tube is extracted from the ground. The fundamental concept of this technique is depicted in Figure 2.21, which has been adapted from the work of (Gniel & Bouazza, 2010).

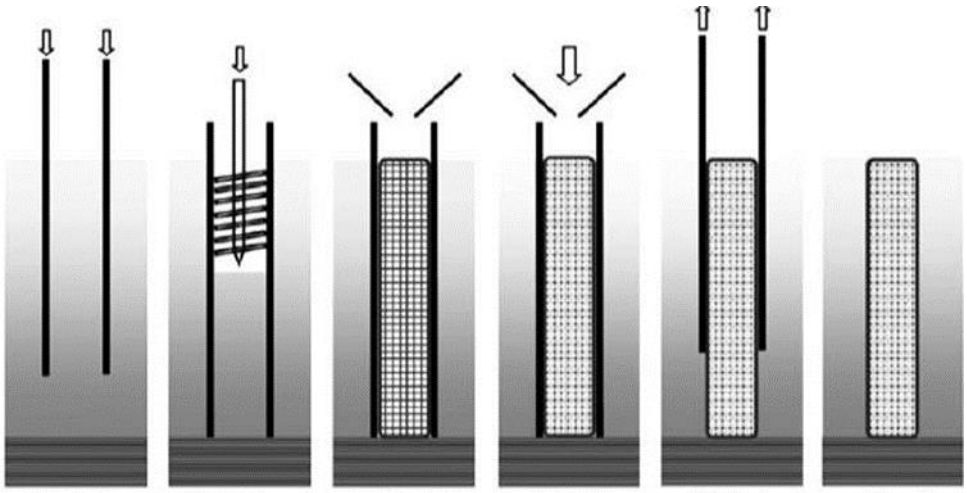

Figure 2.21: Replacement method (adapted from(Gniel & Bouazza, 2010)).

2.2.7.8. Effects of ballasted column installation

The installation of columns has an influence on the surrounding soil, particularly when the columns are installed by vibro-replacement. In this case, the drilling and granular compaction equipment create a radial displacement in the soil surrounding the column(Yu, 2000). In soft clay, this installation effect creates increases in lateral stress and interstitial water pressure, which can be predicted by approximate methods (Castro, 2017; J.-F. Chen et al., 2009; Egan et al., 2008; Muir Wood et al., 2000).

This displacement immediately causes a dissipation of excessive interstitial pressures, accompanied by an increase in effective stress in the column and soft clay. (Guetif et al., 2007; Stuedlein & Holtz, 2013)conducted studies in the field on the effect of column installation methods and concluded that vibro-compacted columns showed a 15% capacity increase compared to columns installed by the replacement method. The installation effects observed in tests on a group of columns were not observed in tests on isolated columns. This led these authors to conclude that the role of soft soil in a group loading could be more important than the effects of installation type and column composition.

It should be noted that for columns installed by the replacement method, the installation effect is negligible and may not be considered.

2.2.7.9. Technical requirements and influencing factors in the implementation

The deformable nature of ballasted columns makes them highly reliable for flexible structures such as embankments on compressible soils, slabs, and flexible rafts. However, the premature application of the method to heavy and sensitive structures can lead to disorders resulting from excessive deformations, unlike conventional deep foundations (piles, beams, and micro-piles). To guard against these sometimes serious consequences, it is imperative to adhere to the following rules:

- In-depth geotechnical study of the soil to be reinforced, the depth of investigation, the consistency of the study (types of tests...), and the different geomechanical parameters to be measured depending on the geology of the site and the importance of the structure to be built;
- Evaluation of the loads to be supported by the foundations.
- Sizing of the ballasted column project, taking into account the absolute and differential settlements that the structure will experience after completion and commissioning;
- During the implementation phase, great attention should be given to the installation of the columns following the mesh plan, checking the depth of refusal, monitoring the consumption of ballast, and recording parameters (amperage, depth, number of buckets, etc.);
- Quality of the vibro-foundation workshop (verticality, support force, equipment with parameter recorders, etc.);
- Power of the vibrator, which plays a crucial role in the quality of the column (verticality, continuity, compactness);
- Quality of the material (ballast) used: soft material can generate fines during the compaction sequences, reducing the draining capacity of the column, depending on the power of the vibrator.

- **The main factors for choosing the technique of stone columns:**

Reinforcement using stone columns stands out as a preferred method for soil stabilization and enhancement due to several compelling reasons:

- Time Efficiency: Stone column installation is known for its efficiency in terms of time. For instance, in the construction of a highway embankment, where soil stabilization is crucial, stone columns can be installed swiftly compared to methods like deep soil mixing or soil nailing. This saves valuable construction time and accelerates project schedules, minimizing disruptions and delays.

- Cost-Effectiveness: Consider a commercial development project requiring soil reinforcement to support the foundation of a high-rise building. Stone columns present a cost-effective solution compared to more elaborate methods like soil grouting or jet grouting. The simplicity of stone column construction translates to lower labor and material costs, contributing to overall project affordability without compromising on quality.

- Availability of Technology: In a large-scale infrastructure project such as a bridge construction over soft soil, the widespread availability of stone column installation technology ensures practicality and accessibility. Contractors and engineers can readily procure the necessary equipment and expertise for stone column implementation, streamlining the construction process and ensuring timely project execution.

- Reliability: In a real-world scenario, consider the construction of a railway track on expansive clay soil prone to settlement. Stone columns have a proven track record of reliability in stabilizing such challenging soil conditions. Their ability to improve soil bearing capacity and reduce settlement risk makes them a preferred choice for railway infrastructure projects worldwide. Engineers and stakeholders can trust in the consistent performance of stone columns, even in varying soil compositions and environmental conditions.

In summary, the efficiency, cost-effectiveness, technological accessibility, and reliability of stone columns make them a preferred choice for soil reinforcement across diverse construction projects, ensuring both structural integrity and project success.

2.2.7.10. Constituent materials of granular columns

The filling material (ballast) must be of high quality (strength) and have controlled and as homogenous as possible particle sizes. It generally consists of natural crushed or rolled gravel

with high mechanical characteristics (Rc> 25 MPa) that is non-expandable and not subject to attrition (Dhouib & Blondeau, 2005).

The main characteristic of ballast is its high drainage potential and its bearing capacity, which is increased by the high percentage of stones. The percentage of fine particles is limited to ensure that the column remains drainable and resistant to internal erosion. The particle size distribution of the material (ballast) must satisfy the following three (3) conditions (Dhouib & Blondeau, 2005):

- d_5> 0,10 mm;
- d_{30}> 10 mm;
- d_{100}> 100 mm.

The physico-mechanical characteristics used for ballast and commonly employed in the construction of stone columns are summarized in Table 2.1.

Table 2.1: Characteristics of ballast for stone columns (Dhouib & Blondeau, 2005).

Characteristics	Ordersofsizes	Remarks
Ballast Dimensions (mm)	40/60 12/40	Wet method Dry method
Crushing index (%)	>80	-
LA (Los Angeles test)	<25–35*	(Standard NCEN 1097-2)
MD (Micro-Deval test)	<20–30 *	(Standard NCIN1097-1)
(LA+MD)	<40–60*	-
Fine content percentage	<5%	-
limiting values *		

Regarding the parameters of the mechanical behavior of ballasted columns, especially the deformation modulus (Ec), they are closely dependent on the type of process used (wet or dry method), degree of compaction during implementation (vibrator performance), and the lateral resistance of the surrounding soil (Dhouib & Blondeau, 2005). Therefore, it is difficult to specify a value for the deformation modulus (Ec) without prior knowledge of all the aforementioned influencing factors.

- The usual values of mechanical parameters accepted for correctly implemented ballasted columns are as follows (Dhouib & Blondeau, 2005):
- Deformation modulus (average over the volume of column):Ec = 60 To 100 MPa,

- Intergranular friction angle: -(rolled material): fc'= 38 degrees
- (material crushed): fc'= 40 degrees
- As for a pulverulent material, the cohesion is zero (C'c =0),
- Poisson's ratio: $\nu = 1/3$,
- Saturated unit weight of the material in place: γ_c = 20 To 21 kN/ m^3.

2.3. Review of previous researches on deferent granular columns

Granular column is a ground improvement technique used to enhance the load-bearing capacity, reduce total and differential settlement, and provide stability to weak soil or fill material. Granular columns involve the installation of cylindrical columns made of locally available stone fill material into compressible soil layers. Several studies have been conducted on the effectiveness of granular column as a ground improvement technique.

2.3.1.Stone Column

The behavior of both single stone columns and groups of columns were examined by (Ambily & Gandhi, 2007b)through experimental studies where they manipulated parameters such as the spacing between the columns, shear strength of the soft clay, and loading conditions. The results of their experiments suggested that no significant improvement was obtained by positioning the columns beyond a spacing of three times the diameter of the column. Although the stiffness improvement factor was found to be unrelated to the shear strength of the surrounding clay soil, it was discovered that it depends on the spacing of the stone columns and the friction angle of the stone aggregates. Figure 2.22 exhibits a typical experimental setup for a single column test.

Figure 2.22 displays the particle size distribution of crushed stones (referred to as aggregates) ranging between sizes 10 and 2 mm, which were implemented to form the stone column. The aggregates exhibit γ_{max} and γ_{min} of 17.3 and 15 kN/m3, respectively, and Table 2 presents additional properties of the aggregate used for the stone column. To determine the angle of internal friction, a direct shear box measuring 300 mm x 300 mm x 100 mm was utilized where the stones were compacted to a density of 16.62 kN/m3, which was the same density achieved during the construction of the stone columns for experimentation. Shearing the stones at a steady rate of 1.25 mm/min was also carried out under ordinary pressures of 75, 100, and 125 kPa, following which the dilation angle was calculated per the suggested method by (Coop & Atkinson, 1993) .The constrained modulus used in the study was obtained by loading the stones

in a cylindrical mold of 150 mm diameter and 180 mm height and at an initial density of 16.62 kN/m3. The Poisson's ratio used was based on typical values proposed by (Bowles, 1988).

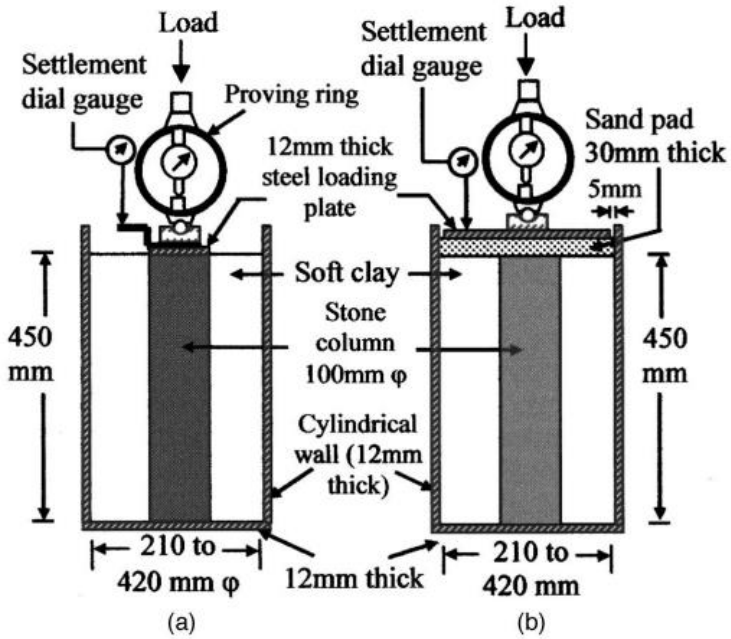

Figure 2.22: Single column test arrangement: **a.**column area loading; **b.** entire area loading (Ambily & Gandhi, 2007b).

Figure 2.23 displays a triangular arrangement of seven columns, for which experimentation was conducted to compare behavior with a single column and investigate stress distribution between the stone column and clay. The area of clay equivalent to the space occupied by seven unit cells is represented by the tank area. To prevent substantial structural deformation, a mild steel plate measuring 16 mm in thickness with stiffeners was utilized to apply the load. The locations of pressure cells affixed along the bottom surface of the loading plate are presented in Figure 2.23.

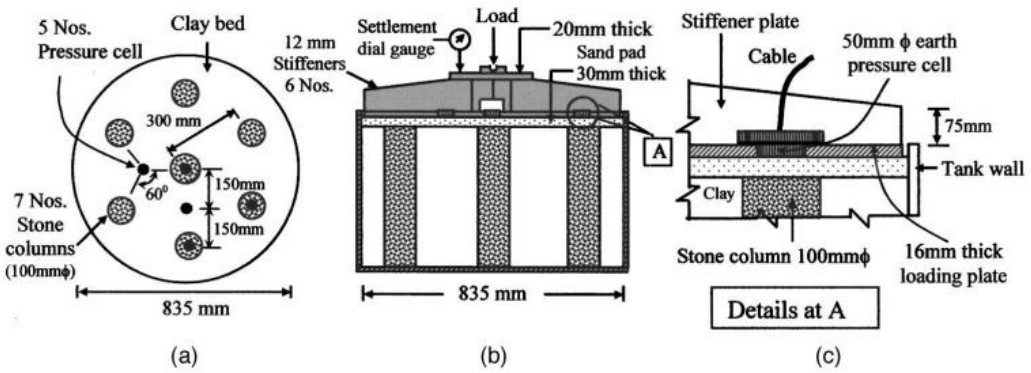

Figure 2.23: Group test arrangement: **a.** plan view; **b.** section of test tank; **c.** details of pressure cell (Ambily & Gandhi, 2007b)

- Materials Properties

This study utilized three fundamental materials: clay, stones, and sand, each characterized by distinct properties.

Clay: The clay, classified as CH, was extracted from the IIT Madras campus. Surface clay, cleared of vegetation, underwent air-drying and pulverization. A 4.75 mm sieve removed coarser particles, and Figure 2.24 displays the particle size distribution. Additional properties include specific gravity (2.6), liquid limit (52%), plastic limit (21%), maximum dry density (16.63 kN/m³), and optimum moisture content (19.26%). Table 2 presents other clay properties at varying moisture levels. The modulus of elasticity was derived from the inverse of the coefficient of volume compressibility, obtained through consolidation tests at pressures ranging from 100 to 200 kPa. For columns' behavior analysis, the constrained modulus from a consolidation test is justified due to the surrounding columns' confinement. Poisson's ratio was determined through a drained triaxial test at the corresponding moisture content.

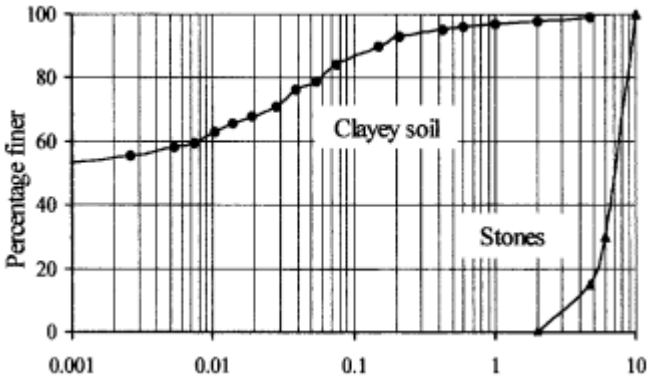

Figure 2.24: Grain size distribution for clay and stones (Ambily & Gandhi, 2007b)

Stones: Stone columns were formed using crushed stone aggregates (particle sizes 10 to 2 mm) with a distribution shown in Figure 2.24. Aggregate properties, detailed in Table 2.2, include max and min densities of 17.3 and 15 kN/m³. Compacted at 16.62 kN/m³, the stones underwent shearing at 1.25 mm/min under normal pressures (75, 100, 125 kPa). The dilation angle was determined following Atkinson's method (1993). The modulus of elasticity was obtained through constrained modulus testing in a cylindrical mold (150 mm diameter, 180 mm height) at an initial density of 16.62 kN/m³. Poisson's ratio adhered to typical values proposed by Bowles (1988).

Sand: The clean river sand used had a size less than 4.75 mm. Table 2.2 reports the angle of internal friction and dilation angle, determined through a direct shear test. Poisson's ratio followed typical values suggested by Bowles (1988).

Table 2.2: Properties of materials used material (Ambily & Gandhi, 2007b)

Material	**w (%)**	**c_v (mm^2/min)**	**E (kPa)**	**μ**	**c_u (kPa)**	**φ (deg)**	**φ' (deg)**	**γ_{dry} (kN/m^3)**	**γ_{bulk} (kN/m^3)**
Clay	25	0.63	5,500	0.42	30	—	—	15.56	19.45
	30	0.99	3,100	0.45	14	—	—	14.60	18.98
	35	1.34	2,150	0.47	7	—	—	13.60	18.38
Stones	—	—	55,000	0.30	—	100	430	16.62	—
Sand	—	—	20,000	0.30	—	40	300	15.50	—

2.3.2. Sand Column

In 2004 (McKelvey et al) his colleagues performed triaxial tests on sand columns modelled in clay as a means of examining the behavior of sand columns under diverse conditions like shifting densities and confining pressures. The findings revealed that the mechanical characteristics of the sand column were impacted by the magnitude of the applied confining pressure. Moreover, the presence of clay was found to have an important impact on said sand column performance, especially with respect to shear strength.

Fine crystal sand that is uniformly graded (D_{50} = 0.25 mm, D_{10} = 0.2 mm, and D_{60} = 0.27 mm) was utilized in the experiment, with a water content of 18% to produce damp but not completely saturated conditions. This sand was meticulously placed into the hole of the specimen in small increments and then compacted by dropping a 175-gram, 25 mm-thick rod from a fixed height of 200 mm. The sand underwent dyeing to differentiate the column of sand from the surrounding clay, and columns ranging from 80 mm to 200 mm in length were produced. While a 200 mm sand column penetrated the complete distance of the clay, smaller columns floated or were only partially penetrating. The mass of the wet sand entering the hole and the depth of the compacted sand layer were monitored consistently, as demonstrated in Figure 2.25-a. This data was used to compute the bulk density of sand, assuming that the column diameter was consistent with the drilled hole's diameter of 32 mm for all experiments. The open circles seen in Figure 2.25-b demonstrate bulk density values that vary from 2300 to 2450 kg/m3, implying that there is significant variation in bulk density which is unacceptable. This

inconsistency can be attributed to the assumption that the column diameters were equivalent to the diameter of the predrilled hole even after adequate compaction.

In accordance with previous clarification, sand columns were inserted into 200 mm high samples of kaolin while still within the consolidation chamber. Both installation methods were employed to place single columns of 80, 120, 160, and 200 mm in length, corresponding to values of Hc/Hs = 0.4, 0.6, 0.8, and 1.0, where Hc denotes the column length and Hs represents the sample length. Additionally, tests were conducted on samples without sand columns (Hc/Hs = 0). Upon installation of the column, the clay-sand composite sample was removed from the consolidation chamber and transferred to a triaxial cell for loading. Samples were consolidated to 100 kPa of effective confining pressure, and a "back" pore-water pressure of 300 kPa was applied to ensure saturation. Drainage was permitted from the bottom of the sample, and pore-water pressures were measured at the top. Undrained loading was then conducted in two ways: (i) The top of the sample was loaded in a similar fashion to a standard consolidated isotropically undrained test (Figure 2.25-a); and (ii) only the area of the top of the sample above the column was loaded, simulating foundation-type loading (Figure 2.25-b). The foundation's diameter was 40 mm. These two loading methods are referred to as uniform and foundation loading, respectively, throughout the subsequent discussion.

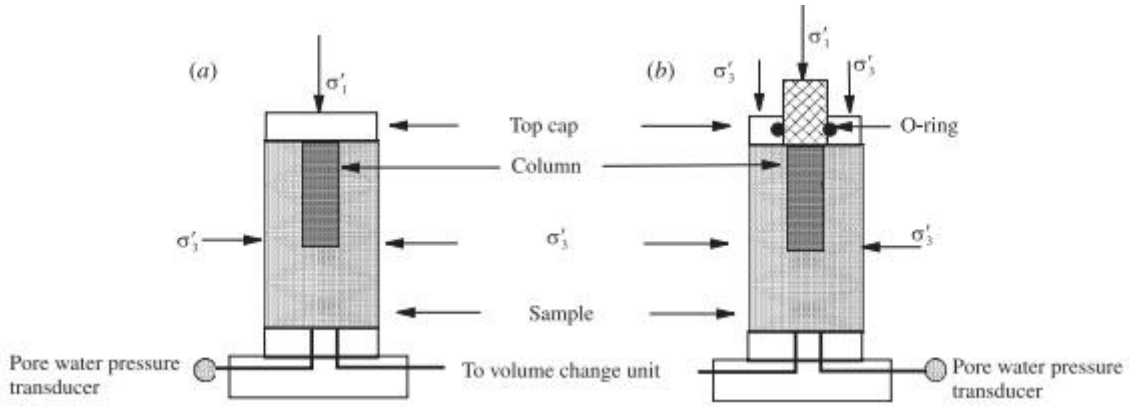

Figure 2.25: Loading pattern in triaxial cell: **a.** uniform loading; **b**. foundation loading (McKelvey et al., 2004).

- **(Sand Fibre Mix) Granular Pile**

The sand-fiber mix is a commonly used combination of sand and fibers in geotechnical engineering applications. The inclusion of fibers in the sand mixture can significantly enhance its mechanical properties, including strength, stiffness, and

deformability. The selection of fiber type and properties relies on the specific performance requirements of the mixture. Several earlier investigations, including (Al-Refeai, 1992; Basu, 2009; Ranjan et al., 1999) have examined the efficacy of Sand Fibre Mix column as a method for ground improvement.

In the (Basu, 2009) study, it was determined that a granular sand pile (GP) with a relative density of 65% should be constructed, corresponding to a dry unit weight of 18.23 kN/m3. However, pilot tests indicated that achieving such a dry unit weight was complicated when utilizing GP with random fibers due to the low specific gravity of the fibers, causing an increase in the mixture volume. As a result, more compaction energy was required to maintain a consistent dry unit weight, leading to GP bulging and GP diameter enlargement. Numerous tests were performed to address this issue, and it was found that adopting a dry unit weight of 18.0 kN/m3 (equivalent to a relative density of 60%) eliminated the problem of bulging. Thus,a dry unit weight of 18.0 kN/m3 for the sand-fiber mixed granular pile was selected for all model tests (Figure 2.26).

a. b.

Figure 2.26:.a- Top view of sand fiber mix pile after construction (upper view). **b-** Longitudinal section of pile after conducting the experiment “Problem of bulging” (side view)(Basu, 2009).

The present experimental work utilized three tanks, two of which were steel tanks for single GP model testing, and one concrete tank was designated for group testing. The thickness of the steel plate for tanks was uniform at 6 mm, and 3 stiffeners were welded onto each steel tank

sheet to prevent buckling. The plan dimensions of the steel tanks were fixed at 525 mm x 525 mm, with depths of 500 mm for d = 50 mm and 650 mm for d = 75 mm. The dimensions of the concrete tank were larger, with a plan size of 1250 mm x 1250 mm and a depth of 500 mm. The concrete tank wall thickness was 250 mm. For the group GP test, the reaction frame was made monolithic with the concrete tank. For single GP tests, the reaction frame was embedded into the ground, and the steel tanks were placed underneath the reaction frame before it was filled (Figure 2.27).

Single GP load tests were conducted on diameters of 50 mm and 75 mm. In the case of GP with an area replacement ratio of a_s = 1.0 (diameter of 75 mm), a 75 mm diameter footing was utilized, whilst for the 50 mm diameter GP, footings with diameters of 50 mm (a_s = -1.0) and 100 mm (a_s = 0.25) were employed. The footings were comprised of mild steel plates with a 15 mm thickness. To measure the footing settlement, 3 L-shaped rods were affixed to the footing at angular intervals of 120° by way of screws.

For load tests on a group of granular piles with an a_s = 0.125, a 250 mm mild steel square plate was utilized, with an 18 mm thickness. Both square and circular plates feature a spherical hole at the center, sufficient to accommodate a steel hull during testing. Four L-shaped rods were fixed to the footing at each corner to determine the footing's settlement. Additionally, two handles were welded to the square footing to facilitate careful placement and lifting. The bases of all footings were rendered rough.

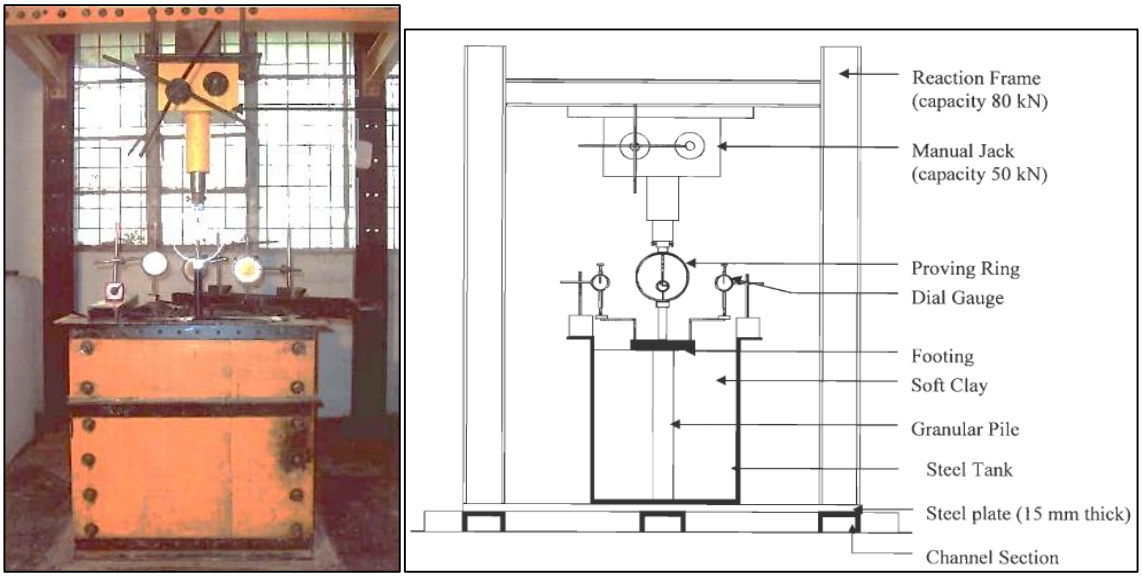

Figure 2.27: Experimental Setup (single GP) (Basu, 2009).

Properties of sand:

The decision was made to utilise coarse sand as the GP material. Sand samples were gathered from different locations, and laboratory tests were conducted to determine its minimum and maximum dry unit weight [IS: 2720 (Part 14) - 1983]. Subsequently, direct shear tests were performed at 60% relative density to derive shear strength parameters.

For the model test, sand with a higher angle of friction and cohesion was selected. Sand from Badshahibag, located 100 km from the campus, was chosen for the model test. Various laboratory tests were carried out on the sand sample to ascertain its fundamental properties. The grain size distribution curve for the sand is illustrated in Figure 2.28, and the sand's properties are detailed in Table 2.3.

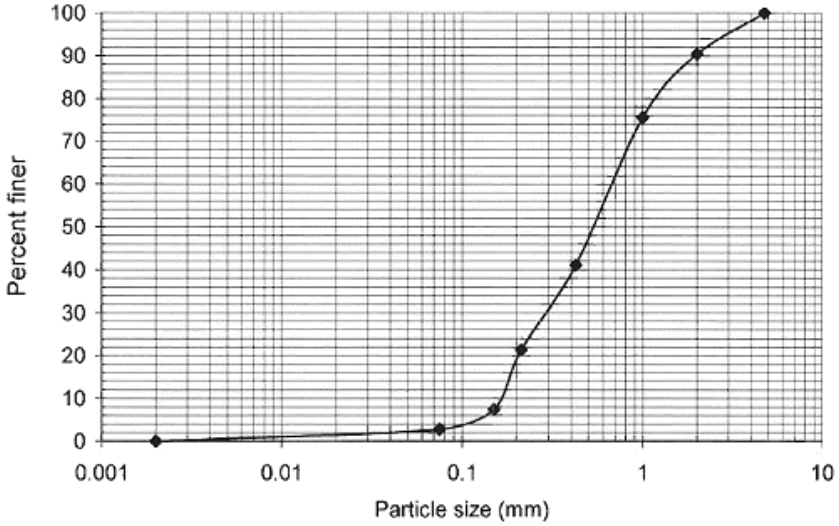

Figure 2.28: Grain size distribution of Badshahibag sand (Basu, 2009).

Table 2.3: Properties of sand (Basu, 2009).

Property	Value
Specific Gravity	2.805
D60	0.68
D30	0.29
D10	0.16
Uniformity Coefficient, Cu	4.25
Coefficient of Curvature, C	0.80
Classification	SP
γ_d, max	19.90 kN/m³
γ_d, min	15.75 kN/m³
Cohesion at 60% relative density	3.45 kPa
Angle of Internal Friction at 60% relative density	40.01°

The sand, collected from the Badshahibag site (8 tonnes), was sun-dried and sieved through a 4.75 mm IS sieve. Particles larger than 4.75 mm were removed, and the portion passing through the sieve was stored in drums for the model test.

Fiber:

Nylon fibers were employed as reinforcement in GP for this study (Figure 2.29). Fiber rolls were procured from the market and cut into various lengths as required. A simple setup was arranged in the laboratory to cut nylon fibers according to the specifications. Tensile strength tests were conducted on the fibers, and the load-elongation curve is presented in Figure 2.30. The properties of the fiber are outlined in Table 2.4.

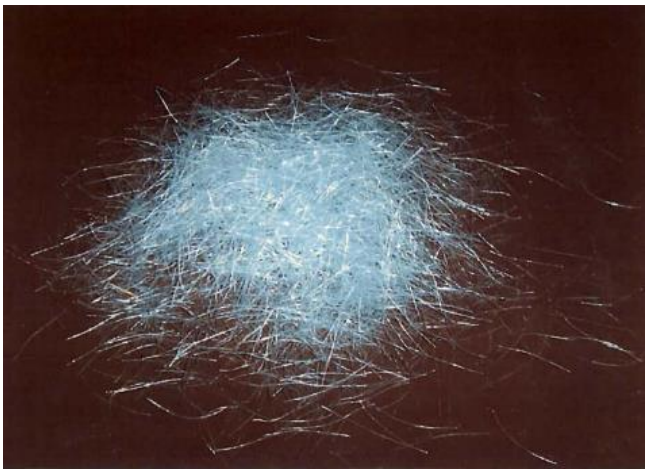

Figure 2.29: Fiber after cutting (Basu, 2009).

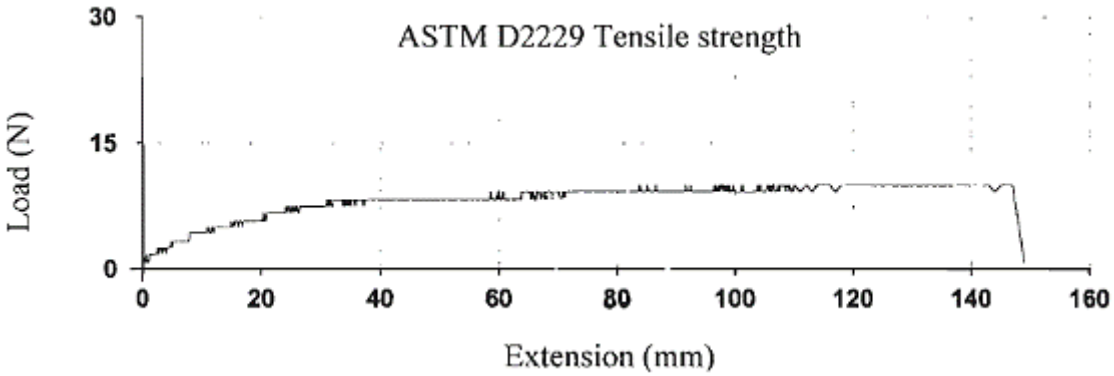

Figure 2.30: Load - elongation curve for fiber (Basu, 2009).

Table 2.4: Properties of fiber (Basu, 2009).

Characteristic	Value
Diameter	0.2 mm
Specific Gravity	0.833
Tensile Strength	0.01 kN

2.3.3. Recycled Aggregate Column

Recycled aggregates encompass materials acquired from dismantled constructions via physical or chemical processing methods, including crushing, sorting, and particle gradation control. These processes serve to transform waste concrete into usable aggregates suitable for use in new construction projects. Recycled aggregates' physical characteristics may differ owing to their diverse origins, resulting in hurdles to their application in new concrete structures. Nonetheless, crushing concrete waste to regulate recycled aggregates' gradation can surmount such complications. Recent research has yielded promising results for using recycled aggregate concrete to construct various structural elements, including beams, columns, beam-column joints, and slabs. Furthermore, recycled aggregates' environmental impact has received attention, with studies being conducted to evaluate their potential pollution and environmental impact via leaching tests and simulations.

Prior studies have contributed significantly to expanding the comprehension and implementation of recycled aggregates in construction. (Marinković et al., 2010) conducted an environmental comparison of natural aggregate cement and recycled aggregate cement, providing valuable insights into the sustainability of the latter. (Petkovic et al., 2004)evaluated the environmental impact of utilizing recycled materials in roadway construction, identifying the potential benefits and obstacles of incorporating recycled materials into such initiatives. (You, 2003) reported on different piling systems' performance, demonstrating the potential of the newly developed recycled aggregate porous concrete pile (RAPP) technique in overcoming traditional system constraints. Moreover, leaching tests and simulations, as illustrated in studies such as those by (Fällman, 1997; Hohberg et al., 2000), have advanced understanding about the environmental hazards associated with recycling aggregates, as well as appropriate tactics for using them sustainably and safely.

On the other hand, (Kim et al., 2012) studied the recycled aggregate porous concrete pile (RAPP), which refers to a concrete pile constructed using recycled aggregates. It was developed to tackle technical problems associated with conventional compaction piling systems and enhance the performance of soft ground. RAPP exhibits a porous structure that transmits load from the soil formation to the pile, improving consolidation through radial drainage. A schematic representation of the RAPP system is depicted in Figure 2.31.

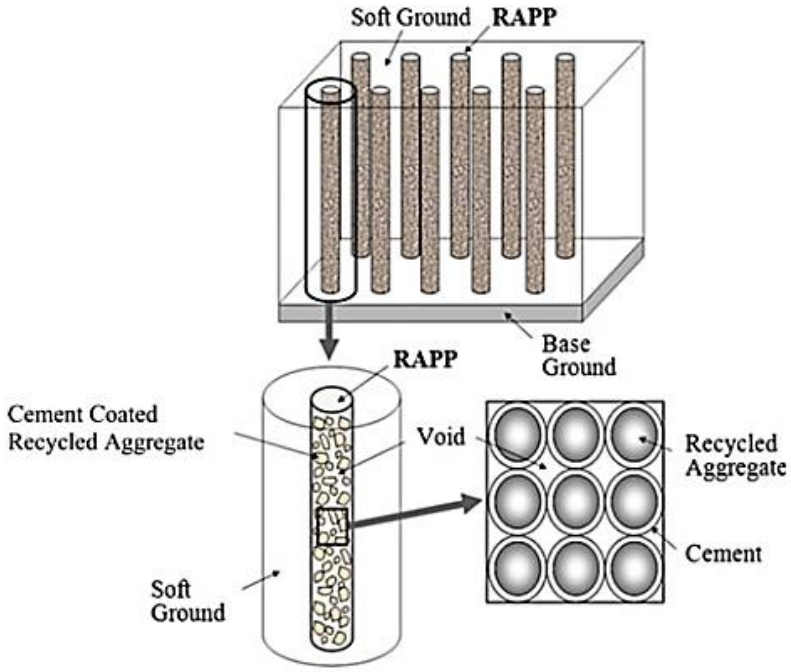

Figure 2.31: Schematic description of the recycled aggregate porous concrete pile system (Kim et al., 2012).

The study utilized a cylindrical mold with two-way drainage and a chrome-plated inside surface to reduce friction. An automatic motor system with a sensor detected unexpected surcharge pressures. Measuring instruments, including pressure transducers and pore pressure transducers, were symmetrically arranged around the RAPP inside the mold, with calibration conducted from preliminary tests. The kaolinite clay was slowly inserted into the mold to preserve the measuring instruments (Figure 2.32).

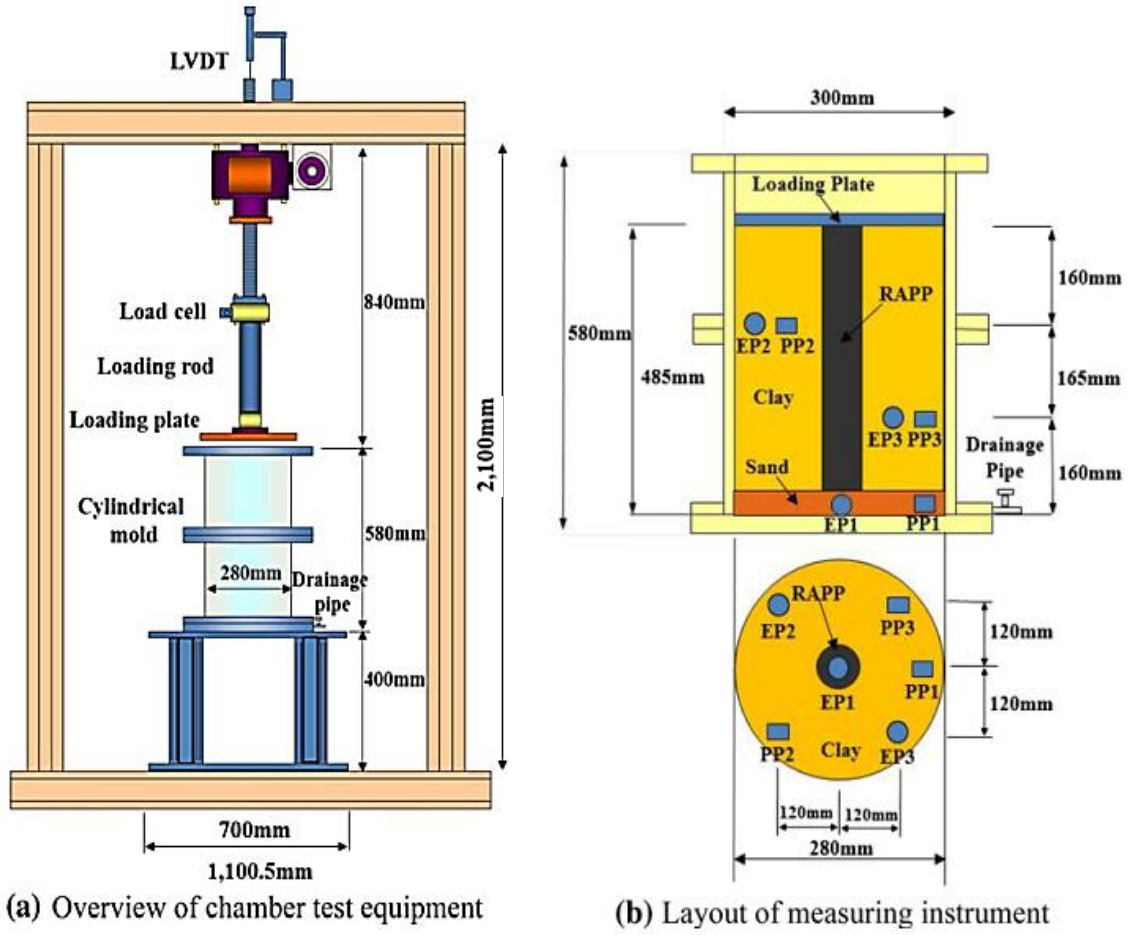

Figure 2.32: Overview of chamber test equipment and measuring instruments: ***a.*** overview of chamber test equipment; ***b.*** layout of measuring instruments (Kim et al., 2012).

In this study, the physical properties of the EPK kaolinite clay used to simulate a soft soil formation in the laboratory chamber test are presented in Table 2.5. These properties, including the Atterberg limits (liquid limit, plastic limit, and plastic index) and compression index in consolidation, are important in determining the engineering behavior of clayey soils. The EPK kaolinite clay is classified as having high plasticity and compressibility by soil classification systems such as AASHTO and USCS.

Table 2.5: Physical properties of kaolinite clay (Kim et al., 2012).

Specific Gravity (GS)	Liquid Limit (WL)	Plastic Limit (WP)	Plastic Index (IP)	Compression Index (CC)
2.62	82.6%	28.6%	54.0%	0.54

Additionally, Tables 2.6 and 2.7 describe the physical properties of the sand used to fabricate the SCP and the recycled aggregate used for the RAPP, respectively. Figure 2.33 compares the particle size distribution curve of the sand and the recycled aggregate obtained by sieve analysis. The sand was classified as well-graded soil, while the recycled aggregate was classified as poorly graded gravels with little or no non-plastic fines.

Table 2.6: Physical properties of sand (Kim et al., 2012).

Specific gravity, G_S	Maximum void ratio, e_{max}	Minimum void ratio, e_{min}	Coefficient of uniformity, Cu
2.64	0.87	0.58	3.71

Table 2.7: Physical properties of recycled aggregate (Kim et al., 2012).

Absolute dry density (g/cm3)	Particle shape decision result ratio (%)	Absorption rate (%)	Attrition weight loss (%)	Stability (%)	Organic material contents (%)
2.28	56.8	3.6	35.4	6.7	0.08

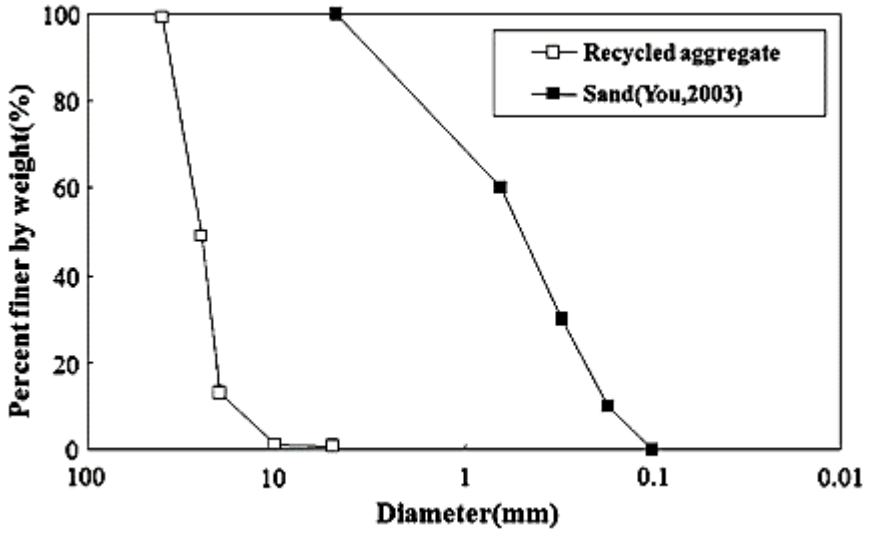

Figure 2.33: Particle size distribution curve of the sand and the recycled aggregate(Kim et al., 2012).

- Recycled aggregate in granular columns

Recycled aggregate in stone columns is a ground improvement technique that involves using recycled materials, typically crushed concrete or reclaimed construction aggregates, in the construction of stone columns. These columns are installed vertically in the ground and serve to reinforce weak soils, improving their load-bearing capacity and overall stability. The use of recycled aggregates aligns with sustainable practices by repurposing materials that would

otherwise be discarded, contributing to environmental conservation. This technique is employed in geotechnical engineering projects to address issues such as settlement, consolidation, and enhancing the performance of foundations. Certainly, here's a Table 2.8 outlining the advantages of using recycled aggregate in stone columns compared to natural aggregate:

Table 2.8: The advantages of using recycled aggregate in stone columns compared to natural aggregate

Feature	Recycled Aggregate in Stone Columns	Natural Aggregate in Stone Columns
Sustainability	Utilizes recycled material, promoting sustainability.	Relies on natural resources, may have environmental impact.
Cost-Effectiveness	Often more cost-effective due to recycling benefits.	Natural aggregate may be subject to market fluctuations.
Resource Conservation	Reduces dependence on virgin aggregates, conserving natural resources.	Requires extraction of natural aggregates, impacting landscapes.
Quality Control	May have variations, but can be controlled through processing.	Natural aggregates may vary, impacting consistency.
Environmental Impact	Low environmental impact due to recycling.	Quarrying natural aggregates can have ecological consequences.
Availability	Widely available, promotes use of recycled materials.	Availability may vary based on local natural deposits.
Engineering Properties	Engineering properties can be tailored through processing.	Natural aggregates possess inherent properties.
Particle Shape and Size	Shape and size can be controlled during recycling.	Natural aggregates come with inherent particle characteristics.
Regulatory Compliance	May align with environmental regulations promoting recycling.	Compliance with regulations may involve sustainable quarrying.

2.4. Conclusion

The literature review on the general characteristics of soft soil reinforcement using stone columns has highlighted the effectiveness of this technique and the advantages it presents compared to other reinforcement methods.

In this chapter, various methods of improving the soft soil are discussed. It defines compressible soils and highlights their different types, including clays, silts, peats, and marls.

The chapter then explores the different applications of soil improvement techniques and focuses on three methods of soil reinforcement: stone columns, geosynthetics, and other reinforcement techniques such as soil nailing, prefabricated vertical drains, compaction grouting, columns of lime-cement-treated soils, and dynamic compaction. The chapter delves into the installation process, technical requirements, and influencing factors that affect stone column implementation, such as diameter, spacing, and arrangement; the coefficient of substitution; the stress concentration ratio; and the settlement reduction factor. It concludes with an examination of the constituent materials for stone columns and the functions and types of geosynthetics, which are used for soil improvement purposes.

Furthermore, the use of geosynthetics to confine the columns has been recognised by several researchers as an effective technique that significantly improves bearing capacity and increases column stiffness, resulting in a substantial reduction of settlements. Geotextiles, with their good resistance characteristics, have been considered more effective than geotextiles for column reinforcement. For these reasons, the geotextile has been used as a confinement element in the parametric study in this work. The different parameters and concepts presented in this chapter will be analysed in further detail in subsequent sections of this work.

Chapter 03:

Numerical Modelling and Behavioural Laws

Chapter 3: Numerical Modelling and Behavioural Laws

3.1. Introduction

The evolution of technology has led engineers to undertake increasingly complex and costly projects that are subject to stringent safety constraints. To carry out these projects, engineers have turned to methods that allow them to simulate the behaviour of complex physical systems, given the complexity of analytical methods for material strength. Conditioned by the progress made in the field of computer science and the advances in mathematics in energy theory, projection methods, and approximation methods, finite element methods have become the most effective numerical methods due to their broad applicability in various industries such as aerospace, nuclear, civil engineering, shipbuilding, mechanics, offshore technology, and more.

Numerical methods, such as the finite element methods, are increasingly used in soil stability analysis. The main advantage of these methods compared to limit equilibrium methods is that they do not require assumptions about the shape and location of the failure surface, as well as the directions and magnitudes of forces. Today, the majority of numerical codes are designed for two-dimensional (plane deformation or axisymmetry) and three-dimensional analyses. Three-dimensional calculations are more computationally intensive than two-dimensional calculations, and the engineer's skill lies in their ability to choose models that are as simple as possible.

In this chapter, we will first provide an overview of the PLAXIS code used in conducting finite element analysis. We will also discuss the type of model and mesh elements used, and provide definitions of the behavioural models employed in this programme.

3.2. Presentation of PLAXIS

The PLAXIS software was originally developed in 1987 by the Ministry of Public Works and Hydrology of the Netherlands with the aim of creating a user-friendly 2D finite element code for analyzing the impact of river dike implementation on the soft clays of the Netherlands. Over time, PLAXIS has expanded its capabilities to cover various aspects of geotechnics. In 1998, the software was developed for Windows, and a 3D version was also created. By 2001, the 3D PLAXIS Tunnel program was released with the primary objective of providing geotechnical engineers with a practical analysis tool, even if they are not experts in numerical methods. Consequently, PLAXIS has gained significant popularity among geotechnical engineers worldwide.

The strengths of PLAXIS are:

- User-friendly interface for data input and result interpretation.
- Automatic mesh generator.
- Comprehensive set of soil behavior laws and the ability to define custom behavior laws.
- Coupling with flow and consolidation calculations.
- Consideration of structural elements and soil-structure interaction.
- Calculation of safety factors.

3.2.1. The finite element code PLAXIS 3D

The PLAXIS finite element code, developed by numerical geotechnical engineers, is considered a cutting-edge tool for both scientific and practical analysis in 2D or 3D pseudo-static analysis. It offers advanced capabilities for non-linear analysis in non-standard elastoplasticity, with the incorporation of interstitial pressures and linear consolidation. Equipped with robust and validated solution methods and algorithms, the software also includes automatic selection procedures to simplify decision-making for users with less experience. In terms of numerical reliability, the code employs high-precision elements, specifically 15-node triangles, and utilizes modern resolution control processes like the arc length method.

From a practical perspective, the hierarchical menu system on the screen enhances usability and convenience, as the operator is not burdened excessively. As the use of manuals is becoming rare, they are now compact and easy to consult. The default options (boundary conditions) make data input easy and fast. Finally, the simplified options for stress initialization and interstitial pressures allow for a direct focus on predicting the behavior of a structure, even if a more refined analysis can be performed later on with the same code and data.

3.2.2 Default options and approximate solutions

The system of default options and specific approximate solutions, which is one of the key features of the geotechnical design tool, is intended to save the operator time, avoid having to make troublesome choices, and ultimately improve the user-friendliness of the software. This system is inseparable from the use of a hierarchical menu. Each branch of the menu is fixed, as it performs a specific, well-defined task, but the diversity of the branches makes it an extremely flexible tool overall.

The default options start with the mesh: The operator can of course specify a very detailed mesh, but if only a general overview is needed, the detailed elements, arranged optimally from a numerical perspective, will be fully generated by the software from a small number of key nodes, with constant control on the screen. In fact, the meshing capability is currently being redesigned to increase its efficiency.

The same applies to boundary conditions in terms of displacements: If they are complex, the engineer will have to specify the subtleties in a precise manner, block by block. On the other hand, if they have a standard nature (zero displacement vector at the base of the domain under study and zero horizontal displacement vector on its lateral faces),the application can be automatically performed (by default) from the menu with immediate control of the result on the screen.

The application of initial stresses due to the weight of the soil can be accurately performed by activating the loading multiplier relative to self-weight. However, in geotechnical engineering, if we know or can estimate a given K_0 state, it can be directly specified. In this case, the soil mass is often slightly unbalanced (incompatibility between K_0 and other mechanical characteristics). The menu allows for a zero fictitious change to rebalance the mass, and then reset the displacements to zero in order to redefine the new origin as the state of the material after gravity application. The K_0 option is particularly interesting (and realistic) in the case of a heterogeneous model of nearly horizontal free surface (e.g., diaphragm wall in soft soil).

Interstitial pressures have been carefully considered in PLAXIS. For those who wish to accurately calculate the field of interstitial pressures in steady-state or transient regimes, it is possible thanks to the porous flow module. However, this operation naturally requires time (operator and machine). If the water table is not too far from horizontal in its initial and final states, we know that the pressure differs little from hydrostatic pressure. Adopting this approximate pressure field makes calculations very simple, as it only involves handling variations in buoyant force; PLAXIS offers this possibility, which is often highly appreciated.

The execution of nonlinear calculations is another example of the flexibility provided by this software. The operator can obviously make their own choices regarding step size, number of steps, interface stiffness, solution method, etc. If they do not wish to make these choices, the software can make them on their behalf, taking into account the experience of the numerical analysts. For consolidation calculations carried out using explicit finite differences over time,

the user can also decide on the time step, or it can be calculated using default options based on known numerical criteria.

The safety factor is a somewhat magical notation in geotechnical engineering, as it summarizes a considerable amount of data in a single piece of information. The classical approach typically evaluates this number based on the theory of limit equilibrium, assuming a proportionate reduction in the mechanical strength of the materials involved, which is clearly not a realistic failure scenario. The same approach, adapted to elastic-plastic finite elements, is used to evaluate the safety factor in PLAXIS. The failure criterion is qualitative and left to the judgment of the observer. In any case, it is based on the displacement level of a control point related to the studied structure. The obtained displacement field is obviously entirely hypothetical.

A finite element calculation provides a massive amount of results: results directly useful to the designer, such as displacements, stresses, interstitial pressures at a given stage of loading, and more mathematical results concerning the progression of the calculation process. All of these results are accessible, depending on whether one is interested in one aspect or another. It is also a tree-like menu system that allows for the selection of desired information.

3.3. Behavioural laws and models used

The choice of behavioural law depends not only on the material being modelled but also on the phenomena being considered. In this study on the bearing capacity of shallow foundations, the behaviour of the soil can vary significantly. It can exhibit different types of behaviour, sometimes acting as an elastic body, sometimes as an elastoplastic or perfectly plastic material.

In general, behavioural laws establish a relationship between the stresses σ and strains ε experienced by the material. They take into account the nature of the material. It is often observed that the stress-strain curve (σ, ε) for many materials consists of two distinct parts: alinear region corresponding to the reversible behaviour of the material (elasticity) and a nonlinear region corresponding to irreversible behaviour beyond the yield point (Figure 3.1).

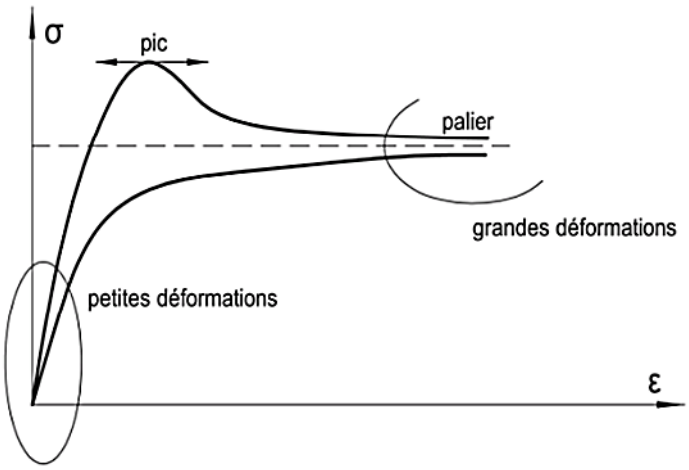

Figure 3.1. Stress-Strain Curve.

The relationships between stresses and strains are often linear and isotropic for deformation calculations. To characterize a material as isotropic, it is defined by two characteristic parameters: the Young's modulus *E* and the Poisson's ratio ν, or the shear modulus *G* and the bulk modulus *K*.

A behavioral law is meaningful if it can represent the various aspects of soil response to applied loads as accurately as possible. Different formulations of behavioral models have been developed to characterize the behavior of soils. In practice, a good behavioral model should be in a sufficiently simple form for practical usability and implementation in a numerical deformation analysis code. It should have a limited number of mechanical parameters that can be easily identified based on common experimental data.

There are numerous rheological laws for soils. In this study, we have chosen representatives from certain classes of behavioral laws that have been used to model shallow foundations with linear elastic behavior in three-dimensional analysis.

3.3.1 Elastoplastic Behavior

The theory of elastoplasticity aims to describe the nonlinear and irreversible behavior of materials. The presence of a yield plateau in the stress-strain curve and the occurrence of irreversible deformations suggest the application of elastoplasticity framework to soils. Furthermore, the elastoplastic model remains relatively simple and is well-suited for implementation in analysis software.

- Strain partitioning: It decomposes the tensor of total strains (ε_{ij}) into the sum of the tensor of elastic strains and the tensor of plastic strains.

- Yield surface: It defines the stress threshold beyond which the material behavior becomes irreversible.
- Plastic flow rule: It describes the evolution of plastic strains.
- Hardening: It allows for the evolution of the yield surface in the stress space, and thus the elasticity domain.

Elastoplastic behaviour can be effectively represented using a one-dimensional model, consisting of a spring with stiffness K to represent the elasticity of the material and a yield pad with threshold S_0 (Figure 3.1).

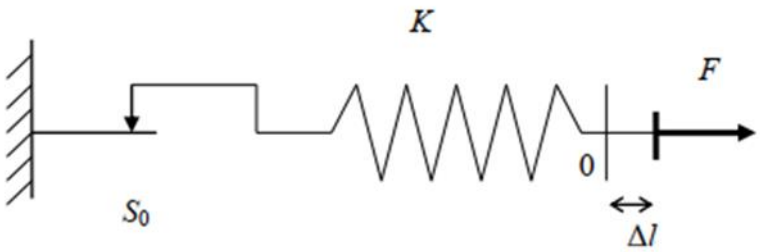

Figure 3.2: One-dimensional model of elastoplastic behavior.

The stress-strain or force-displacement curve obtained is shown in Figure 3.2.

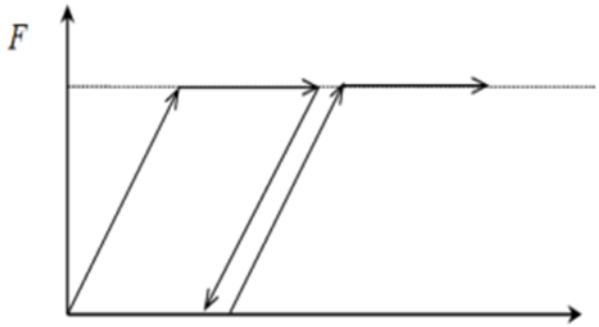

Figure 3.3: Representation of perfectly plastic elastic behavior.

During unloading, the behavior is elastic and reversible. The magnitude of plastic deformation is initially undetermined.

The type of behavior represented by Figures 3.2 and 3.3 is an elastoplastic behavior without hardening. Figure 3.4 represents an elastoplastic behavior with hardening.

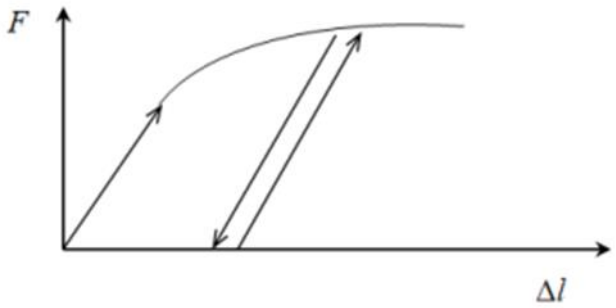

Figure 3.4: Representation of elastoplastic behavior with hardening.

3.3.2. Linear Elastic Model (LEM):

This model corresponds to the application of Hook's Law, which describes linear and isotropic elasticity. It relies on two key parameters: the Young's modulus *E*, and the Poisson's ratio *v*, stipulating the elastic stiffness of the material. However, its capabilities are limited when it comes to accurately simulating soil behavior. This model is primarily suitable for analyzing the response of rigid and massive structures that interact with the soil, and it may also have some applicability in specific scenarios within rock mechanics.

The linear elastic model used in PLAXIS is a classical one. The input data tables require the shear modulus, *G*, and the Poisson's ratio, ν. The advantage of using *G* is its independence from the drainage conditions of the material (G_u = G'), which is not the case with the Young's modulus - the undrained Young's modulus is higher than the drained Young's modulus. It might have seemed logical, if *G*is used as an elastic parameter, to use *K* as the second parameter. However, K_u is infinite (corresponding to νu = 0.5) and it is less commonly used. *G* is actually the modulus measured in pressuremeter tests.

The relationship between the Young's modulus, *E*, and the other moduli is givenby the equations:

$$G = \frac{E}{2(1+\nu)} \tag{3.1}$$

$$K = \frac{E}{3(1+\nu)} \tag{3.2}$$

$$E_{oed} = \frac{(1-\nu)E}{(1-2\nu)(1+\nu)} \tag{3.3}$$

The linear elastic model in PLAXIS can be used primarily to model structural elements made of concrete or metal interacting with the soil. It can also be useful for certain rock mechanics problems.

The related parameters are linked by the equation:

$$E_{actual} = E_{ref} + (z_{ref} - z)E_{increment} \quad \text{avec} \quad z < z_{ref} \tag{3.4}$$

$E_{increment}$: Increase in stiffness [kN/m2/m]

z_{ref}: Depth unit [m]

The equation proposed by(Dias, 1999) to relate these various parameters is represented in Table 3.1.

Table 3.1: Relationships between parameters of linear isotropic elasticity (Dias, 1999).

Couple of parameters used	**Expression of parameters**			
	Shear modulus G	*Young's modulus E*	*Volume modulus K*	*Poisson coefficient* ν
G,E	*G*	*E*	$\frac{G.E}{9G-3E}$	$\frac{E-2G}{2G}$
G,K	*G*	$\frac{9GK}{3K+G}$	*K*	$\frac{3K-2G}{2(3K+G)}$
G,ν	*G*	$2G(1+\nu)$	$\frac{3G(1+V)}{3(1-2\nu)}$	*V*
E,K	$\frac{3KE}{9K-E}$	*E*	*K*	$\frac{3K-E}{6K}$
E,ν	$\frac{E}{2(1+\nu)}$	*E*	$\frac{E}{3(1-2\nu)}$	*ν*
K, ν	$\frac{3K(1-2\nu)}{2(1+\nu)}$	$3K(1-2\nu)$	*K*	*ν*

3.3.3. Linear perfectly plastic elastic model (Mohr-Coulomb)

In this thesis, the proposed model is employed to simulate the behavior of granular backfill with friction. This model incorporates isotropic linear elasticity based on Hooke's law (E, v), a stress surface described by $F(\sigma_{ij})$, and a plastic potential defined by $G(\sigma_{ij})$. It is a 5-parameter model featuring 2 elastic parameters (E, v) and 3 failure parameters (c, φ, and ψ).

The criterion utilized in this model adopts Coulomb's line as the envelope curve on the Mohr plane. Coulomb's line is represented by a straight line equation, defined as follows:

$$\tau = c + \sigma_n \tan(\varphi) \tag{3.5}$$

In the equation, σ_n represents the normal stress and τ represents the shear stress acting on a specific plane.

The Mohr-Coulomb criterion can be visualized in the Mohr plane, as illustrated in Figure 3.5. It should be noted that the intermediate stress does not influence its formulation. When dealing with a material that is purely cohesive ($\varphi = 0$), this criterion is referred to as the Tresca criterion.

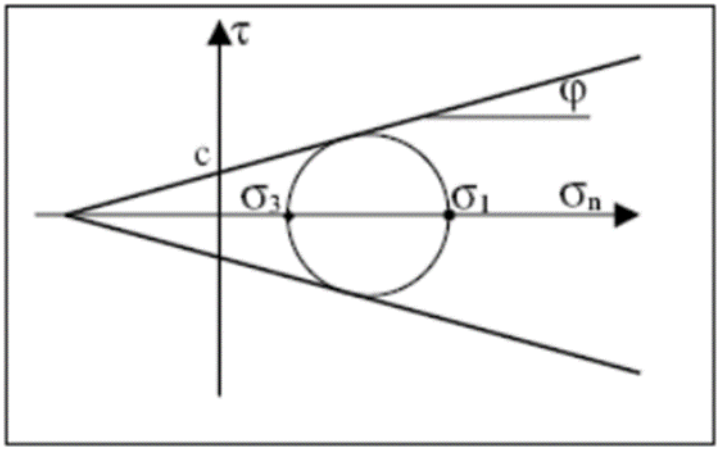

Figure 3.5: Representation of the Mohr-Coulomb criterion in the Mohr plane.

In the principal stress space, the yield function for the Mohr-Coulomb criterion forms a pyramid shape, with the trisectrix serving as its axis. This can be visualized in Figure 3.6. When examining its section in the deviatoric plane, it takes the form of an irregular hexagon, similar to the shape observed in the Tresca criterion. It is worth noting that the Tresca criterion is a specific case of the Mohr-Coulomb criterion when the angle of internal friction φ is equal to zero.

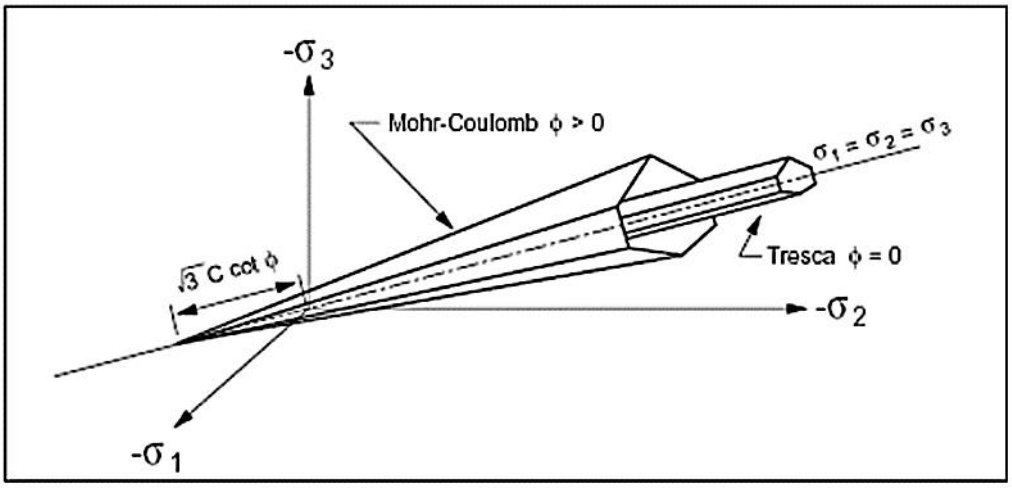

Figure 3.6: Comparison of the Mohr-Coulomb and Tresca criteria in the principal stress space.

The analytical expression for one of the planes of the pyramid in terms of principal stresses can be given by the equation:

$$F(\sigma_1,\sigma_2,\sigma_3) = \sigma_1 - \frac{1+\sin\varphi}{1-\sin\varphi}.\sigma_3 - \frac{2c.\sin\varphi}{1-\sin\varphi} \tag{3.6}$$

with:

- σ_1: major principal stress.
- σ_3: minor principal stress.

An additional parameter that can be significant is σ_t, which represents the tensile rupture stress. Its inclusion introduces a separate criterion, along with its own flow law, thereby altering the original Mohr-Coulomb model that does not account for this parameter.

The equation describes the non-associated flow law and its relation to the plastic shear potential:

$$F(\sigma_1,\sigma_2,\sigma_3) = \sigma_1 - \frac{1+\sin\psi}{1-\sin\psi}.\sigma_3 \tag{3.7}$$

When the angle of friction φ is equal to the angle of dilation ψ, the flow rule is classified as associated. Dilation refers to the volumetric change that occurs concurrently with the deformation of a material under shear. It is quantified by the angle ψ, which represents the ratio of the incremental volumetric plastic strain to the incremental shear plastic strain $\Delta\varepsilon^{pv} / \Delta\varepsilon^{pc}$. The angle of dilation can be determined from triaxial tests or shear box tests. It's determined

from the graphical representation of the variation of volumetric strain ε_v as a function of axial strain ε_1 (Vermeer & De Borst, 1984).The modeling of dilation, based on the Mohr-Coulomb criterion, is shown in figure 3.7.

In materials that exhibit internal friction and follow a Mohr-Coulomb plasticity criterion, an associated flow rule often overestimates the swelling effect that occurs during shear plasticization. The discrepancy between experimental results and calculations has led to the introduction of non-associated flow rules. In these rules, the plastic strains are determined based on a plastic potential that shares the same mathematical form as the yield function. However, instead of using the angle of friction φ, the angle of dilation ψ is employed, where ψ is typically smaller than φ (ψ < φ). This modification helps to improve the agreement between experimental observations and computational predictions by accounting for the reduced degree of swelling during shear-induced plasticity.

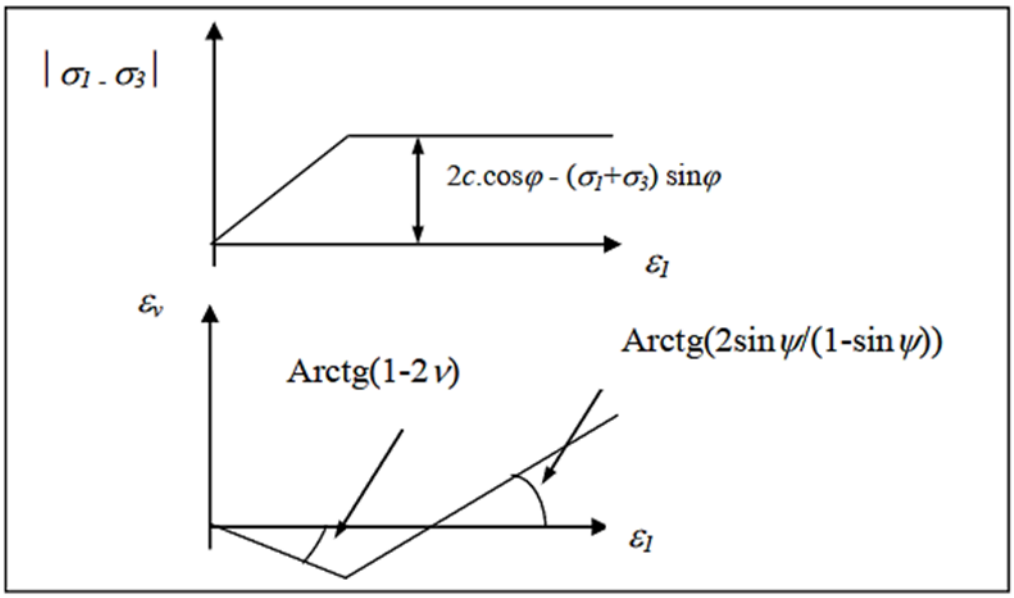

Figure 3.7: Modeling of dilation based on triaxial testing (Vermeer & De Borst, 1984).

It is worth mentioning that research conducted by Vermeer & De Borst in 1984indicated that dilation angles typically range between 0° and 20° for various materials, including soils, rocks, and concrete.

3.3.4. Hardening Soil Model (HSM)

The Hardening Soil Model is a hyperbolic elastoplastic model that is developed based on plasticity theory with shear hardening. This model takes into account both shear hardening and compression hardening to accurately capture the irreversible compaction of soil during initial

compression loading. It is a second-order model that enables the simulation of a wide range of soil types, including sands, gravels, as well as softer soils including clays and silts. By incorporating both shear and compression hardening, the Hardening Soil Model offers an improved representation of the complex behavior exhibited by soils under various loading conditions.

The HSM (Hardening Soil Model) has been developed with the aim of improving upon the limitations of the Mohr-Coulomb model in several key aspects. These improvements include:

- Evolution of Deformation Modulus: Unlike the Mohr-Coulomb model, the HSM considers the nonlinear evolution of the deformation modulus as stress levels increase. This is important because oedometer stress-strain curves for soils do not follow straight lines and exhibit varying stiffness at different stress levels.
- Nonlinear Evolution of Shear Modulus: The HSM acknowledges the nonlinear evolution of the shear modulus. In contrast, the Mohr-Coulomb model often relies on a fixed value, such as the E_{50} modulus. This fixed value is not realistic, as stress-strain curves typically exhibit curvature before reaching plasticity.
- Loading and Unloading Phases: The HSM distinguishes between loading and unloading phases, recognizing that soil behavior can differ during these phases. This allows for a more accurate representation of the soil's response under varying stress conditions.
- Dilation: The HSM accounts for dilation in a defined and realistic manner. Dilation refers to the volumetric expansion that can occur when a soil undergoes shear deformation. By considering this phenomenon

One could say that this model is derived from the hyperbolic model proposed by Duncan-Chang, as it incorporates and improves upon the hyperbolic formulations of stress-strain curves.

Les paramètres spécifiques au modèle HSM sont les suivants :

- **Parametres of Mohr-Coulomb :**

c : cohesion (effective) ; [kN/m2]

ϕ :effective friction angle; [°]

ψ :dilation angle; [°]

- **Stiffness parameters:**

E_{50}^{ref} : secant modulus in a triaxial test; [kN/m2]

E_{oed}^{ref} : tangent modulus in an oedometer test; [kN/m2]

m : Exponent (approximately 0.58 for sands)

- Janbu in 1963reports values of m around 0.5 for sands and Norwegian silts.

- Von Soos in 1990reports various different values in the range 0.5 < m < 1.0.

- **Advanced parameters:**

E_{ur}^{ref} : unloading modulus (default E_{ur}^{ref} = 3 to 4 E_{50}^{ref}) [kN/m2]

ν_{ur} : Poisson's ratio under loading and unloading (default ν_{ur} = 0.2)

p^{ref} : Reference stresses (default p_{ref} = 100) [kN/m2]

K_0^{NC} : K_0-consolidation (default; $K_0^{NC} = 1 - sin\varphi$)

$c_{increment}$: Refer to the Mohr-Coulomb model (default $c_{increment}$ = 0) [kN/m3]

y_{ref}: Depth unit [m]

R_f: Coefficient at failure q_f/q_a (default Rf = 0.9)

$\sigma_{tension}$: Tensile strength (default σtension = 0) [kN/m2]

- **Effort-deformation curves:**

An essential principle underpinning the formulation of the Hyperbolic Stress Model (HSM) is the establishment of a hyperbolic correlation between vertical stress ε_1, and deviatoric stress q, within the primary triaxial loading conditions. Consequently, standard drained triaxial tests demonstrate tendencies towards yield curves that can be aptly characterized by:

$$-\varepsilon = \frac{1}{2E_{50}} . \frac{q}{1 - q/q_a} \qquad pour \quad q < q_f ; \tag{3.8}$$

With:

$$q_f = (\, c.cot\varphi - \sigma_3^{'}) . \frac{2sin\varphi}{1\text{-}sin} \text{ and; } \quad q = q_f / R_f \tag{3.9}$$

q_a: asymptotic value of shear strength. The parameter R_f is analogous to the one introduced by Duncan.

- **The modules:**

The secant modulus in a triaxial test is determined by the formula:

$$E_{50} = E_{50}^{ref}\left(\frac{\sigma_3^{'}}{p^{ref}}\right)^m \text{ with; } \quad p^{ref} = 100kN/m^2 \tag{3.10}$$

For unloading, it is given by:

$$E_{ur} = E_{ur}^{ref}\left(\frac{\sigma_3^{'}}{p^{ref}}\right)^m \tag{3.11}$$

The tangent oedometer modulus is given by:

$$E_{oed} = E_{oed}^{ref}\left(\frac{\sigma_1^{'}}{p^{ref}}\right)^m \tag{3.12}$$

Figure 3.8 provides a visual representation of the HSM (Hardening Soil Model) definitions within the stress-strain coordinate system. This figure serves as a valuable tool to enhance our understanding of the HSM and its implications. It allows us to clearly visualize the relationships between stress and strain parameters and provides insights into the deformation behavior of soils. By referring to Figure 3.8, researchers and practitioners can effectively analyze and interpret stress-strain responses and gain valuable insights into the mechanical behavior of soils under different loading conditions.

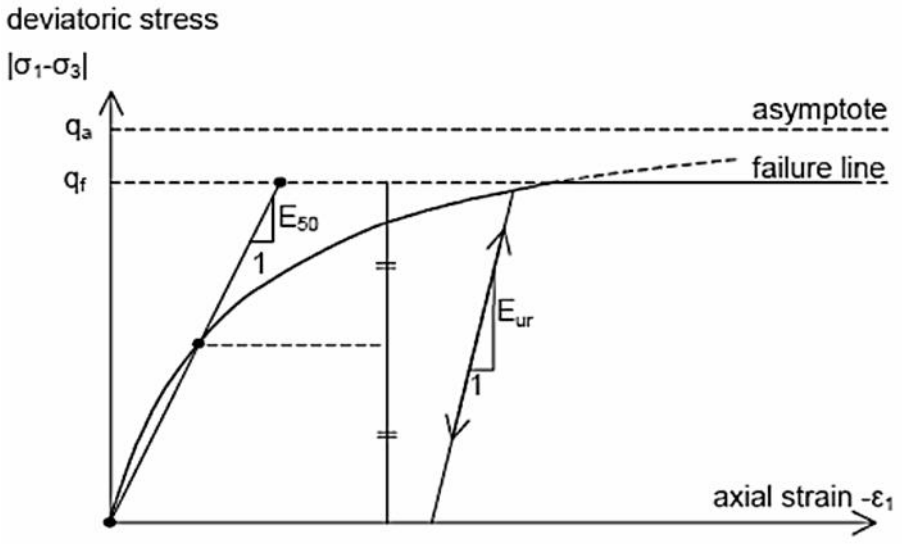

Figure 3.8: Representation of the HSM in the stress-strain coordinate system.

3.3.5. Soft Soil Model (SSM):

The Soft Soil model, based on the Cam-Clay approach, is specifically designed to replicate the intricate behavior observed in soft soils like normally consolidated clays or peat. Developed by (Roscoe et al., 1958), this model considers the phenomenon of hardening that occurs due to the impact of average pressure on clays. The average pressure induces a reduction in water content within the clay, consequently enhancing its strength. The model exhibits an elastoplastic nature, featuring a yield surface. Material behavior remains elastic below the yield surface, whilst crossing the yield surface leads to the manifestation of plastic deformations characterized by non-reversible tendencies.

3.3.6. Soft Soil Creep Model (SSCM):

The Soft Soil Creep model, formulated as a second-order model, operates within the framework of viscoplasticity. This model is specifically designed to capture the time-dependent behavior exhibited by soft soils like normally consolidated clays or peat. Being based on the concept of logarithmic compression, the model incorporates the logarithmic strain measure to account for the deformations occurring over time.

The SSCM takes into account the strain hardening of soft clays but does not consider secondary consolidation, which is manifested by the axial deformation evolution over time in an oedometer test, after primary consolidation has completed.

This deformation evolves logarithmically over time (at least for observable time scales) and is characterized by the parameter C_u. It gives rise to what is referred to as quasi-preconsolidation in soils that have been deposited for a long time (Boulon et al., 2004).

3.3.7. The Jointed Rock Model (JRM):

The Jointed Rock model serves as a specialized anisotropic elastic-plastic model tailored to accurately simulate the behavior of rock formations that comprise distinct layers, exhibiting stratification and specific fault orientations. Plastic deformations are limited to a maximum of three shear directions, also known as shear planes, each of which possesses its unique strength parameters represented by φ and c. The model assumes intact rock to exhibit purely elastic behavior with consistent stiffness properties denoted as E and v. For the stratification direction, it is possible to define reduced elastic properties to account for the variations in behavior along that particular axis.

3.3.8. Modified Cam-Clay Model (MCC):

The renowned critical state model is widely applicable for simulating the behavior of normally consolidated soft soils. This model incorporates a logarithmic correlation between volumetric strain and average effective stress, facilitating a comprehensive representation of the soil's response to various loading conditions.

3.3.9. The NGI-ADP Model:

The NGI-ADP model finds application in analysing the capacity, deformation, and soil-structure interaction induced by undrained clay loading. This model allows for the definition of distinct anisotropic stress forces based on different stress paths, enabling a more accurate representation of the complex behavior exhibited by clay soils under various loading scenarios.

3.3.10. The Hoek-Brown Model (HBM):

The widely recognized Hoek-Brown model, a well-established perfectly plastic elastic model, is frequently employed to simulate the isotropic behavior of rock. In this model, a constant stiffness is assumed for the rock mass, providing a simplified representation of the mechanical properties. Shear failure and tensile failure are characterized by nonlinear stress curves, effectively capturing the nonlinear behavior exhibited by the rock mass under various loading conditions.

3.3.11 User-defined Soil Models (UDSM):

With this option, it is possible to utilize constitutive models other than the standard PLAXIS models. Researchers and practitioners have the flexibility to define and implement their own customized soil models based on their specific requirements and research findings. This feature allows for greater adaptability and accuracy in analyzing and simulating the behavior of soils with unique characteristics or complex material properties.

3.4. Interfaces

Interfaces within the context of this study comprise interface elements that connect to soil elements in a specific manner, as illustrated in Figure 3.9. For 15-node soil elements, the associated interface elements are determined by five node pairs, while for 6-node soil elements, the interface elements consist of three node pairs. Although Figure 3.9 portrays the interface elements with a finite thickness, their representation in the finite element formulation assumes zero thickness, with the coordinates of each node pair being identical.

To define the material properties of the interfaces, a "virtual thickness" is assigned, which serves as an imaginary dimension. This virtual thickness is determined by multiplying the virtual thickness factor with the average element size. The average element size is derived from the mesh accuracy employed in the two-dimensional analysis.

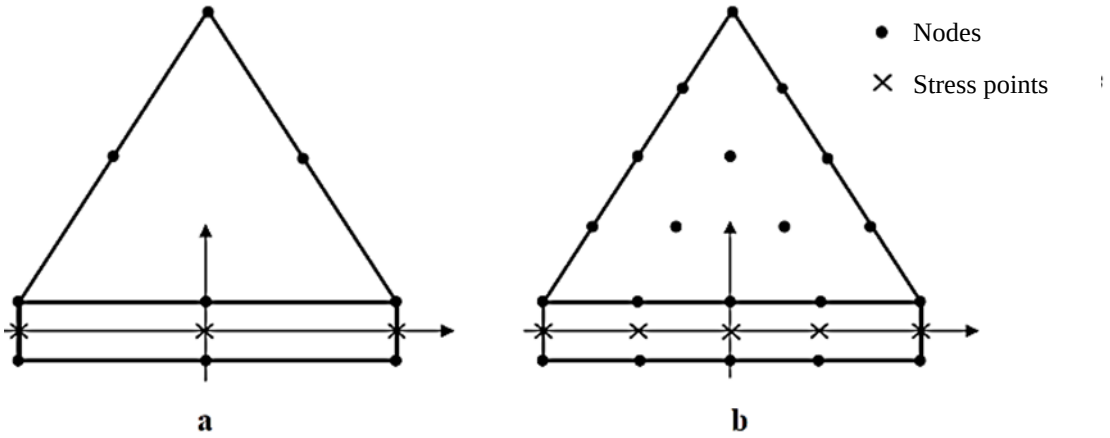

Figure 3.9: The distribution of nodes and stress points in the interface elements and their connection with soil elements: **a.** 6-node element;**b.** 10-node element.

The stiffness matrix for the interface elements is determined using Newton-Cotes integration. In this process, the Newton-Cotes stress points are coincident with the node pairs of the interface elements. Consequently, a 10-node interface element utilizes five stress points, while a 6-node interface element utilizes three stress points.

In the modeling of soil-structure interactions, an elastoplastic model is employed to characterize the behavior of interfaces. The Coulomb criterion is utilized to distinguish between elastic and plastic behavior at the interfaces. Under elastic behavior, small displacements can occur, while plastic behavior allows for permanent sliding to take place. Through this modeling approach, the response of the interfaces can be accurately captured by considering both the elastic and plastic deformation mechanisms.

For interfaces with elastic behavior, the tangential stress τ is given by:

$$|\tau| \prec c_i + \sigma_n . \tan \varphi_i \tag{3.13}$$

And for plastic behavior, the tangential stress τ is given by:

$$|\tau| = c_i + \sigma_n . \tan \varphi_i \tag{3.14}$$

In the given expression, c_i represents the interface friction angle, φ_i denotes the cohesion of the interface, σ_n signifies the normal stress acting on the interface, and τ represents the tangential stress of the interface. The strength properties of the interface are interconnected with the strength characteristics of the corresponding soil layer.

For each dataset, a reduction factor for interface strength (R_{inter}) is designated. The interface characteristics are computed by considering the properties of the associated soil layer and applying the reduction factor. The following rules outline how the interface characteristics are determined in relation to the reduction factor:

$$c_i = R_{inter} c_{sol} \tag{3.15}$$

$$\tan\varphi_i = R_{inter}.\tan\varphi_{sol} \leq \tan\varphi_{sol}$$

$$\psi_i = 0 \quad \text{Where ; } R_{inter} < 1 \quad \text{otherwise it is ;} \quad \psi_i = \psi_{sol}$$

In addition to the Coulomb shear criterion, the previously described tensile suppression criterion applies to interfaces (if not disabled), where σ_t is the tensile strength of the soil.

$$\sigma_n < \sigma_{t,i} = R_{inter}.\sigma_{t,sol} \tag{3.16}$$

Where σ_r is the tensile strength of the soil.

3.5. Geotextile

Geotextiles are slender elements that possess normal stiffness yet lack bending stiffness. They can only resist tensile forces and are commonly employed in modelling soil reinforcements. Geogrids, on the other hand, are characterised by their elastic axial stiffness, denoted as *EA*, which is measured in force per linear meter. The axial stiffness *EA*is typically provided by the geogrid manufacturer and can be obtained from diagrams depicting the elongation of the geogrid versus the applied force in the longitudinal direction. This axial stiffness is calculated as the ratio of the axial force per unit length to the axial deformation (*Δl/l)*, where *Δl* represents the elongation and *l* refers to the length.

$$EA = \frac{F}{\Delta l / l} \tag{3.17}$$

Geotextiles consist of linear elements with two degrees of freedom in translation at each node, namely (u_x; u_y). When employing 15-node soil elements, a geogrid element is defined by five

nodes. Conversely, 6-node soil elements are paired with 3-node geogrid elements. Axial forces are evaluated at the stress points determined through Newton-Cotes integration. These stress points coincide with the nodes of the geogrid element. Figure 3.10 illustrates the positioning of nodes and stress points on the geogrid elements.

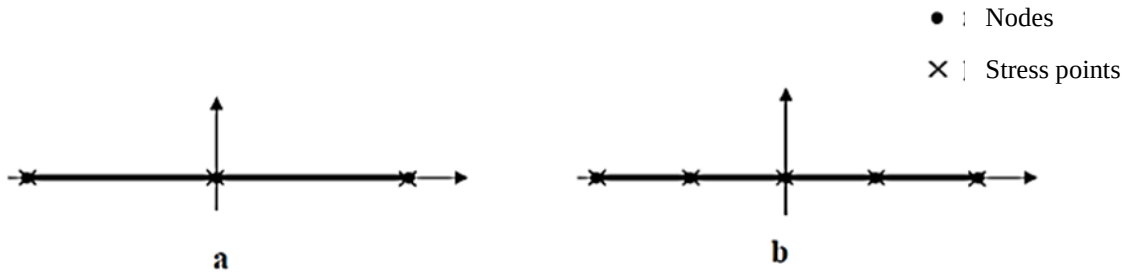

Figure 3.10: The position of nodes and stress points on geogrid elements: **a.** 3-node element;**b.** 5-node element.

3.6. Conclusion

This brief overview of some models used in PLAXIS shows that they are simple enough for their parameters to be determined through conventional geotechnical studies or correlations. These models do not involve any calibration parameters or physically meaningless parameters often found in more sophisticated models. Determining the parameters often requires optimization techniques. The user must focus on two choices: one related to geotechnical engineering in general, and the other concerning numerical simulation.

Determining the geotechnical parameters to input into PLAXIS is no different from choosing "manual" calculation parameters for settlement or stability analysis. Based on partial tests, it is essential to create what can be called a geotechnical field model. Some of the parameters have different expressions but are always related to conventional geotechnical parameters. The least common parameter is likely the dilatancy angle.

Regarding the constitutive behavior laws, we have chosen the perfectly plastic linear elastic model of Mohr-Coulomb for this study.

Chapter 04:

Numerical Analysis of a 3D Unit Cell Model for Soft Soil Reinforced with Different Granular Columns

Chapter 04: Numerical Analysis of a 3D Unit Cell Model for Soft Soil Reinforced with Different Granular Columns

4.1.Introduction

This chapteris based on a number of numerical tests using the finite element method of the PLAXIS 3D software with the elastic-perfectly plastic behavior model and the Mohr flow criterion for all materials.

In the present study, a unit cell model of soft soil treated by three types of granular columns: ordinary stone columns (OSC), sand-fiber mix (SFM) and recycled aggregate porous concrete pile (RAPP) was loaded to failure. Where an extensive study was conducted to investigate the effects of the column type; angle of friction, modulus of elasticity, column length and geosynthetic effective stiffness on the behavior of soft soils.

Results of the numerical tests indicated that the bearing capacity of the columns of recycled aggregates is three times greater than that the columns of natural aggregates. The findings of this research are given in the form of load-settlement graphs, which made it possible to release constructive recommendations for the realization of the work on this technique. Figure 4.1 shows a flowchart of the research methodology.

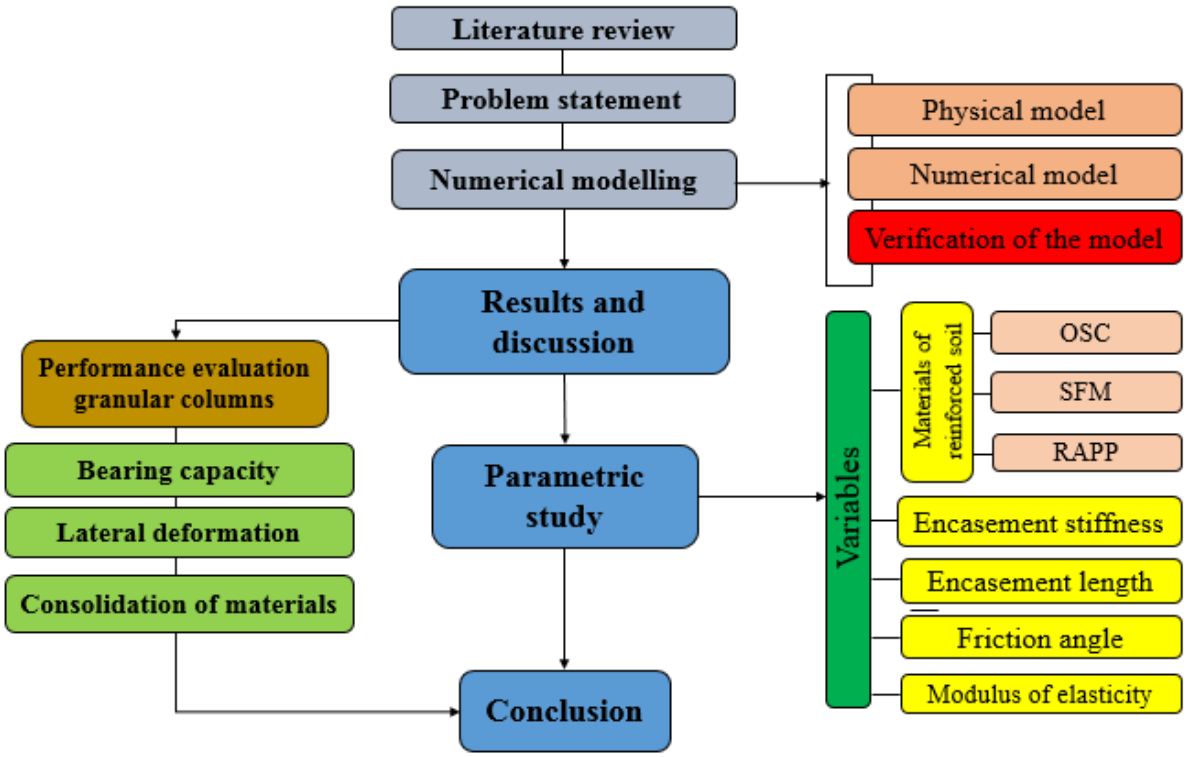

Figure 4.1: Research methodology flowchart.

4.2. Numerical modeling

4.2.1 Presentation of the finite element model

A series of numerical analyses have been carried out using the PLAXIS 3D finite element analysis software (Rajan & Krishnamurthy, 2022; Shooshpasha et al., 2013; Tüter & Ertugrul, 2022) to simulate the three types of granular columns to reinforce soft soil. Figure 4.2 shows the numerical model and mesh configurations used in the analysis. The cylindrical unit cell model can be simplified as a 3D model, where the vertical axis passes through the center of the column. Due to geometry limitation in PLAXIS, therefore (Ambily & Gandhi, 2007b; Hasan & Samadhiya, 2016; Mohanty & Samanta, 2015; Murugesan & Rajagopal, 2006)used a square unit cell equivalent to a cylindrical unit cell. Accordingly, in this study, a square unit cell model was created.

Basu in 2009 formed a stone column of 7.5 cm diameter and 60 cm length in the center of a rectangular tank size (262.5×262.5×600) mm of weak clay and loaded it with a 7.5 cm diameter circular plate perpendicular to the center. In this numerical study, simulations of short-term load tests on granular column were carried out. Assuming that the load applied to the plate is solid; the vertical load is defined as a prescribed displacement. Moreover, the vertical displacements were allowed at the lateral border, but at the bottom borders of the unit cell, vertical and horizontal displacements were constrained. The left, right, and bottom boundaries are treated as impermeable. The pore pressures are set to zero above the ground-water level.

The "coarse element distribution" mode in PLAXIS 3D is generally used when modeling relatively simple geometries or when conducting preliminary analyses. This mode generates a relatively coarse mesh, which can reduce computational time and memory requirements compared to a finer mesh. This mode is used for small, relatively simple numerical models with few details, the coarse mesh may provide sufficiently accurate results for preliminary analyses or design studies (bearing capacity, vertical and lateral deformation curves).

The characteristics and sizes of the mesh in this numerical model are:

- Number of soil elements: 7893
- Number of nodes: 11374
- Average element size: 2.29e-3 m

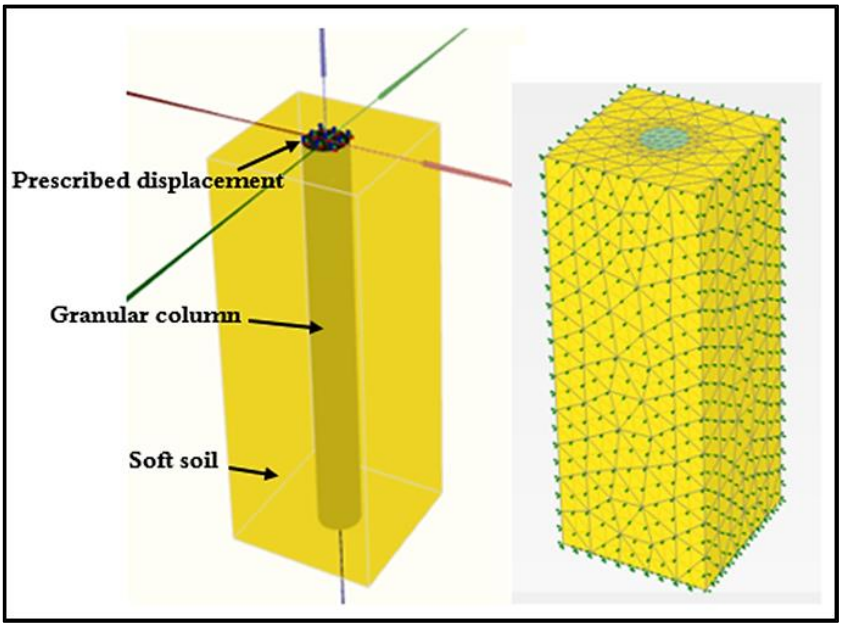

Figure 4.2: The numerical model with the finite-element mesh.

4.2.2. Validation of the numerical model

The Load-settlement curves were compared with the laboratory and numerical curves obtained (Figure 4.3). The model is validated by simulation of the load settlement behavior of the soft soil reinforced by a single SFM column, based on small case model test performed in the laboratory by(Hasan & Samadhiya, 2016). (Basu, 2009)also worked on this model numerically and verified it with the same curves. The validation results were good as the difference between the experimental model (Basu, 2009)is approximately 7.97 % and the numerical model (Hasan & Samadhiya, 2016)is 4.01 %.

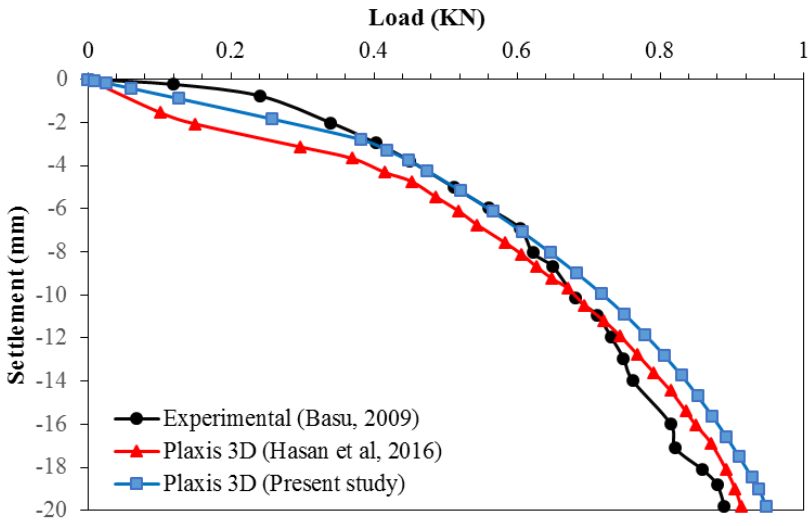

Figure 4.3: Numerical validation through (Basu, 2009; Hasan & Samadhiya, 2016) results.

4.2.3. Properties of materials used

Based on the experimental and numerical studies of (Basu, 2009; Kim et al., 2012; Labed & Mellas, 2016), the mechanical properties of the soils achieved for the studied numerical model were obtained. After verifying the experimental model of (Basu, 2009)in which weak clay and SFM were used, this model was relied upon to follow the evolution of soil behavior by replacing the reinforcement soil SFM with OSC (Labed & Mellas, 2016)and RAPP (Kim et al., 2012).

The linear elastic perfectly plastic Mohr-Coulomb model was adopted for the four types of soils, which was also adopted by many authors, who used it in soft soil reinforced with stone columns (Ambily & Gandhi, 2007b; J. F. Chen et al., 2015; Debbabi et al., 2020; Ghazavi & Nazari Afshar, 2013; Mohanty & Samanta, 2015; Pulko & Majes, 2005). This model is characterized by the volumetric weight (γ), Poisson's coefficient (ν), Young's modulus (E), Internal friction angle of the soils (φ), Dilation angle (Ψ) and the cohesion (c). The values of the parameters used are presented in Table 4.1.

Table 4.1: Material characteristics used for the numerical analysis.

Material properties	Clay	SFM	OSC	RAPP
Previous studies	(Basu, 2009)	(Basu, 2009)	(Labed and Mellas, 2016)	(Kim et al., 2012)
Modulus of Elasticity, E (kPa)	250	6700	40000	16400
Friction Angle φ (°)	0	34.47	38	32.70
Dilation Angle ψ (°)	0	4.47	8.00	2.70
Cohesion (kPa)	16.00	15.55	1	727.9
Poisson's Ratio μ	0.30	0.30	0.30	0.30
Dry Unit Weight γ_d (kN/m^3)	14.90	18.00	17.00	18.46
Wet Unit Weight γ_s (kN/m3)	19.37	19.00	18.00	19.00

4.3. Results and Discussion

4.3.1. Bearing capacity and (lateral/vertical) deformation behavior of soils

Numerical analyses of the unit cell simulation were carried out on the proposed granular column of three soils and the optimization of the behavior is determined based on a reduction in the settlement, vertical and lateral deformation of the column. In addition, note the improvement in the characteristics of each soil in bearing capacity. Considering that the bearing capacity is directly proportionate to the vertical and horizontal displacement. Only bearing capacity curves were dealt with for their importance in this research.

It was mentioned earlier that the vertical loading is applied in the form of a prescribed displacement; therefore, 20 mm was determined as a constant value of displacement for all models presented in this study. Consequently, it was sufficient to determine the bearing capacity and to show the differences between the types of soils. Figure 4.4 shows the FEM results in relation to the load settlement behavior of all soils used; therefore, it was revealed that RAPP gave excellent results compared to OSC and SFM. Thus, it was found that the bearing capacity increased by 88.53, 117.77, and 770.25 % for the OSC, SFM and RAPP columns respectively as compared to untreated soil (US). Furthermore, it was noted that the RAPP gave high results compared to OSC and SFM, with the values reaching 299.62 and 361.60 % respectively, while the comparison between OSC and SFM were almost identical between them by the value of 15.51 %.

The SFM and OSC are effective ground improvement techniques, they may not be as effective as RAPP in certain situations. For example, SFM may not be effective in areas with high water tables, as the water may cause the sand-fiber mixture to wash out. Similarly, OSC may not be effective in areas with soft or compressible soil, as the stone columns may sink or settle over time.

Overall, the difference between RAPP and other ground improvement techniques in Figure 4.4 can be attributed to several factors, including the materials used, the construction method, and the effectiveness of the technique in reinforcing weak soil. RAPP's ability to control permeability, reduce environmental impact, and improve the strength and stability of soft soil make it a promising ground improvement technique for future applications.

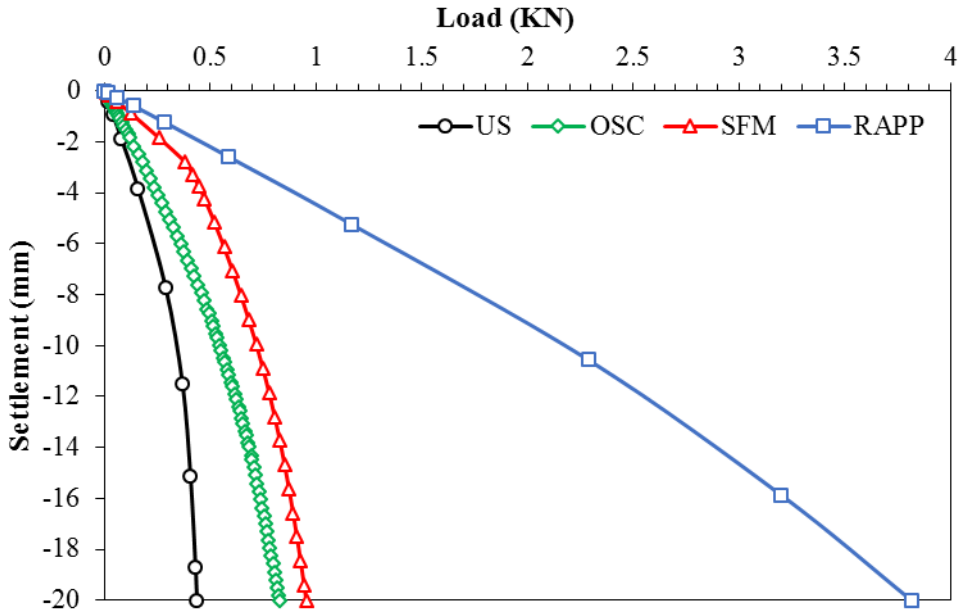

Figure 4.4: Vertical load-settlement behavior of soils.

The lateral deformation of the column occurs when the vertical load is greater than the confined internal stress. When the depth increases, the internal confining stress increases. So we note that a lateral deformation is formed in the top of the column. Knowing that the surrounding soil gives some additional lateral support to limit the expansion of the column (W. E. T, 1995).

Figure 4.5-a shows the distribution of the mesh deformation of the granular column through a depth of 0.6 m, to illustrate the effect of lateral bulge and how important the reinforcing soil used is in reducing it, When the column is of SFM, the bulge in the critical zone is slightly smaller than in the case of the OSC by an estimated 19.05 %. While RAPP achieved as a more effective result compared to SFM and OSC, the swelling value was smaller by 282.88 and 221.62%, respectively (Figure 4.5-b). The value of β (vertical distance between the surface of the column and the maximum value of the lateral displacement U_x) was almost convergent at a value of 4.52×10^{-2}m for the OSC and 4.75×10^{-2}m for the SFM, while RAPP achieved twice the result with a value of 8.27×10^{-2}m. Comparing the lateral deformation curve (Figure 4.5) with the vertical load-settlement curve (Figure 4.4) it turned out that the deeper the distance β was, the greater the endurance, and the less lateral bulge.

In (Figure 4.5-b), the maximum lateral deformation of the Recycled Aggregate Porous Concrete Pile (RAPP) is shown to be 0.001 mm, indicating that there is no lateral deformation

or movement. This can be attributed to several factors, including the high cohesion factor of the material and the careful installation and alignment of the piles.

The high cohesion factor of the RAPP, which is 727.9 kPa according to the information provided, indicates that the material has a high degree of internal strength and resistance to shear forces. This means that the RAPP is able to maintain its shape and stability even under external loads or forces that would cause weaker materials to deform or fail.

Additionally, the RAPP is typically installed with a high degree of precision and care to ensure that it is properly aligned and supported. This helps to minimize any potential for lateral deformation or movement during or after installation.

Overall, the combination of the high cohesion factor of the RAPP and the careful installation and alignment of the piles contributes to the very small deformation of the RAPP in Figure 4.5-b. This indicates that the RAPP is a reliable and effective ground improvement technique for providing stable support to the soil above it.

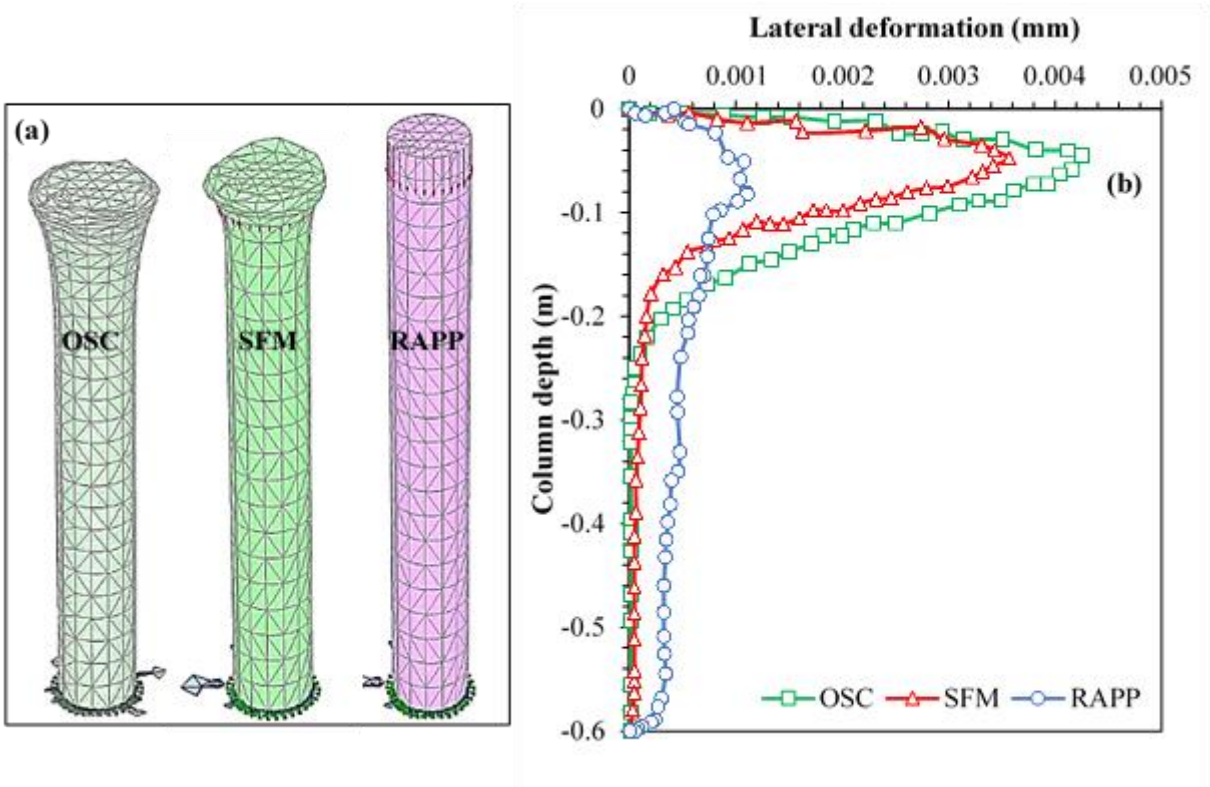

Figure 4.5:a. Deformation of finite element mesh in the columns, **b**. Lateral deformation of the columns.

In addition, to prove the validity of the investigations conducted in bearing capacity and lateral deformation, vertical deformation curves were added as a function of time during one day. Which in turn proved the validity of the model, since the study of the vertical deformation behavior is proportionally consistent with the bearing capacity and lateral deformation. Therefore, it was observed that the results presented in the vertical deformation curves gave preference to RAPP at the expense of OSC and SFM, where the comparison ratio of improvement between RAPP and SFM was 247 %, and RAPP with OSC was 438 % (Figure 4.6).

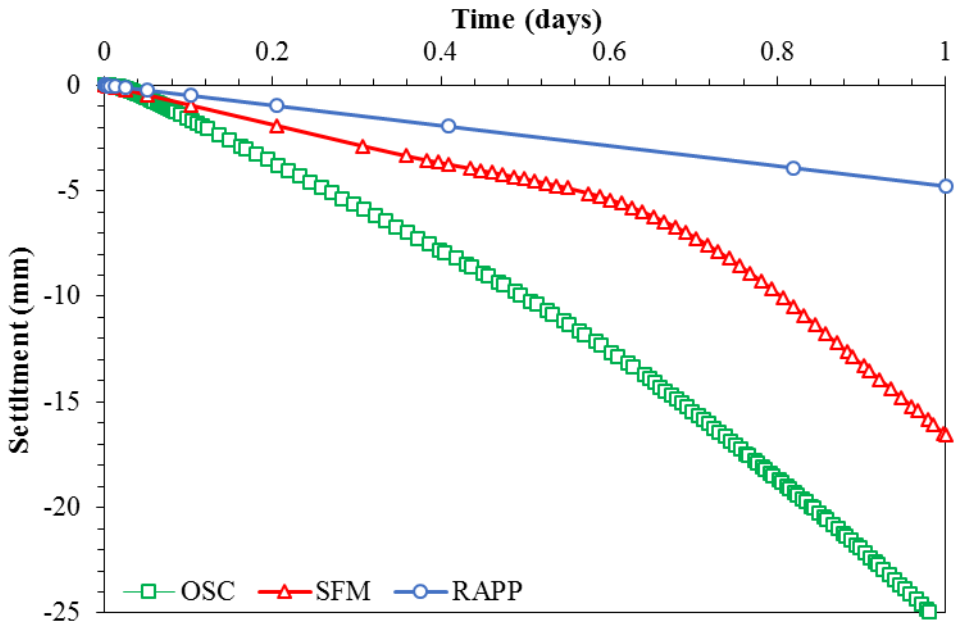

Figure 4.6: Vertical deformation of the columns as a function of time.

4.3.2. The Plastic Point

In Plaxis 3D, the plastic point refers to a specific location or zone within the soil or material where plastic deformation occurs. It is a critical parameter used to analyze the behavior of soils and determine their stability.

In the case output of Plaxis 3D, the plastic point provides information about the location and extent of plastic deformation within the analyzed soil or material. It is represented by colored contour plots or iso-surfaces, where different colors indicate different degrees of plasticity. The plastic point output helps visualize and understand the plastic behavior of soils under loading conditions and assess their stability.

By examining the plastic point output in Plaxis 3D, (Figure 4.7) illustrates the identification of potential failure zones in red color resulting from the effects of applied loads on the behavior of the soil. It was observed that the granular column bears a significant portion of the applied load effects, and it demonstrates the distribution and transfer of loads through it. Regarding the reinforcement materials, it was noticed that the upper third of the column experienced deformation in all three cases, despite the RAPP column yielding better results with consistent deformation, as observed.

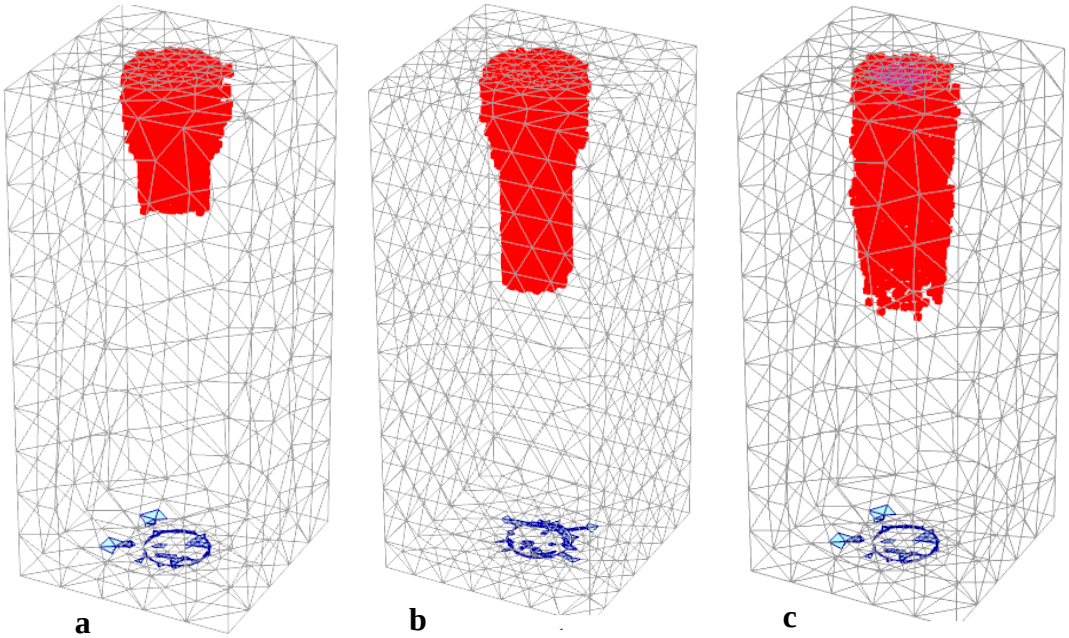

Figure 4.7: The plastic point behaviour .**a.**OSC ,**b.**SFM,**c**. RAPP

4.3.3. The Maximum Shear Stress

The maximum shear stress τ_{max} is a principal stress value that represents the maximum resistance of a material against shearing forces. In the context of geotechnical engineering, the maximum shear stress is often considered in the analysis of soil stability and failure. inPlaxis 3D or any other finite element software, the maximum shear stress can be obtained by analyzing and post-processing the results of a model. The software calculates the stresses within the soil or rock materials based on the applied loads and material properties. To determine the maximum shear stress within a model, you would typically need to review the post-processed results, such as stress contours or stress envelopes, provided by Plaxis 3D. These visualizations can show the distribution of shear stresses within the soil or rock elements and identify the areas

of highest shear stress. It's worth noting that the maximum shear stress can vary depending on the specific conditions and loading scenarios applied in the model (Figure 4.8).

In this study, the behavior of a unit cell model of soft soil treated with three types of granular columns (ordinary stone columns, sand-fiber mix, and recycled aggregate porous concrete pile) was studied. The main goal was to evaluate the effectiveness of these treatments in enhancing the stability and strength of the soft soil. Numerical experiments were carried out to analyze the shear stress levels achieved at failure for each treatment. The results consistently showed that the recycled aggregate porous concrete pile treatment (RAPP) outperformed the other treatments, exhibiting a maximum shear stress τ_{max} of 846.3 kN/m^2. In comparison, the ordinary stone column treatment (OSC) achieved a maximum shear stress of 134.2 kN/m^2, while the sand-fiber mixtreatment (SFM) reached 170.9 kN/m^2. This noteworthy performance of the RAPP treatment can be attributed to the physical properties of the material, specifically its higher cohesion coefficient. These findings emphasize the significance of considering material properties during the design of granular column treatments for enhancing the stability of soft soil.

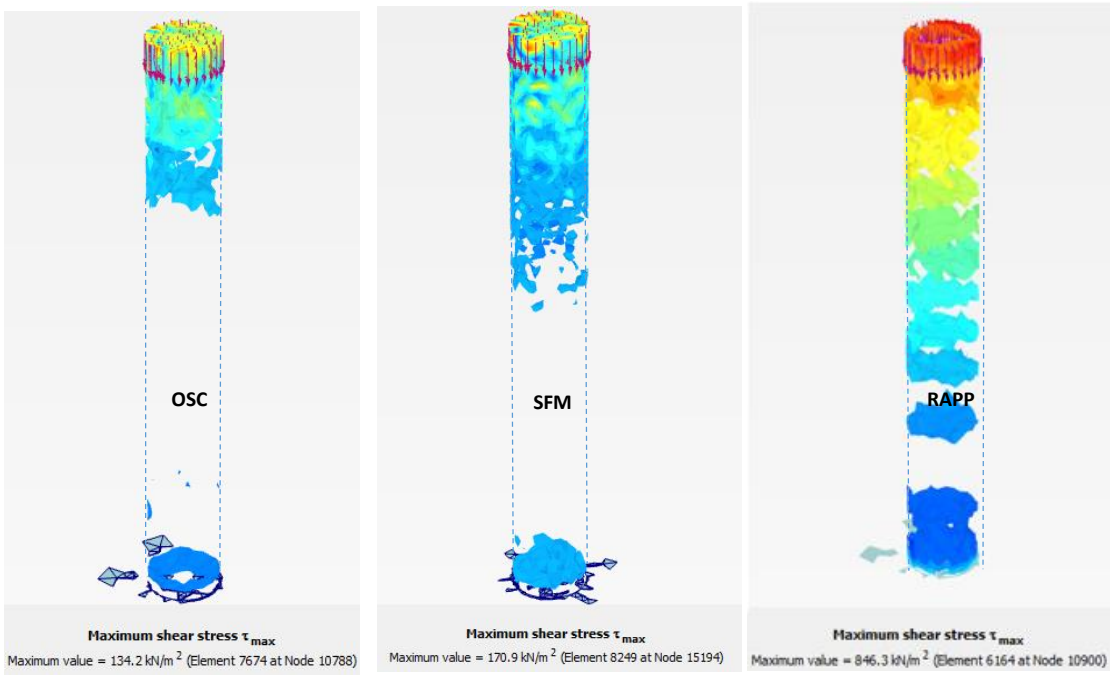

Figure 4.8: The maximum shear stress failure

4.3.4. Parametric study

Investigate impact of input parameters on the behavior of soft soil reinforced by granular columns. A number of parametric numerical analyses have been carried out. Each parameter is isolated and examined separately to determine the effects of the model. The values of the soil

materials and geometric parameters used for the analysis are displayed in Table 4.2, they are selected according to the typical range adopted in the latest studies (Basu, 2009; Boumekik et al., 2021; Mahiyar & Patel, 2000; Petkovic et al., 2004). The results are presented as the load-displacement curves, the parameters analyzed in this study are the Friction angle of the soil column, Young's modulus, Column length and the Encasement stiffness of geosynthetic.

Table 4.2: The values of the material properties used for parametric research.

Category		**Description/Range**	**Base values**
Encasement stiffness, (J), (kN/m)		0, 4.5, 6, 8.5	0
Encasement length, (m)		0.1, 0.2, 0.3, 0.4, 0.5, full encasement	0.6
Friction angle of (φ°)	OSC	35, 38, 40, 45	38
	SFM	30, 34.47, 40, 45	34.7
	RAPP	32.7, 35, 40, 45	32.7
Young's modulus of (E), (kPa)	OSC	30000, 40000, 50000, 60000	40000
	SFM	6700, 8000, 10000, 12000	6700
	RAPP	12000, 14000, 16400, 18000	16400

4.3.4.1. Effect of encasement length

In the search for strengthening weak soils with stone columns, the study of the change in column length is often resorted to or more specifically studying floating columns. These studies mostly summarize the search for the ideal length of the corresponding column for optimal bearing capacity. Thus, the evolution of the change in the column depth from 0 to 0.6 m was studied, while studying the importance of each soil in further improving the bearing capacity.

Figure 4.9 shows the load-settlement curves of three numerical models that vary by column type (a. OSC b. SFM c. RAPP). It was noted that the ideal length for OSC and SFM was 0.2 m. That is, it has achieved the maximum value of the bearing capacity achieved at the total length of the column with a value of 0.827 KN for OSC and 0.955 KN for SFM. While RAPP reaches above these values by only 1.05 KN with a length of 0.1 m. Furthermore, it has been observed that RAPP gives excellent results the greater the depth of reinforcement, the percentage increase between each of the two consecutive lengths were estimated at values ranging from 16 to 54%.

As a result, it can be said that RAPP achieved better results than SFM by 6.63 times, and OSC by 8.88 times, in the percentage of increase in bearing capacity at the total length of the column.

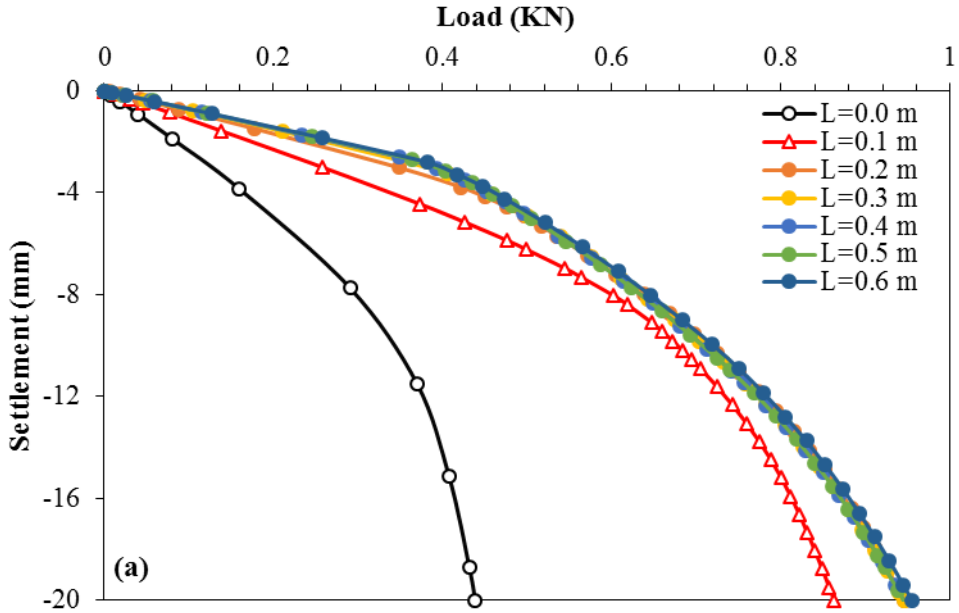

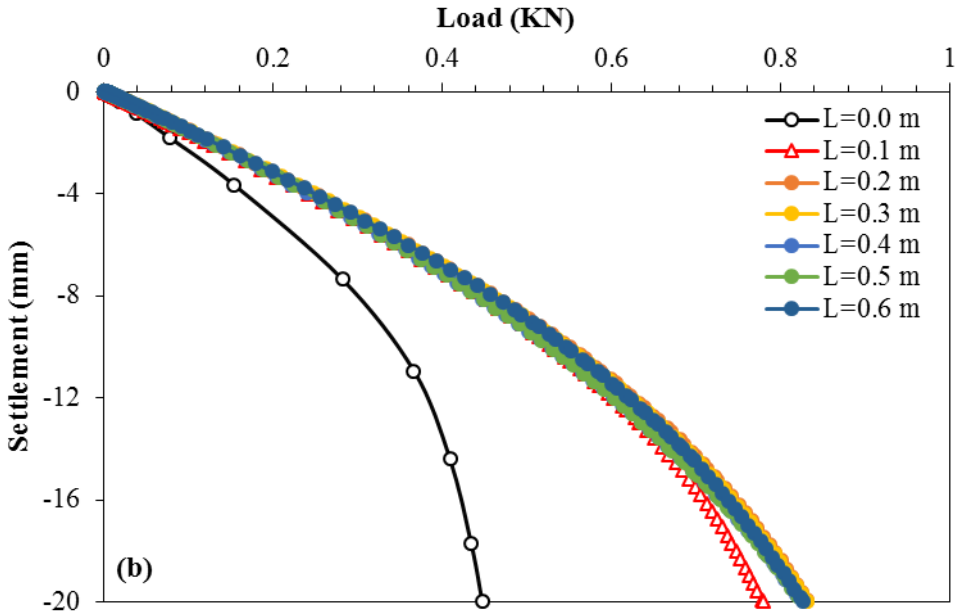

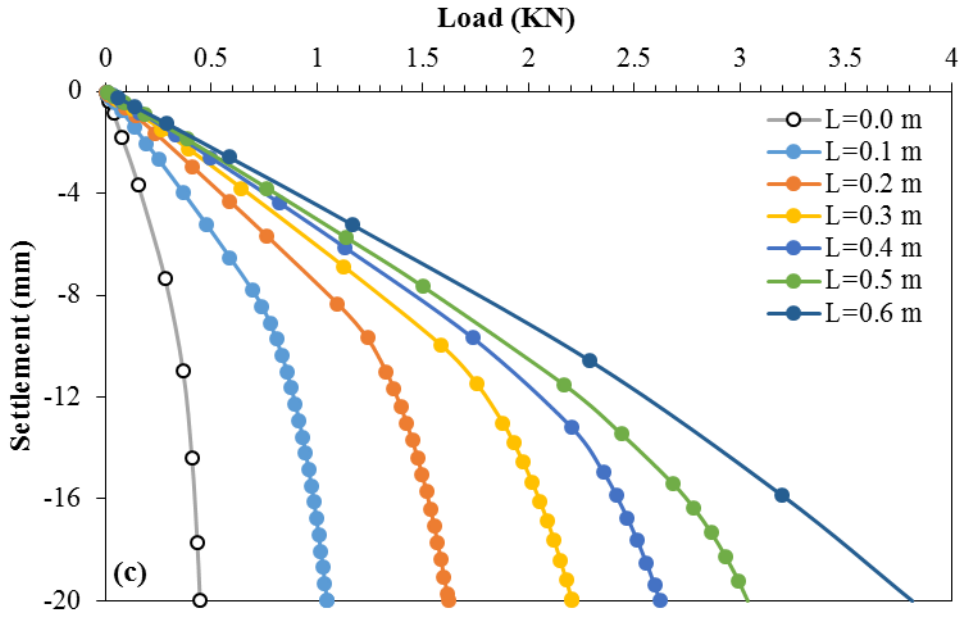

Figure 4.9: Effect of encasement length on vertical load intensity settlement behavior of column: **a.** OSC, **b.** SFM, **c.** RAPP.

4.3.4.2. Influence of the stiffness of geosynthetic encasement

Geosynthetics were modeled using the PLAXIS 3D code using the geotextile-type structural elements which behaves as an isotropic, linear elastic material without failure limitations. The boundary conditions of the unit cell only allow deformations along the vertical direction (Figure 1). The vertical and horizontal displacements at the base of the unit cell were restrained. Using the geotextile element requires the specification of mechanical and geometric characteristics, Therefore, in this research, the properties of the PLAXIS 3D geotextile were determined using the following parameters: elastic, isotropic material type and tensile stiffness J , Knowing that the geotextile was confined laterally along the column.

The tensile strength of geosynthetic material has been reduced in accordance with the scaling law proposed by(Hasan & Samadhiya, 2016; Iai, 1989). Moreover, several researchers (Ghazavi & Nazari Afshar, 2013; Gniel & Bouazza, 2009; Murugesan & Rajagopal, 2006; Pulko & Majes, 2005)employed geosynthetic materials with tensile strengths ranging from 1.5 to 20 kN/m. Geogrids and geotextiles having tensile strengths of 4.4 - 8.96 kN/m respectively were used in the laboratory study. Based on the parametric study, it was noted that there is a distinct effect and an excellent scientific value when using geotextile with each type of column. The findings showed that geotextile encasement with stiffness J improved bearing capacity, according to the curves given in Figure 4.10.

Previously, it was found that the reinforcement with SFM is slightly better than OSC, on the contrary when adding the geotextile to the column; the latter gave better results than SFM (Figure 4.10-a,b). For the OSC, as compared with a stone column devoid of geotextile encasement J= 0.0kN/m, the bearing capacity is improved by 38.34, 45.94 and 57.47% when the column is surrounded in geotextile with stiffness of J= 4.5,6,8.5kN/m, respectively. Moreover, for the OSC at the same values of stiffness (J), the bearing capacity was 22.32, 26.55 and 32.93%, respectively. More importantly, clear that RAPP achieved better results than OSC and SFM even if the RAPP was without geotextile encasement. However, it should be mentioned that RAPP with encasement has achieved a maximum approximate value at J = 4.5kN/m estimated at 12.00% in comparison to a column devoid of geotextile encasement (Figure 4.10-c).

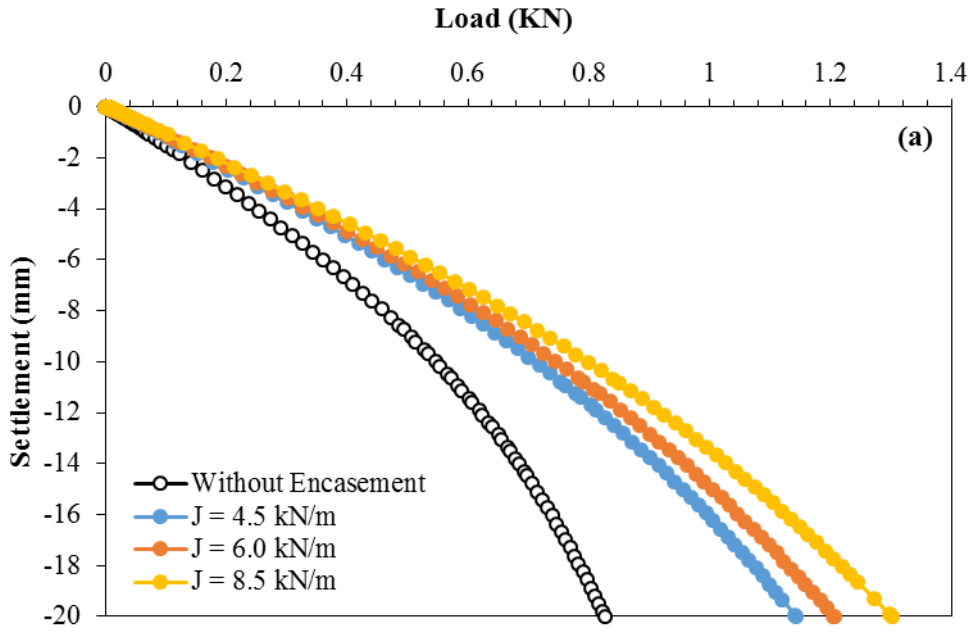

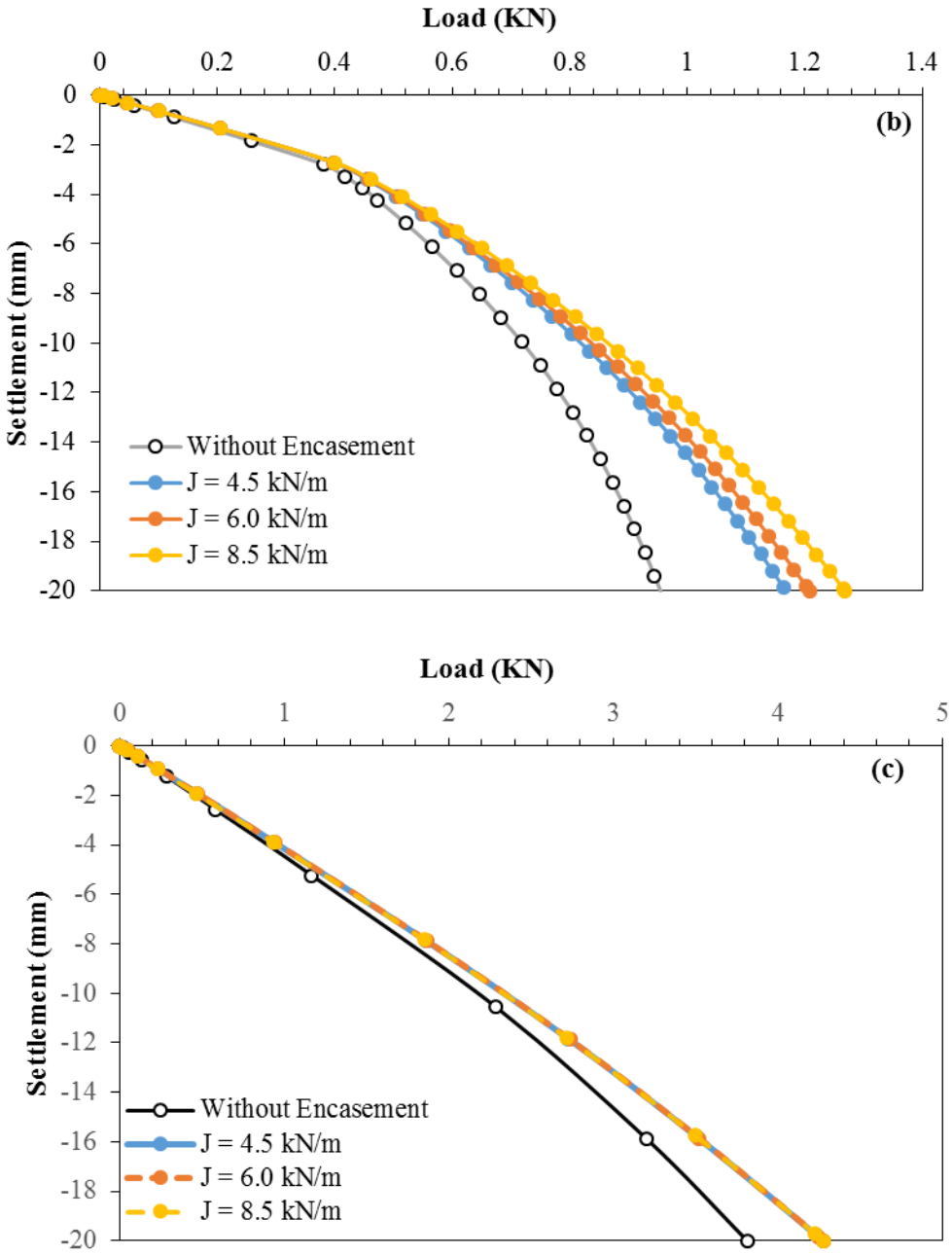

Figure 4.10: Effect of the stiffness of geosynthetic encasement on vertical load intensity settlement behavior of column: **a.** OSC, **b.** SFM, **c.** RAPP.

4.3.4.3. Effect of friction angle of reinforcement materials

To investigate the impact of column material friction angle on column bearing capacity. Analyses were conducted with a series of four angles of friction for each type of column, OSC (38, 40, 42, 45°), SFM (34.47, 40, 42, 45°) and RAPP (32.7, 35, 40, 45°).

Figure 4.11 shows the curves of the loading of columns as a function of settlement for various friction angles of the column material. It can be observed that the more the bearing capacity,

the greater the friction angle value. The difference between the bearing capacity of angle 38° and angle 40° in OSC is estimated to be 6.26%, (38°,42°) is 18.36% and (38°,45°) is 35.12% (Figure 4.11-a). In contrast, SFM achieved better results than OSC. Where the ratio of the difference between angles in the bearing capacity was as follows, (34.47°,40°) is 32.64%, (34.47°,42°) is 39.72% and (34.47°,45°) is 51.64% (Figure 4.11-b). This shows that the friction angle of the granular column (OSC and SFM) has an important role in improving the bearing capacity.

On the other hand, the curves of the loading of RAPP columns as a function of settlement for different friction angles (35°, 40°, and 45°) are shown. It can be observed that all the lines overlap on each other, indicating that the bearing capacity of RAPP columns is not affected by changes in the friction angle (Figure 4.10-c).

This is because RAPP has a high cohesion factor of 727.9 KPa, which means that the material is able to resist shear forces without relying on friction between particles. Cohesion is a measure of the internal strength of a material that arises from the attractive forces between its particles. In contrast, friction is a measure of the resistance to movement between particles that arises from the contact forces between them. Since RAPP has a high cohesion factor, it is less dependent on the friction angle of the material for its bearing capacity. This is in contrast to granular materials like OSC and SFM, which are more dependent on the friction angle for their bearing capacity. Therefore, the results in (Figure 4.11-c) suggest that when using RAPP as a column material, the friction angle may not need to be a major consideration in the design process. However, other factors, such as the elasticity module and durability of the material, should still be taken into account when designing RAPP columns.

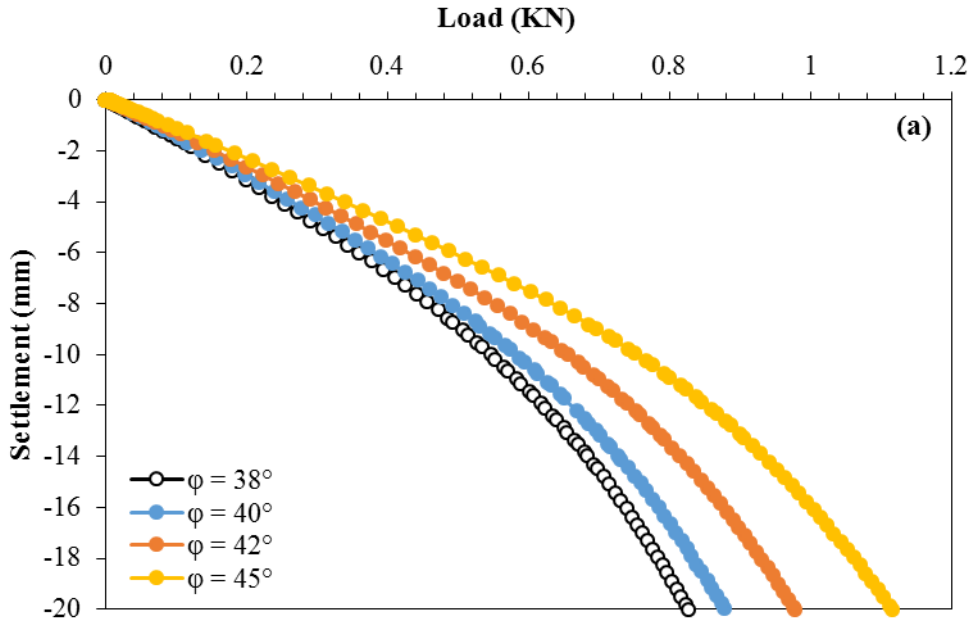
Load (KN)
0
0.2
0.4
0.6
0.8
1
1.2
Settlement (mm)
0
-2
-4
-6
-8
-10
-12
-14
-16
-18
-20
(a)
φ = 38°
φ = 40°
φ = 42°
φ = 45°

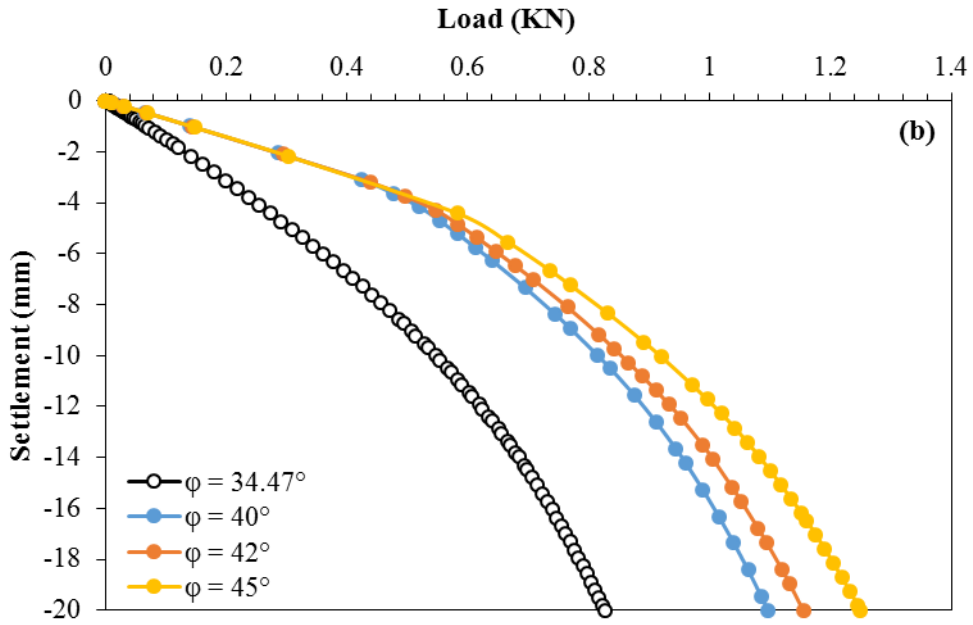
Load (KN)
0
0.2
0.4
0.6
0.8
1
1.2
1.4
Settlement (mm)
0
-2
-4
-6
-8
-10
-12
-14
-16
-18
-20
(b)
φ = 34.47°
φ = 40°
φ = 42°
φ = 45°

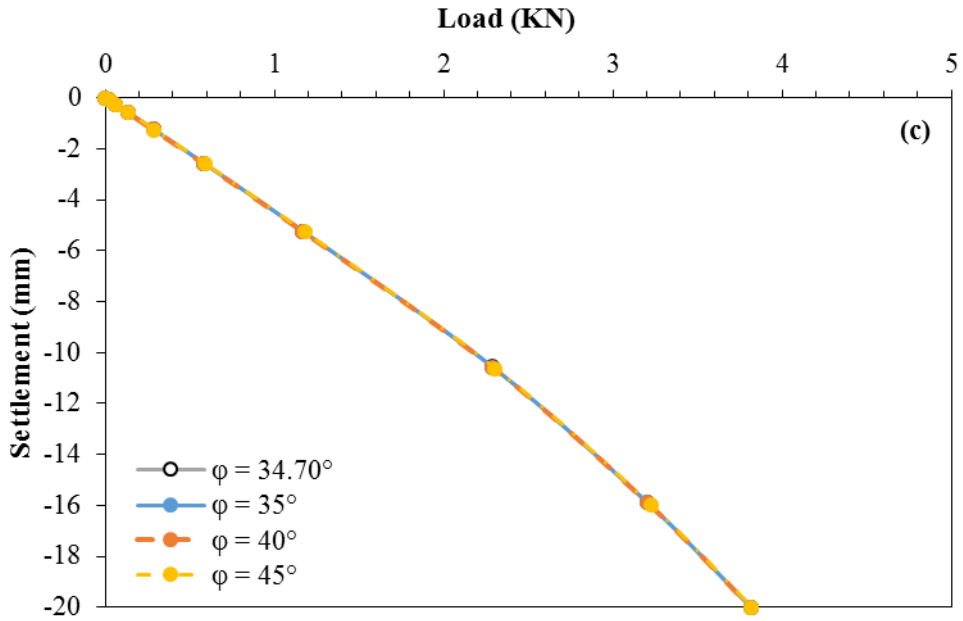

Figure 4.11: Effect of friction angle on vertical load intensity settlement behaviour of column: **a.** OSC, **b.** SFM, **c.** RAPP

4.3.4.4. Effect of Young's module of reinforcement materials

One of the main differences between the three soils used in this reinforcement is the value of Young's coefficient. The elasticity module range for OSC is from 30 to 60 MPa, SFM from 6.7 to 12 MPa, and RAPP from 12 to 18 MPa. These values are used to highlight the effectiveness and effect of Young's modulus in improving the bearing capacity of the soil.

In (Figure 4.12-a), the curves of the loading of OSC columns as a function of settlement for different values of Young's modulus are shown. It can be observed that all the lines overlap on each other, indicating that the bearing capacity of OSC columns is not significantly affected by changes in Young's modulus.

This result may be due to the fact that the range of Young's modulus for OSC is relatively narrow (30-60 MPa), and therefore, the increase in stiffness from one value to another was not significant enough to have a noticeable impact on the bearing capacity. Additionally, the material properties of OSC, being natural stone, may also contribute to the insensitivity of bearing capacity to changes in Young's modulus. As is well known, When working on small numerical and experimental models, it is common practice to scale down the properties of materials, including the Young's modulus. Scaling down the Young's modulus can be necessary when working on small-scale models, as the actual Young's modulus of the material may be

too large to be accurately modeled or measured at the reduced scale. Additionally, scaling down the Young's modulus can help to reduce the complexity of the model.

It is important to note that while the results in Figure 4.12-a suggest that Young's modulus has little impact on the bearing capacity of OSC columns, other factors such as the friction angle and density of the material are still important considerations in the design of OSC columns.

On the other hand, the results shown in (Figure 4.12-b) showed that the increase in Young's modulus of SFM gave a slight effect of 1%. While, the data in (Figure 4.12-c) showed that the change in the value of Young's module for RAPP gave a good effect in increasing the bearing capacity. It can be seen that the higher the elasticity module value, the greater the bearing capacity. Where the ratio of the difference between modules in the bearing capacity was as follows: (12000; 14000) kPa is 10.06%, (14000; 16400) kPa is 10.77% and (16400; 18000) kPa is 6.34%. As a result, the stiffness of RAPP plays an important role in soil improvement. Thus, the properties of the recycled materials in the column have a direct impact on the behavior of the granular column.

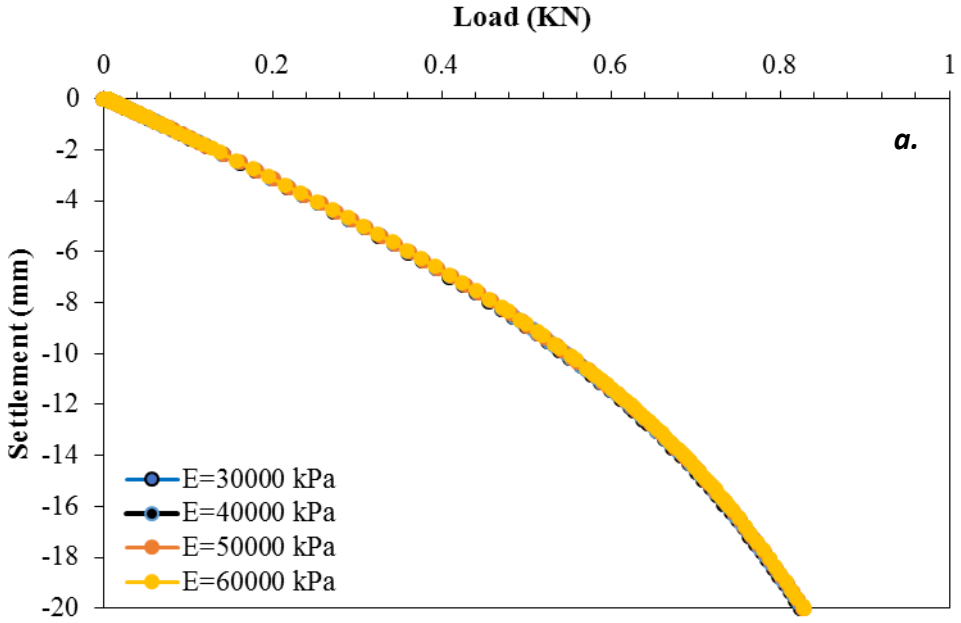

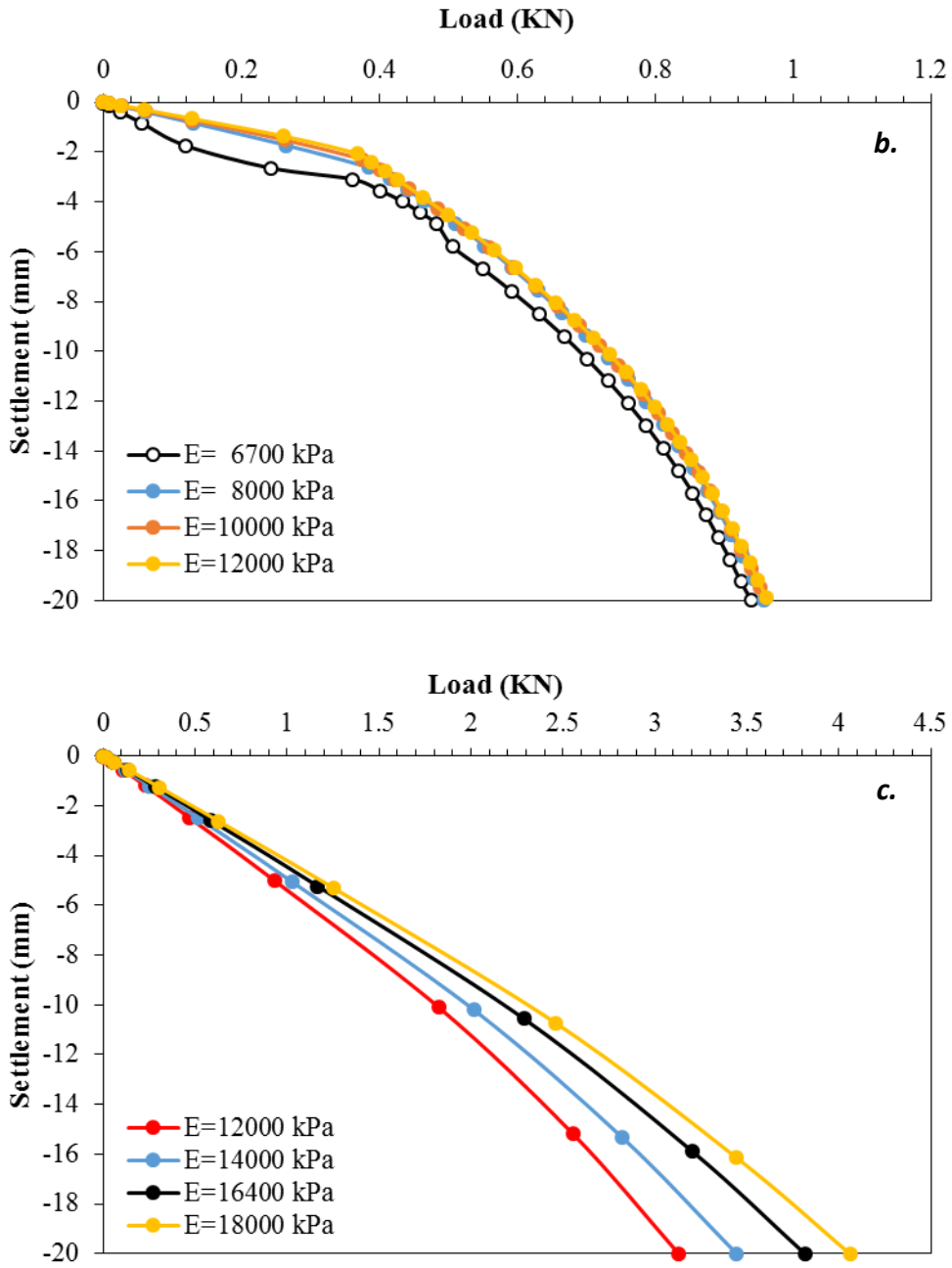

Figure 4.12: Effect of Young's modulus on vertical load intensity settlement behavior of column: **a.** OSC, **b.** SFM, **c.** RAPP.

4.4. Conclusion

This chapter explores the behavior of soft soil supported by three types of granular columns through numerical simulation. The (RAPP) demonstrated the most favourable behavior, improving bearing capacity and displacement. The depth of reinforcement was influential, with RAPP achieving positive results at a shorter length. Increasing the geotextile encasement's tensile strength enhanced column stiffness. Initially, the (SFM) performed slightly better than (OSC), but OSC outperformed SFM when geotextiles were added. RAPP achieved superior outcomes even without geotextiles. Higher internal friction angles in the column material increased the bearing capacity, particularly in OSC and SFM. Friction angles did not affect RAPP. Increasing Young's modulus had no significant effect on OSC and SFM's bearing capacity but improved RAPP's performance.

General Conclusion and Perspectives

This research studies the behavior of soft soil supported by three types of granular columns. A numerical simulation was confirmed by comparison with data available in the literature. Several numerical simulations were run to investigate the impact of column material (OSC, SFM, RAPP) on the weak soil with respect to bearing capacity and load-settlement behavior.

Chapter 1 discusses the importance of understanding compressible soils in civil engineering. It aims to provide a comprehensive analysis of various aspects related to compressible soils, such as their characteristics and behavior. The discussion focuses on the bearing capacity of shallow foundations and the effectiveness of using stone columns for soil reinforcement.

Chapter 2 explores different methods of improving soft soil, including the use of stone columns, geosynthetics, and other reinforcement techniques. It discusses the installation process, technical requirements, and factors that affect the implementation of stone columns. The chapter also highlights the use of geosynthetics to confine columns, which has been found to significantly improve bearing capacity and reduce settlements.

Chapter 3 provides an overview of models used in PLAXIS for numerical simulation. It emphasizes the simplicity of these models and their parameter determination through conventional geotechnical studies. The chapter also discusses the choice of geotechnical parameters and the constitutive behavior laws used in the study.

Chapter 4 investigates the behavior of soft soil supported by different types of granular columns through numerical simulation. It compares the performance of different column types, such as RAPP, SFM, and OSC, and examines the influence of factors like geotextile encasement and internal friction angles. The chapter concludes that RAPP demonstrates the most favourable behavior, improving bearing capacity and displacement. The depth of reinforcement and the tensile strength of geotextile encasement also play roles in column stiffness. Higher internal friction angles in the column material increase bearing capacity, particularly in OSC and SFM. Young's modulus has no significant effect on the bearing capacity of OSC and SFM but improves RAPP's performance.

The results of this study indicate the following conclusions:

- ✓ The RAPP showed good behavior in improving bearing capacity, vertical and lateral displacement, as it was about 7 times greater in SFM and 9 times greater in OSC.

- ✓ The RAPP gives good results whenever the depth of reinforcement increases, while the increase in SFM and OSC stops at 0.2 m as the ideal length, knowing that the RAPP achieved better than these results at only 0.1 m in length.
- ✓ Increase in the tensile strength of the geotextiles encasement of granular columns leads to increases in the column stiffness, it turns out that the reinforcement with SFM is slightly better than OSC initially, but when geotextiles were added to the column, OSC gave better results than SFM. More importantly, RAPP obviously achieved better results than OSC and SFM even if RAPP was without geotextile.
- ✓ Another key finding from this numerical analysis is that as the internal friction angle of the column material rises, so does the bearing capacity. This demonstrates that the granular column's friction angle (OSC and SFM) has a crucial influence on improving bearing capacity. On the contrary, it was concluded that RAPP was not affected by the change in the values of friction angles.
- ✓ In contrast to the previous result, the study showed that the increase in Young's modulus in OSC and SFM had no significant effect on the bearing capacity, while in RAPP it had the opposite effect and made good improvements.

Ultimately, this numerical study proved the effectiveness of using recycled aggregates in soil reinforcement at the expense of natural aggregates, despite all the attempts made in the parametric study to improve the performance of OSC and SFM columns. However, RAPP in the general case only had the best performance, and accordingly, it can be said that this scientific research has addressed part of the problem of environmental pollution (construction waste and concrete) and also addressed the problem of excessive use of natural aggregates in the field of construction and the strengthening of weak soils in economical and sustainable ways.

Based on the findings presented, it is recommended that future research activities focus on two aspects: creating an experimental model of the unit cell and developing an enlarged numerical model.

- ➢ Experimental Model: Building an experimental model of the unit cell would involve physically simulating the research presented. This would allow for a more practical and tangible understanding of the behavior and performance of different column types. The experimental model can be used to validate the numerical simulations and provide additional insights into the effectiveness of various reinforcement techniques.

- Enlarged Numerical Model: Developing an enlarged numerical model that simulates large-scale studies would enable researchers to investigate the behavior and performance of soil reinforcement techniques on a broader scale. This can help in understanding how different factors, such as soil properties, column dimensions, and external loads, affect the overall stability, bearing capacity, and displacement of the reinforced soil.
- Use of Recycled Concrete Materials: Given the positive results and benefits of using recycled aggregates in soil reinforcement, it is recommended that future research activities explore the use of recycled concrete materials specifically in soil consolidation. This would involve investigating the effectiveness of incorporating crushed or processed recycled concrete as a stabilizing agent in compressible soils

By combining both experimental and numerical approaches, researchers can gain a comprehensive understanding of the behavior and performance of various soil reinforcement techniques. This multidimensional approach will enhance the reliability and applicability of the research findings. In other hand, By utilizing recycled concrete materials, two important issues can be addressed simultaneously: sustainable waste management and soil consolidation. The problem of excess construction waste can be tackled, while also reducing the demand for natural resources. Concrete waste can be reused in soil consolidation, providing an environmentally-friendly solution.

References Bibliographie

Aboshi, H. (1979). The compozer-a method to improve characteristics of soft clay by inclusion of large diameter sand columns. *Proceedings, International Conference on Soil Reinforcements: Reinforced Earth and Other Techniques*, *1*, 211–216.

Ahlem, G. (2019). *Capacité portante des fondations sous charge inclinée par approche numérique Guetari Ahlem.Université Mohamed Khider-Biskra.*.

Ahmad, J., Md Zain, N. H., & Ashaari, Y. (2010). *The modelling of lateral movement of soft soil using finite element analysis and laboratory model*.

Al-Refeai, T. O. (1992). Strengthening of soft soil by fiber-reinforced sand column. *International Symposium on Earth Reinforcement Practice*, 677–682.

Alexiew, D., Brokemper, D., & Lothspeich, S. (2005). Geotextile encased columns (GEC): load capacity, geotextile selection and pre-design graphs. In *Contemporary issues in foundation engineering* (pp. 1–14).

Ambily, A. P., & Gandhi, S. R. (2007a). Behavior of stone columns based on experimental and FEM analysis. *Journal of Geotechnical and Geoenvironmental Engineering*, *133*(4), 405–415.

Ambily, A. P., & Gandhi, S. R. (2007b). Behavior of Stone Columns Based on Experimental and FEM Analysis. *Journal of Geotechnical and Geoenvironmental Engineering*, *133*(4). https://doi.org/10.1061/(asce)1090-0241(2007)133:4(405)

Auvray, R. (2010). Influence d'une colonne ballastée sur le comportement des sols argileux. *Université de Strathclyde, Glasgow*.

Balaam, N. P., & Booker, J. R. (1981). Analysis of rigid rafts supported by granular piles. *International Journal for Numerical and Analytical Methods in Geomechanics*, *5*(4). https://doi.org/10.1002/nag.1610050405

Balaam, N. P., & Booker, J. R. (1985). Effect of stone column yield on settlement of rigid foundations in stabilized clay. *International Journal for Numerical and Analytical Methods in Geomechanics*, *9*(4). https://doi.org/10.1002/nag.1610090404

Barksdale, R. D., & Bachus, R. C. (1983). Design and Construction of Stone Columns Volume II, Appendixes. In *National Technical Information Service*.

Basu, P. (2009). *Behaviour of sand-fiber mixed granular piles*. Ph. D. Thesis. Indian Institute of Technology Roorkee, Roorkee, India.

Bell, A. L. (2004). The development and importance of construction technique in deep vibratory ground improvement. In *Ground and soil improvement* (pp. 101–111). Thomas Telford Publishing.

BENMOUSSA., S. (2013). *BENMOUSSA Samir. Doctorat en sciences en G.C 2013(analyse numérique de l'influence de la stratification sur la portance des fondations superficielles). Unv M.khider_Biskra*. Unv M.khider_Biskra.

Benmoussa, S. (2006). *ANALYSE 3D DE LA CAPACITE PORTANTE D'UNE FONDATION SUPERFICIELLE REPOSANT SUR UN BICOUCHE*. Université de Batna 2.

Berrabah, F. (2015). *Évaluation numérique de l'effet du renforcement par nappes de géosynthétique sur la stabilité et le tassement des remblais sur sol compressible*. Université Mohamed Khider-Biskra.

BETEHI, C. (2010). *Thème: Comportement Des Sols Compressibles*. Université 8 mai 1945 de Guelma.

Boulon, M., Flavigny, E., & Malcot, Y. (2004). d'autres:«Pratique éclairée des éléments finis en Géotechnique», document1. *Laboratoire 3S et Terrasol*.

Boumekik, N. E. I., Labed, M., Mellas, M., & Mabrouki, A. (2021). Optimization of the ultimate bearing capacity of reinforced soft soils through the concept of the critical length of stone columns. *Civil Engineering Journal (Iran)*, *7*(9), 1472–1487. https://doi.org/10.28991/cej-2021-03091737

Bowles, J. E. (1988). *Foundation analysis and design*.

Brauns, J. (1978). Initial bearing capacity of stone columns and sand piles. *Int. Symp. on Soil Reinforcing and Stabilizing Techniques in Engineering Practice*, *1*, 497–512.

Brauns, J. (1980). Untergrund verbesserung mittels sandpfihlen oder schottersiulen. *Tiefbau22*, *8*, 678–683.

Caquot, A. I., & Kérisel, J. L. (1948). *Tables for the calculation of passive pressure, active pressure and bearing capacity of foundations*. Gautier-Villars.

CARTIER, G., WASCHKOWSKI, E., & DUNOYER, H. (1986). Expérimentation d'une technique innovante de stabilisation de remblais instables par colonnes de sol traité en place. *BULL LIAISON LAB PONTS CHAUSS*, *144*.

Castro, J. (2017). Modeling stone columns. *Materials*, *10*(7). https://doi.org/10.3390/ma10070782

Chen, J.-F., Han, J., Oztoprak, S., & Yang, X.-M. (2009). Behavior of single rammed aggregate piers considering installation effects. *Computers and Geotechnics*, *36*(7), 1191–1199.

Chen, J. F., Li, L. Y., Xue, J. F., & Feng, S. Z. (2015). Failure mechanism of geosynthetic-encased stone columns in soft soils under embankment. *Geotextiles and Geomembranes*, *43*(5), 424–431.

https://doi.org/10.1016/j.geotexmem.2015.04.016

Coop, M. R., & Atkinson, J. H. (1993). The mechanics of cemented carbonate sands. *Geotechnique*, *43*(1), 53–67.

Costet, J., Sanglerat, G., Biarez, J., & Lebelle, P. (1969). *Cours pratique de mécanique des sols*. Dunod Paris.

Das, B. M. (2017). *Shallow foundations: Bearing capacity and settlement*. CRC press.

Das, B. M. (2021). *Principles of geotechnical engineering*. Cengage learning.

Datye, K. R. (1982). Settlement and bearing capacity of foundation system with stone columns. *Int. Symp. on Soil and Rock Improvement Techniques Including Geotextiles, Reinforced Earth, and Modern Piling Methods*.

DEBBABI, I. E. (2021). *Contribution à l'analyse numérique des remblais sur sols mous*. Université Mohamed Khider–Biskra.

Debbabi, I. E., Saddek, R. M., Rashid, A. S. A., & Muhammed, A. S. (2020). Numerical modeling of encased stone columns supporting embankments on sabkha soil. *Civil Engineering Journal (Iran)*. https://doi.org/10.28991/cej-2020-03091569

Dhouib, A., & Blondeau, F. (2005). *Colonnes ballastées: techniques de mise en œuvre, domaines d'application, comportement, justification, contrôle, axes de recherche et développement*. Presses de l'École nationale des ponts et chaussées.

Dias, D. (1999). *Renforcement du front de taille des tunnels par boulonnage: Etude numérique et application à un cas réel en site urbain*. Villeurbanne, INSA.

DURVILLE, J.-L., & SEVE, G. (1996). Stabilité des pentes: glissements en terrain meuble. *Techniques de l'ingénieur. Construction*, *1*(C254), C254-1.

Egan, D., Scott, W., & McCabe, B. (2008). Installation effects of vibro replacement stone columns in soft clay. In *Geotechnics of soft soils: Focus on ground improvement* (pp. 35–42). CRC Press.

Fällman, A.-M. (1997). Performance and design of the availability test for measurement of potentially leachable amounts from waste materials. *Environmental Science & Technology*, *31*(3), 735–744.

Feng, S.-J., Shui, W.-H., Gao, L.-Y., & He, L.-J. (2010). Application of high energy dynamic compaction in coastal reclamation areas. *Marine Georesources and Geotechnology*, *28*(2), 130–142.

Frank, R., Cuira, F., & Burlon, S. (1999). *Calcul des fondations superficielles et profondes*. Techniques

de l'Ingénieur.

Ghazavi, M., & Nazari Afshar, J. (2013). Bearing capacity of geosynthetic encased stone columns. *Geotextiles and Geomembranes*, *38*. https://doi.org/10.1016/j.geotexmem.2013.04.003

Gniel, J., & Bouazza, A. (2009). Improvement of soft soils using geogrid encased stone columns. *Geotextiles and Geomembranes*, *27*(3), 167–175. https://doi.org/10.1016/j.geotexmem.2008.11.001

Gniel, J., & Bouazza, A. (2010). Construction of geogrid encased stone columns: A new proposal based on laboratory testing. *Geotextiles and Geomembranes*, *28*(1), 108–118.

Greenwood, D. A. (1991). *Load tests on stone columns*. ASTM International.

Guetif, Z., Bouassida, M., & Debats, J. M. (2007). Improved soft clay characteristics due to stone column installation. *Computers and Geotechnics*, *34*(2), 104–111.

Hansen, J. B. (1970). *A revised and extended formula for bearing capacity*.

Hasan, M., & Samadhiya, N. K. (2016). Experimental and Numerical Analysis of Geosynthetic-Reinforced Floating Granular Piles in Soft Clays. *International Journal of Geosynthetics and Ground Engineering*, *2*(3). https://doi.org/10.1007/s40891-016-0062-6

Hohberg, I., De Groot, G. J., Van der Veen, A. M. H., & Wassing, W. (2000). Development of a leaching protocol for concrete. *Waste Management*, *20*(2–3), 177–184.

Holtz, R. D. (2001). Geosynthetics for soil reinforcement. *Seattle, Washington*.

HOUDA, M. H. (2010). Etude numérique d'un mur de soutènement en sol stabiles et renforce avec fibres et geogrilles. *Mémoire de Mgister, Université Badji Mokhtar d'Annaba*.

Hughes, J. M. O., & Withers, N. J. (1974). Reinforcing of soft cohesive soils with stone columns. *International Journal of Rock Mechanics and Mining Sciences & Geomechanics Abstracts*, *11*(11). https://doi.org/10.1016/0148-9062(74)90643-3

Hughes, J. M. O., Withers, N. J., & Greenwood, D. A. (1975). A Field Trial of the Reinforcing Effect of a Stone Column in Soil. *Geotechnique*, *25*(1). https://doi.org/10.1680/geot.1975.25.1.31

Iai, S. (1989). Similitude for shaking table tests on soil-structure-fluid model in 1g gravitational field. *Soils and Foundations*. https://doi.org/10.3208/sandf1972.29.105

Indraratna, B., Rujikiatkamjorn, C., Wijeyakulasuriya, V., McIntosh, G., & Kelly, R. (2010). *Soft soils improved by prefabricated vertical drains: performance and prediction*.

Janbu, N. (1963). Soil compressibility as determined by oedometer and triaxial tests. *Proc. European*

Conf. SMFE, Wiesbaden, 1963, 1, 19–25.

Kempfert, H.-G., & Gebreselassie, B. (2006). *Excavations and foundations in soft soils*. Springer Science & Business Media.

Kim, S., Lee, D., Lee, J., You, S. K., & Choi, H. (2012). Application of recycled aggregate porous concrete pile (RAPP) to improve soft ground. *Journal of Material Cycles and Waste Management*, *14*(4). https://doi.org/10.1007/s10163-012-0076-7

Labed, M., & Mellas, M. (2016). *fst Stability of geosynthetic reinforced embankments over stone column - improved soft soil*. *2*(October), 65–74.

Liang, R. Y., Shilong, X., & Edil, T. B. (2015). Innovative soft soil improvement method through intelligent use of vacuum de-watering and dynamic compaction techniques. *Geotechnical Engineering*, *46*(4), 57–67.

Lundgren, H. (1953). Determination by the theory of plasticity of the bearing capacity of continuous footings on sand. *3rd Int. Conf. Soil Mech.*, *1*, 409–412.

Magnan, J., Construction, G. P.-T. de l'ingénieur., & 1988, undefined. (n.d.). Amélioration des sols. *Pascal-Francis.Inist.Fr* . Retrieved May 30, 2023, from https://pascal-francis.inist.fr/vibad/index.php?action=getRecordDetail&idt=16005963

Mahfoud, O. A. (1990). *Modélisation numérique des écoulements et des déformations dans les barrages en terre construits sur des sols mous*. Ecole Nationale des Ponts et Chaussées.

Mahiyar, H., & Patel, A. N. (2000). Analysis of Angle Shaped Footing under Eccentric Loading. *Journal of Geotechnical and Geoenvironmental Engineering*, *126*(12). https://doi.org/10.1061/(asce)1090-0241(2000)126:12(1151)

Marinković, S., Radonjanin, V., Malešev, M., & Ignjatović, I. (2010). Comparative environmental assessment of natural and recycled aggregate concrete. *Waste Management*, *30*(11), 2255–2264.

McKelvey, D., Sivakumar, V., Bell, A., & Graham, J. (2004). Modelling vibrated stone columns in soft clay. *Proceedings of the Institution of Civil Engineers: Geotechnical Engineering*, *157*(3), 137–149. https://doi.org/10.1680/geng.2004.157.3.137

Meyerhof, G. G. (1951). The ultimate bearing capacity of foudations. *Geotechnique*, *2*(4), 301–332.

Meyerhof, G. G. (1963). Some recent research on the bearing capacity of foundations. *Canadian Geotechnical Journal*, *1*(1), 16–26.

Meyerhof, Gg. (1953). The bearing capacity of foundations under eccentric and inclined loads. *Proc. of 3rd ICSMFE*, *1*, 440–445.

Mitchell, J. K., & Huber, T. R. (1985). Performance of a stone column foundation. *Journal of Geotechnical Engineering*, *111*(2). https://doi.org/10.1061/(ASCE)0733-9410(1985)111:2(205)

Mohanty, P., & Samanta, M. (2015). Experimental and numerical studies on response of the stone column in layered soil. *International Journal of Geosynthetics and Ground Engineering*, *1*, 1–14.

Mokhtari, M., & Kalantari, B. (2012). Soft Soil Stabilization using Stone Column--A Review. *Electronic Journal of Geotechnical Engineering*, *17*, 1459–1466.

Morales, E. M., & Morales, M. K. (2003). *State of practice in soil liquefaction mitigation and engineering countermeasures*. Available in: http://www. pgatech. com. ph/State of Practice in Soil ….

Muir Wood, D., Hu, W., & Nash, D. F. T. (2000). Group effects in stone column foundations: model tests. *Geotechnique*, *50*(6), 689–698.

Murugesan, S., & Rajagopal, K. (2006). Geosynthetic-encased stone columns: Numerical evaluation. *Geotextiles and Geomembranes*, *24*(6), 349–358. https://doi.org/10.1016/j.geotexmem.2006.05.001

Nour, B., & Islam, E. (2021.). *Doctorat LMD en Génie Civil Intitulé Analyse numérique de la portance d ' un massif de fondation renforcé par des colonnes ballastées confinées dans des nappesgéosynthétiquesUniversity of Biskra.*

Orense, R. (2008). Liquefaction Remediation by Compaction Grouting, sl: Dept of Civil & Environmental Engineering. *University of Auckland*.

Orense, R. P., Morita, Y., & Ide, M. (2000). Assessment and mitigation of liquefaction risk for existing building foundation. *ISRM International Symposium*, ISRM-IS.

Petkovic, G., Engelsen, C. J., Håøya, A. O., & Breedveld, G. (2004). Environmental impact from the use of recycled materials in road construction: Method for decision-making in Norway. *Resources, Conservation and Recycling*. https://doi.org/10.1016/j.resconrec.2004.04.004

Prandtl, L. (1921). Uber die eindringungfestigkeit plastisher baustoffe und die festigkeit von scneifen. *Zeitschrift Fur Angewandte Mathematik Und Mechanik*, *1*.

Prashant, A., & Mukherjee, M. (2010). Soil nailing for stabilization of steep slopes near railway tracks. *Research Design and Standard Organization (RDSO), Lucknow, Indian Istitute of Technology Kanpur*.

Priebe, H. J. (1991). *Vibro replacement-Design criteria and quality control*. ASTM International.

Pulko, B., & Majes, B. (2005). Simple and accurate prediction of settlements of stone column reinforced

soil. *Proceedings of the 16th International Conference on Soil Mechanics and Geotechnical Engineering: Geotechnology in Harmony with the Global Environment*, *3*.

Rajan, P. M., & Krishnamurthy, P. (2022). *Adequacy of Stone Column Dimensions Supporting Isolated Footing when Subjected to Earthquake Loading*. 1–13.

Raju, V. R., Hari Krishna, R., & Wegner, R. (2004). Ground improvement using vibro replacement in Asia 1994 to 2004-a 10 year review. *5th International Conference on Ground Improvement Techniques, Kuala Lumpur*.

Raju, V. R., & Sondermann, W. (2005). Ground improvement using deep vibro techniques. In *Elsevier Geo-Engineering Book Series* (Vol. 3, pp. 601–638). Elsevier.

Ranjan, G. (1989). Ground treated with granular piles and its response under load. *Indian Geotech J*, *19*(1), 1–86.

Ranjan, G., Singh, B., & Charan, H. D. (1999). Experimental study of soft clay reinforced with sand-fiber core. *Indian Geotechnical Journal*, *29*(4), 281–291.

Rankine, W. J. M. (1857). II. On the stability of loose earth. *Philosophical Transactions of the Royal Society of London*, *147*, 9–27.

Rima, H. (2012). *Analyse Numerique De La Capacite Portante D ' Une Fondation Filante Implantee Sur Un*.

Roscoe, K. H., Schofield, An., & Wroth, andC P. (1958). On the yielding of soils. *Geotechnique*, *8*(1), 22–53.

Sayehvand, S., & Kalantari, B. (2012). Use of Grouting Method to Improve Soil Stability Against Liquefaction--A Review. *Electronic Journal of Geotechnical Engineering*, *17*, 1559–1566.

Schlosser, F., Jacobsen, H. M., & Juran, I. (1984). Le renforcement des sols. *Revue Française de Géotechnique*, *29*, 7–33.

Schultze, H. E., & Schwick, G. (1952). *Über den Mechanismus der Thrombinbildung im isolierten System*.

Shivashankar, R., Dheerendra Babu, M. R., Nayak, S., & Rajathkumar, V. (2011). Experimental studies on behaviour of stone columns in layered soils. *Geotechnical and Geological Engineering*, *29*, 749–757.

Shooshpasha, I., Hasanzadeh, A., & Taghavi, A. (2013). Prediction of the axial bearing capacity of piles by SPT-based and numerical design methods. *International Journal of GEOMATE*, *4*(2), 560–564. https://doi.org/10.21660/2013.8.2118

Singh, D., Kumar, V., & Rawat, A. (2016). *Review on Various Techniques to Improve Bearing Capacity of Soil*. *October 2018*.

Skempton, A. W. (1951). The bearing capacity of clays. *Selected Papers on Soil Mechanics*, 50–59.

Soyez, B. (1985). Méthodes de dimensionnement des colonnes ballastées. *Bulletin de Liaison Des Laboratoires Des Ponts et Chaussées*, *135*(135), 35–51.

Stuedlein, A. W., & Holtz, R. D. (2013). Bearing capacity of spread footings on aggregate pier reinforced clay. *Journal of Geotechnical and Geoenvironmental Engineering*, *139*(1), 49–58.

Tandel, Y. K., Solanki, C. H., & Desai, A. K. (2012). Numerical modelling of encapsulated stone column-reinforced ground. *International Journal of Civil, Structural, Environmental and Infrastructure Engineering (IJCSEIERD)*, *2*(1), 82–96.

Taube, M. G., & Herridge, J. (2002). Stone columns for industrial fills. *33rd Ohio River Valley Soil Seminar (ORVSS)*, *18*.

Terzaghi, K. (1943a). Theoretical Soil Mechanics. In *Theoretical Soil Mechanics*. https://doi.org/10.1002/9780470172766

Terzaghi, K. (1943b). Theory of consolidation. *Theoretical Soil Mechanics*, 265–296.

Terzaghi, K., Peck, R. B., & Mesri, G. (1996). *Soil mechanics in engineering practice*. John wiley & sons.

Tüter, F., & Ertugrul, Ö. L. (2022). *Numerical modeling of geogrid reinforced stone column groups with Plaxis 3D*. *December*, 158–160.

Vermeer, P. A., & De Borst, R. (1984). Non-associated plasticity for soils, concrete and rock. *HERON*, *29 (3), 1984*.

Vesic, A. S. (1974). Analysis of ultimate loads of shallow foundations: Closure of discussion of original paper J. Soil Mech. Found. Div. Jan. 1973. 1F, 6R. J. GEOTECH. ENGNG. DIV. V100, N. GT8, 1974, P949–951. *International Journal of Rock Mechanics and Mining Sciences & Geomechanics Abstracts*, *11*(11), A230.

Vipulanandan, C., Bilgin, O., Guezo, Y. J. A., Vembu, K., & Erten, M. B. (2009). *Prediction of embankment settlement over soft soils.* Center for Innovative Grouting Materials and Technology.

Von Soos, P. (1990). Properties of soil and rock. *Grundbautaschenbuch Part*, *4*.

W. E. T, H. (1995). *Physical Modelling of Group Behaviour of stone column foundations*. University of Glasgow.

Wakeman, R. C., Evenson, A., Morgan, T., Pastore, J., & Blackburn, J. T. (2010). *Compaction grouting for seismic mitigation of sensitive urban sites*.

Welsh, J. P., & Burke, G. K. (2000). Advances in grouting technology. *ISRM International Symposium*, ISRM-IS.

Yeung, V. (2008). Application of soil nailing for slope stability purpose. *B. Tech. Project, University of Technology, Sydney. P*, *21*.

You, S. K. (2003). Experimental study on stress sharing behavior of composition ground improved by sand compaction piles with low replacement area ratio. *Journal of KGS*, *19*(5), 253–261.

Yu, H.-S. (2000). *Cavity expansion methods in geomechanics*. Springer Science & Business Media.

Zhu, H.-H., Yin, J.-H., Yeung, A. T., & Jin, W. (2011). Field pullout testing and performance evaluation of GFRP soil nails. *Journal of Geotechnical and Geoenvironmental Engineering*, *137*(7), 633–642.

Zighmi, I. (2011). *Etude numérique de l'influence des paramètres geotechniquesn sur le comportement des sols renforcés par colonnes ballastées*. Tizi Ouzou.